Remote Sensing the Signatures of Upwelling in South Eastern Arabian Sea

Ch.V.Chiranjivi Jayaram

Department of Physical Oceanography

Cochin University of Science and Technology

Thesis submitted in partial fulfilment for the award of

Doctor of Philosophy

in

Oceanography

Under Faculty of Marine Sciences

MAY 2011

Declaration

I herewith declare that the thesis entitled **"Remote Sensing the Signatures of Upwelling in South Eastern Arabian Sea"** is an authentic record of research work carried out by me under the supervision and guidance of Prof.(Dr).A.N.Balchand, Department of Physical Oceanography, Cochin University of Science and Technology, towards the partial fulfilment of the requirements for the award of Ph.D degree under the Faculty of Marine Sciences and no part thereof has been presented for the award of any other degree in any University / Institute.

Ch.V.Chiranjivi Jayaram
Registration Number: **3456**
Department of Physical Oceanography
Cochin University of Science & Technology
Kochi - 682016
India

Certificate

This is to certify that this thesis entitled **"Remote Sensing the Signatures of Upwelling in South Eastern Arabian Sea"** is an authentic record of research work carried out by Mr.Ch.V.Chiranjivi Jayaram, under my supervision and guidance at the Department of Physical Oceanography, Cochin University of Science and Technology, towards the partial fulfilment of the requirements for the award of Ph.D degree under the Faculty of Marine Sciences and no part thereof has been presented for the award of any other degree in any University / Institute.

Prof. (Dr). A.N.Balchand
Supervising Guide
Department of Physical Oceanography
Cochin University of Science & Technology
Kochi - 682016
India

Acknowledgements

I am deeply indebted to my guide Prof.(Dr). A.N. Balchand, Department of Physical Oceanography, Cochin University of Science & Technology, Kochi, for his guidance, constant encouragement and support, which enabled me to complete this thesis. I am especially grateful to him for the freedom given to me to select the topic and methodology to be adopted. It is indeed an honor to be his student. Without his guidance, support and encouragement, this thesis would not have materialized.

I am particularly grateful to Dr. K. Ajith Joseph, Director, Nansen Environmental Research Centre (India), Kochi, for giving me an opportunity to work in the Oceansat-II utilization project and providing an excellent working environment at NERCI. It is indeed he, who introduced me to upwelling during my M.Tech days and it is true to say that without his enthusiasm, support and encouragement, I could not have finished my thesis in time. I really enjoyed working with him at NERCI.

I acknowledge all the support and help rendered to me by Dr. S.S.C. Shenoi, Director, Indian National Centre for Ocean Information Services, Hyderabad during the tenure of the Doctoral Work.

Also, I acknowledge the support and encouragement given to me by Prof. H.S.Ram Mohan, Director, School of Marine Sciences, Cochin University of Science and Technology during my Doctoral work.

I sincerely thank Dr.T.V.S.Udaya Bhaskar, Scientist, Indian National Centre for Ocean Information Services, for his encouragement and also spending long hours after office to discuss my doubts and going

through my thesis to provide critical insights towards improvement. It is really a privilege to have such a senior colleague to work with.

I am thankful to Dr.R.Sajeev, Head, Dept. of Physical Oceanography, CUSAT, for providing the necessary facilities and encouragement throughout the study period. I also thank Sri.P.K.Saji, Assistant Professor, Dept. of Physical Oceanography for his support.

My sincere thanks are due to Dr.P.V.Joseph, Emiretus Professor, Cochin University of Science and Technology, for enlightening me with highly meaningful ideas and concepts that helped me during this work.

I express my sincere thanks to Prof. Ola. M. Johannessen and Lasse. H. Pettersson, of Nansen Environmental and Remote Sensing Centre, Bergen, Norway for their support, love and encouragement. Also, my thanks to Nansen Scientific Society for funding my stay at Seoul to attend PICES school on Satellite Oceanography.

My sincere thanks are due to Dr.N. Nandini Menon for the constant support and encouragement throughout my work. The insights she provided had made me understand some of the biological processes that take place within the ocean.

I express my sincere gratitude to Dr.Sudheer Joseph, Scientist, Indian National Centre for Ocean Information Services, for his support and the discussions I had with him during my work. I express my gratitude to Dr.M.S.Madhusoodanan, NERCI for his advice on programming and for the fruitful discussions we had during our stay at NERCI.

My thanks are due to Dr. P.V. Hareesh Kumar, Scientist, NPOL, Kochi for sparing his time during the initial days of my research and especially enlightening my thoughts on the oceanic phenomenon along the southwest coast of India and also my sincere thanks to Dr.K.V. Sanil Kumar, Scientist, NPOL, whose critical review of my work helped me immensely for my first publication.

My sincere gratitude to Dr.Gael Alory of LEGOS, France, for sparing his time to discuss my work and enlightening me on his model simulations to compute the heat budget.

I am indebted to the Space Applications Centre, Ahmedabad, for the financial help rendered as fellowship under the Oceansat-II utilization project that helped me to accomplish this task.

I thank PICES for selecting me and providing travel support to attend the summer school on Satellite Oceanography for Earth Environment held during August 2009 at Seoul, South Korea.

My heartfelt thanks to my dearest friends Neethu, Krishna Mohan, Johnson Zacharia, Nithin, Sandeep, Jayakrishnan, Sivaprasad, Vijaya Kumar and especially Geetu Rose of NERCI for their invaluable scientific and personal support during this study and for the warm friendship and love which has been a pillar of strength in all the challenges during these years. I take this opportunity to express my gratitude to all my colleagues at INCOIS for the moral support and encouragement.

Mr. N. Kumar presently librarian at SAC, Ahmedabad, helped a lot during his tenure at INCOIS by providing me the necessary literature for my work.

I sincerely thank Phiroz Shah, Tara, Smitha, research scholars of Dept. of Physical Oceanography and Smitha of NERCI for their encouragement and the help rendered during my work.

My sincere thanks to the office staff of Dept. of Physical Oceanography, CUSAT, for their help and co-operation extended to me during the period of study. My special thanks to Sri.Manual Prakasia of NERCI for his encouragement and all the help rendered to me during my work at NERCI.

I thank the data centers of AVISO, PO-DAAC, Oceancolor Group of NASA, SSMI, IFREMER, CORIOLIS, INCOIS, BODC and all the

people who put in untiring efforts to bring out quality data products that I made use of in this study.

I am deeply indebted to my parents, brothers and cousins, who have done so much and have always been a source of inspiration. They gave me unconditional love and support throughout my life and have enabled me to achieve this goal. Last but not the least, I thank each and every person who had directly or indirectly helped me to complete this thesis in time.

Most importantly, I thank God for His blessings throughout my life that enabled me to fulfil this endeavour.

To ...My Parents and Teachers...

Contents

List of Figures

List of Tables

Glossary

ARMEX Arabian Sea Monsoon Experiment

AVHRR Advanced Very High Resolution Radiometer

AVISO Archiving, Validation and Interpretation of Satellite Oceanographic data

BoB Bay of Bengal

BoBMEX Bay of Bengal Monsoon Experiment

CEI Chlorophyll Extension Index

CHLA Chlorophyll-a Concentration

CP Coastal Pumping

EICC East India Coastal Current

EM Spectrum Electromagnetic Spectrum

ENSO *El-Nino* Southern Oscillation

EOF Empirical Orthogonal Function

ESSA Environmental Science Services Administration Satellite Program

GPCP Global Precipitation Climatology Project

IIOE International Indian Ocean Expedition

IITM Indian Institute of Tropical Meteeorology

IOD Indian Ocean Dipole

IR Infra Red

JGOFS Joint Global Ocean Flux Studies

LHF Latent Heat Flux

LTG Latitudinal Temperature Gradient

MLD Mixed Layer Depth

MJO Madden Julian Oscillation

MO Meridional Overturning

MOS Modular Optical Sensor

NEM North East Monsoon

NHF Net Heat Flux

OCM Ocean Color Monitor

OLR Outgoing Longwave Radiation

SEAS Southeastern Arabian Sea

SeaWiFS Sea viewing Wide Field of view Sensor

SF Surface Flux

SHF Sensible Heat Flux

SLA Sea Level Anomaly

SMC Summer Monsoon Current

SST Sea Surface Temperature

SWM South West Monsoon

SWR Shortwave Radiation

TMI TRMM-Microwave Imager

TRMM Tropical Rainfal Measuring Mission

WICC West India Coastal Current

WOA World Ocean Atlas

1

Introduction

1.1 Evolution of Ocean Sciences and Disciplines

Oceanography is the branch of science that deals with all studies relevant to the sea. It covers a wide range of topics such as its physical conditions like ocean currents, waves and circulation pattern, the chemical nature of sea water, the biological life forms that thrive within and topography beneath the ocean water and the atmosphere above it [Sverdrup et al., 1942]. Though oceanography is one among the newest fields of science, its roots date back to several centuries when people began to venture in to their neighbouring seas for day-to-day needs. Their experiences and understanding of the oceans over a period of time were passed down the generations. The early modern oceanographic explorations were primarily focussed on cartography and were limited mainly to the surfaces (www.wikipedia.org). Over the period, with the development of technology and knowledge, regarding the oceans, great advancements were made in all the fields of marine sciences.

Modern oceanography began as a field of science only a little less than 150 years in the late 19th century, after the Americans, British and Europeans launched expeditions to explore the oceans. The first such scientific expedition is the Challenger expedition from 1872 to 1876 onboard the British warship HMS Challenger. Oceanography gained immense importance during the two world wars and from then onwards numerous studies have been conducted to understand the oceans

in detail (www.divediscover.whoi.edu/history-ocean/index.html) and its importance vis-a-vis the environment where we dwell. The growth of oceanography has been stimulated not only by its intellectual character and by the everyday practical needs of maritime affairs, but also by the understanding that oceans play a significant role in influencing both weather and climate over land and sea.

Oceanography basically is a data dependent science and therefore the need of accurate measurements is of greater importance [Apel, 1987]. The observation techniques range from traditional *in-situ* and ship based data collection to the recent developments in satellite technology in order to better grasp the premise(s) of theories in oceanography and thus lead to improved parameterization of numerical models for climate prediction. Broad disciplines of oceanography are classified into:

- Physical Oceanography: The study of currents, waves, tides, physical water properties, air-sea interaction
- Biological Oceanography: The study of marine life and its productivity, life cycles and ecosystems
- Geological Oceanography: The study of plate tectonics, geology of ocean basins, coastal process like erosion, sedimentation and
- Chemical Oceanography: The study of chemical properties of sea water, trace organics, carbon cycle, metal speciation, drugs and alike.

Figure 1.1 shows the different processes that take place within the ocean.

1.2 Oceanography in India

During the early years in the evolution of oceanography, very little had been studied and understood on the Indian Ocean owing mainly due to the socio - economic conditions surrounding it. This gap was filled up to some extent by the International Indian Ocean Expedition (IIOE) held between 1960 and 1965. A major share of the present understanding on the processes in Indian Ocean is the fruit of IIOE [Panikkar, 1963]. One of the main intentions of IIOE was to

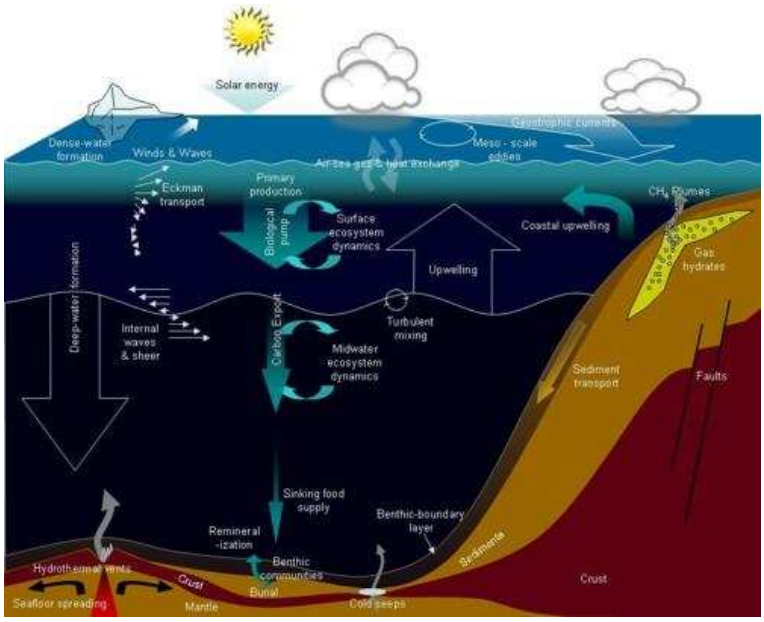

Figure 1.1: Schematic of different oceanic process, taken from Southampton Oceanographic Centre, UK

train Indian scientists in oceanography and establish national level laboratories in India. These two objectives resulted in the establishment of the National Institute of Oceanography in Goa with a team of dedicated researchers.

India has a long coast line of 7517 kms and 25% of its population resides in the coastal regions [Sanil Kumar et al., 2006]; therefore it is imperative for the Indians to well understand the seas around it. In this line of progression, numerous studies had been conducted by India alone and also in collaboration with other nations / interested agencies around the world to further enhance the knowledge on the Indian Ocean. Some of the recent studies that were undertaken by India are Bay of Bengal Monsoon Experiment (BoBMEX), Arabian Sea Monsoon Experiment (ARMEX) and Joint Global Ocean Flux Studies (JGOFS) in the Arabian Sea region. These studies have helped to reveal the role of the Indian ocean in modulating the monsoon(s) (Bhat et al., 2001 and Sengupta et al., 2008) and also on the features of the biogeochemistry of the northern Indian Ocean region [Muraleedharan and Kumar, 1996].

1.3 Remote Sensing as a tool to monitor Oceans

Monitoring the oceans is essential to learn about global climate change issues, fisheries, coastal zone management and of course, just out of scientific curiosity. There are several approaches to achieve this aim of understanding the oceans like observations, numerical models based solely on pure theory and combined observational - numerical models (data assimilation), etc. Among observational techniques, satellite remote sensing is an excellent tool for monitoring the oceans. Satellite overpasses allows continuous and cost effective collection of a variety of observations over large and often inaccessible regions of the oceans within a short period of time. Due to the availability of a variety of sensors, techniques and platforms employed satellite observations differ in their temporal, spatial and spectral characteristics. Consequently, different sensors also vary in their ability to meet the demands of a particular application. In order to efficiently utilize these systems, one must consider the capabilities and limitations of each and choose an appropriate sensor for their application(s) and environment [Brown et al., 2005]. The purpose of an earth observing sensor on a satellite or aircraft is to obtain information about the Earth and its environment. This information may be as complex as a detailed map of temperature or the spatial patterns of surface circulation [Brown et al., 2005].

The information transfer mechanism from sea to the satellite is a major constraint in remote sensing of oceans. This is because of the medium through which electromagnetic radiation has to pass through [Robinson, 2004]. Atmospheric medium is opaque for many sections of the electromagnetic spectrum, and in those parts where the atmosphere is transparent; radiation passing through may still be hampered by various other atmospheric constituents [Stewart, 1985]. Retrieval of information from these signals lays the foundation for remote sensing. Capability of ocean remote sensing is subject to the nature of information about the sea that is possible to be retrieved and communicated by the electromagnetic radiation Maull [1985]. Principal parameters that could be monitored remotely from satellites are ocean colour, sea surface temperature (SST), sea surface height(SSH) and sea surface roughness for estimating winds [Robinson, 2004]. In a way, these

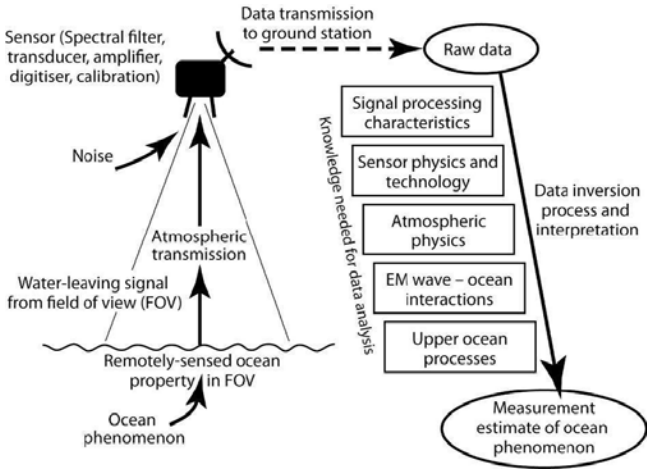

Figure 1.2: Schematic of remote sensing,from [Robinson, 2004]

entire phenomena are pertaining to the upper ocean and thus are known as surface signatures of the ocean. If quantitative information about these signatures is to be retrieved from the satellite data, we need to understand the processes that cause them to have a surface signature in the primary detectable variables. It is with these challenges that satellite oceanography has evolved to unravel, with the advancement of physics of remote sensing and the understanding of oceans as well.

Figure 1.2 presents the complete schematic of the processes involved in remote sensing, right from data collection to data dissemination. The major component of remote sensing as far as oceans are concerned is the atmospheric correction [Robinson, 2004]. The signals that were observed from the ocean will get attenuated while passing through the atmosphere at especially certain wavelengths and those parts where the atmosphere is nearly transparent are known as Atmospheric Windows. All windows are not transparent to every part of the electromagnetic spectrum - they are selective [Stewart, 1985]. Figure 1.3 shows the different spectral bands used in remote sensing. The most important bands that are often used in ocean remote sensing are:

- Visible band - Ocean Color,
- Thermal Infrared Sea Surface Temperature,

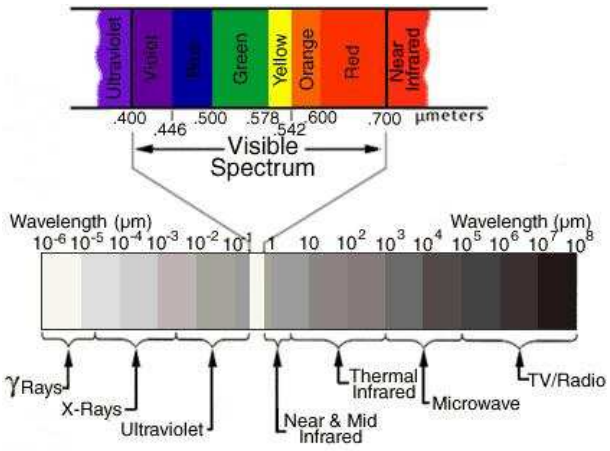

Figure 1.3: Figure showing EM Spectrum, from www.astro.virginia.edu

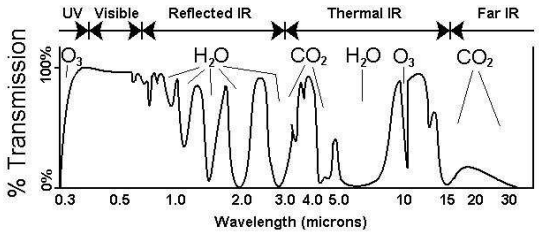

Figure 1.4: Atmospheric Windows, from http://frigg.physastro.mnsu.edu

- Passive Microwave - Sea Surface Temperature, Sea Surface Salinity and
- Active Microwave Sea Surface Height, Sea Surface Roughness.

Constituents of the atmosphere that hamper the information are the presence of Carbon Dioxide, Water vapour and Aerosols. Figure 1.4 presents the schematic of atmospheric windows and transmission percentage for each of the atmospheric constituents at different wavelengths of the electromagnetic spectrum. If features of land and ocean are to be observed by the reflection of incident solar radiation in the same way as the human eye observes, then the frequency range of high energy solar radiation should be used [Robinson, 2004]. Depending on the nature of observation and the resources available, different satellite missions were launched by various countries over the past three decades [Robinson, 2004]. This

growth in the data has made it possible to understand global oceans and their phenomenon more explicitly. Some of the most notable contributions of satellites in oceanography are the understanding on general circulation and eddies, *El-Nino* southern oscillation (ENSO) phenomenon, global productivity regions [Saitoh et al., 2011] and in the Indian Ocean, the satellite observations have paved the way for discovering the Indian Ocean Dipole [Saji et al., 1999]. Also, the knowledge on monsoon pattern now stands enhanced by the application of satellite data products [Joseph, 1990].

1.4 Satellite Oceanography in India

One of the early works on Indian Ocean particularly related to surface oceanographic conditions off west coast of India from satellite observations are available from Saha [1972]. A critical study from the ESSA - 2 satellite photographs linked with aerial data collection had been applied to study the sea state and its surface temperature. Indian remote sensing program started to experiment with sensors specific to oceanographic studies in 1996 with the launch of Modular Optical Sensor (MOS) onboard IRS - P3. This was later followed by an exclusive ocean color sensor named Ocean color monitor (OCM-1) onboard IRS - P4 in 1999 [Chauhan et al., 2002]. This satellite gave vital information on the optical properties and productivity of the Indian Ocean region as reported by Chauhan et al. [2002] and Chauhan et al. [2003]. Later on OCM - 1 was followed by OCM - II that was recently launched onboard Oceansat - II in 2009. This satellite carried another ocean related payload called as scatterometer that is used to estimate ocean surface winds. Apart from the Indian satellite sensors, scientific community is vastly utilizing the data provided by other popular satellite missions launched by various space agencies of the USA and European Union. After the advent of satellite sensors specific to oceanographic observations, it had been possible to monitor the global productive zones, thereby identifying the spatial extent of large marine ecosystems. The abundance of satellite data had made possible the monitoring of the inter-annual variability of the major upwelling zones as reported by Chavez and Messie [2009]. This has prompted to undertake a similar study to expand the knowledge on the upwelling phenomenon that takes place in the south Eastern

Arabian Sea(SEAS), annually. In order to enhance our knowledge on upwelling in local Indian waters and also to demonstrate the significance of satellites in the field of oceanography, present study is envisaged with a series of objectives, listed in section 1.9.

1.5 Upwelling, by definition

Upwelling is the physical process of ascending motion of water column for a minimum duration and extent by which water from subsurface layers is brought into the surface layer (Smith, 1968, Bakun, 1990). As a result of upwelling, cool, nutrient rich subsurface waters replaces the warm surface waters of the ocean. This process has profound influence on the primary productivity and climate in different time scales.

1.5.1 Classification of Upwelling

Coriolis force and Ekman transport are the main physical forces attributed to drive upwelling in the oceans. Rotation of earth causes the moving objects to deflect along their paths, to the right in the Northern Hemisphere and to the left in the Southern Hemisphere, which is known as Coriolis Effect. Observations demonstrate that the water in the ocean moves in curved paths under the Coriolis Effect as it is not attached to the earth (www.wikipedia.org). Winds blowing over the sea surface produce a thin, horizontal boundary layer called Ekman layer. In the ocean, the surface layer or Ekman layer flows towards right of the wind direction in the northern Hemisphere and to the left of the wind direction in the Southern Hemisphere due to the Coriolis deflection [Pond and Pickard, 1983]. This wind induced surface layer transport has strong dynamic implications on coastal surface currents. This will result in the movement of water away from the shore and if there is no sufficient horizontal flow to replace this displaced water, then water must rise from the depth resulting in upwelling [Stewart, 2005].

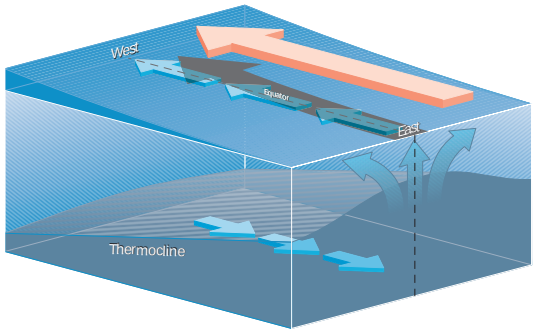

Figure 1.5: Schematic of equatorial upwelling, pink arrow indicates the direction of wind blowing and the blue arrows indicate the water movement, taken from http://atmos.washington.edu

1.5.2 Upwelling characteristics based on driving forces

Upwelling is of two kinds - depending on the nature of driving force: a. Wind-driven and b. Dynamic (www.es.flinders.edu.au/ mattom/ShelfCoast/notes/chapter06). Wind driven upwelling occurs due to the divergence of Ekman layer. Dynamical upwelling results due to the divergence in the upper ocean or convergence in the deeper waters which is caused by large scale oceanic current systems [Rao and Ram, 2005].

1.5.3 Upwelling based on its spatial occurrence

The different types of upwelling, classified [Pond and Pickard, 1983] on the basis of their spatial occurrence are: a. Equatorial, b. Coastal and c. Open Ocean.

- Equatorial upwelling: Equatorial upwelling is caused by trade winds blowing from East to West in the vicinity of the equator. Water flows away from the equator to right in the Northern Hemisphere and towards left in the Southern Hemisphere. The deficit of water at the equator is filled by the upwelled waters from below [Stewart, 2005]. Equatorial upwelling is most prominent in the Pacific Ocean. Figure 1.5 shows a schematic of equatorial upwelling in the oceans.

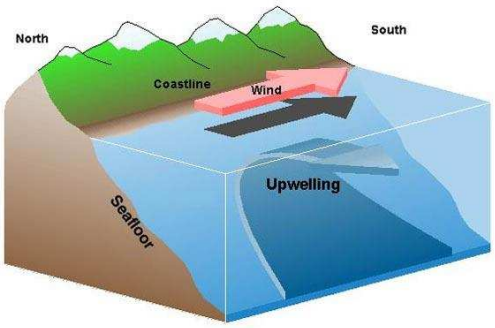

Figure 1.6: Schematic of Coastal Upwelling, from http://en.wikibooks.org

- Coastal upwelling: Coastal upwelling results from the divergence of the flow that occurs when surface waters are transported offshore from a coastal boundary as the wind blows parallel to the coastline on its left (right) in the northern (southern) hemisphere as shown in figure 1.6 . Deficit in water near to the coast is filled by the upwelled waters from the deep. In other terms, upwelling will occur when the wind blows equator-ward along an Eastern boundary of an Ocean in either Hemisphere or pole-ward along a Western boundary [Pond and Pickard, 1983]. Coastal upwelling is most prominent along Somalia coast, Southwest coast of India, the Java-Sumatra Islands, coasts of California and Peru, the Southwestern and Northwestern tips of Africa and recently reported in South China Sea [Su et al., 2011].

- Open Ocean upwelling: Away from the equator, wind stress curl plays an important role in forcing the oceanic movement. Positive wind stress curl is conducive for upwelling in the Northern Hemisphere and negative wind stress curl is favourable for upwelling in the Southern Hemisphere [Stewart, 2005]. Vertical motion of water results in cyclonic and anti-cyclonic circulation of water, where cyclonic circulation gives rise to upwelling and anti-cyclonic circulation results in down-welling [Rao and Ram, 2005]. In general, it is understood that different types of upwelling occur depending upon the topography, prevailing wind directions and conditions in the adjacent deep ocean as in figure 1.7 .

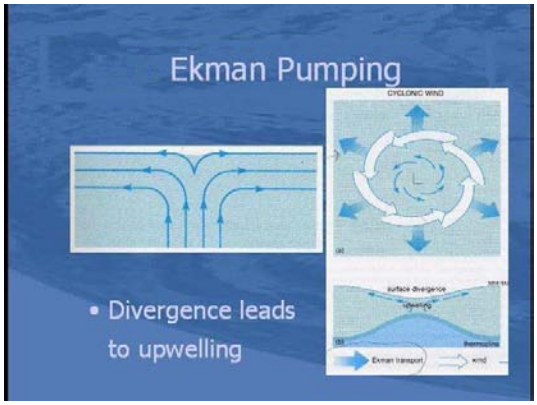

Figure 1.7: Schematic of Open Ocean upwelling as a result of Ekman pumping, from www.ias.ac.in

The driving force for coastal upwelling is the wind stress blowing parallel to the coast, whereas the driving force in open ocean is the wind stress curl [Bakun and Agostini, 2001]. The areas where upwelling is influenced by winds are said to comprise the large productive regions of the world. Some of the major upwelling zones around the world are Bengula upwelling in the south Atlantic, Canara upwelling off the northwest African coast, California upwelling system of the west coast of the United States, Peruvian upwelling region in the equatorial Pacific and the Somalia upwelling system in the Arabian Sea. Though upwelling in SEAS is not as dominant as those listed above, it has considerable impact(s) on the Indian coastal region and importantly, on economics. Figure 1.8 shows the major upwelling zones around the world. If there is a greater increase in the uplift of the nutrients from the subsurface to the surface waters, then that will lead to a phenomenon called Eutrophication [Naqvi et al., 2000]. Eutrophication is a negative impact of upwelling on the marine life. Increase in the nutrients will often lead to the depletion of oxygen [Naqvi et al., 2000] in the subsurface waters which eventually prove fatal to the marine life. If there is a greater increase in the uplift of the nutrients from the subsurface to the surface waters, then that will lead to a phenomenon called Eutrophication. Eutrophication is a negative impact of upwelling on the marine life. Increase in the nutrients will often lead to the depletion of oxygen [Naqvi et al., 2000] in the subsurface waters which

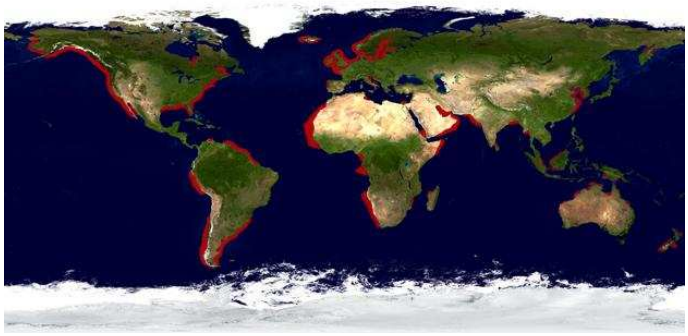

Figure 1.8: Major upwelling zones across the world are marked in red, taken from http://greenseaupwelling.com

eventually prove fatal to the marine life.

1.6 Upwelling in the Indian Ocean

Upwelling in the Indian Ocean is mostly influenced by monsoon winds. The regions where upwelling is predominantly observed are off the Oman coast in the northern Arabian Sea which is both open ocean and the coastal upwelling region [Wyrtki, 1973], Somalia coast (Wyrtki, 1973, Raghu et al., 1999), the southwest coast of India (Muraleedharan and Kumar, 1996, Madhupratap et al., 2001), around Sri Lanka coast, both in the coastal and the open ocean regions [Vinayachandran and Mathew, 2003], south of Madagascar [Lutjeharms and Machu, 2000], coasts of Java and Sumatra (Wyrtki, 1973, Susanto et al., 2001) and east coast of India (Shetye et al., 1991, Naidu et al., 1999). Among these regions that were studied and observed as upwelling zones, the present thesis concentrates on southwest coast of India within SEAS, which is of considerable interest in the Indian context.

1.6.1 Northern Arabian Sea

Northern Arabian Sea provides a good example for coastal upwelling inuenced by the seasonal reversal of the monsoon winds. The physical characteristics of the

Arabian Sea are firstly, strong wind stress during the SW monsoon resulting in widespread upwelling and later, mixing in summer; secondly, moderate strength, relatively cool and dry winds during the winter (NE) monsoon to promote evaporative cooling, thereby forcing strong convective mixing in the offshore region.

1.6.2 Somalia Coast

Upwelling along the Somalia Coast is a seasonal phenomenon during the SWM from June to September [Wyrtki, 1973]. In this region, upwelling occurs due to strong winds blowing parallel to the coast and results in intense upwelling between 5° and 11°N latitudes. At 11°N, the Somali current turns to the East and the upwelling waters may extend to a few hundred kilometres [Shankar et al., 2002]. Nutrient concentration in the Arabia (Oman) coast is often greater than the Somali coast.

1.6.3 Southwest Coast of India

Upwelling along the southwest coast of India commences from the southern tip of India by end May/ early June and propagates northward with time. This upwelling phenomenon is attributed to the influence of south-westerly winds [Madhupratap et al., 2001]. The upwelling exists till September month and then progressively decreases. Upwelling in the Minicoy region was observed during the IIOE near 8°N latitude during the Northeast monsoon in November. The primary cause for this upwelling was observed to be the presence of diverging currents [Rao and Jayaraman, 1966]. As a result of the confrontation of the currents in the Arabian Sea with the coast, a north-north westerly current develops. These currents diverge in the vicinity of Minicoy resulting in upwelling. In the month of July, a peak in upwelling was observed due to the pole-ward propagating coastal Kelvin waves [Shenoi et al., 1999]. Thus, it is understood that the upwelling in this region is a combined effect of winds together with conducive circulation pattern.

1.6.4 Sri Lanka Region

Off the southern coast of Sri Lanka, coastal upwelling driven by the monsoon winds has been reported [Vinayachandran and Mathew, 2003]. In this region, the southwest monsoon current flowing into the Bay of Bengal advects the upwelled waters along its path. Herein, the upwelling was observed to be seasonal. In this region, the maximum intensity in upwelling was observed during July / August and these upwelled waters had an SST of 24° -25°C. Basically, the upwelling favourable conditions in this region are the presence of along shore wind.

1.6.5 East Coast of India

Compared to the Arabian Sea, upwelling phenomenon is less known in Bay of Bengal. Along the eastern coast of India, upwelling was observed in July /August [Shetye et al., 1991] and was found to be due to local alongshore wind forcing. Upwelling ceases by the end of SWM [Shetye et al., 1991]. Also, there are reports on open ocean upwelling in the southwestern part of Bay of Bengal during NEM [Vinayachandran et al., 2003]. A phytoplankton bloom was observed between 8° - 16°N and west of 88°E and this bloom weakens in January. As stated by the author, the upwelling in this region is related to the Ekman Pumping forming a cyclonic gyre with an anti-clockwise wind stress curl during the northeast monsoon.

1.6.6 Java - Sumatra region

An upwelling area develops south of Java during SWM accompanied by strong winds. Ekman transport along with winds cause strong upwelling, but only a mild decrease in the SST was observed [Wyrtki, 1973]. Along shore winds cause upwelling along the Sumatran coast and by January / February, bloom had shifted to 5°-10°N and centred on 90°E [Raghu et al., 1999]. The upwelling centre migrated westward and this process terminated with the onset of northeast monsoon [Susanto et al., 2001]. The variability of upwelling is related to the ENSO and anomalous easterly wind and also, the annual upwelling occurs in June - October months with cold SST and low SSH.

1.6.7 Madagaskar region

Upwelling was also observed in the continental slope and shelf regions of southern Madagascar. The reason for upwelling in this region was attributed to the high pseudo wind stress. Dimarco et al. [2000] observed upwelling in the months of February and March. Upwelling was also observed to be present with varying intensities even in the absence of upwelling favourable winds in this region. This was, of course, attributed to the complex nature of the currents south of the Island and due to the retroflection of the East Madagascar Current (EMC) [Lutjeharms and Machu, 2000]. The upwelling in south Madagascar persists under all wind conditions and the reason was given as the passage of a strong western boundary current from a narrow to a much wider shelf.

In general, can be inferred from the definition, that upwelling is a localized phenomenon with a limited duration, often occurring each year. It influences primary productivity of the region and also the cold upwelled waters do influence the local weather. Atmosphere of the region will be stable with little convection. The important feature of upwelling in the Indian Ocean region is the seasonality of its occurrence. Noteworthy, the seasonal reversal of the monsoon winds has a profound impact on upwelling. Upwelling is more pronounced in the Arabian Sea than in the Bay of Bengal as the Bay is more influenced by the fresh water inputs from the large rivers of India [Prasanna Kumar et al., 2002].

1.7 Southeastern Arabian Sea (SEAS)

Southeastern Arabian Sea (SEAS) is a unique oceanic basin within the Arabian Sea where a suite of phenomenon take place over a year, ranging from coastal upwelling during summer monsoon season along the southwest coast of India to monsoon onset vortex to the Arabian Sea mini warm pool before the onset of summer monsoon and formation of algal blooms in the spring inter-monsoon period [Jayaram et al., 2010b]. All these phenomena make SEAS a natural laboratory to study oceanography in detail. Figure 1.9 presents the topography of the region. As like the rest of the Arabian Sea region, SEAS also shows seasonal reversal of the circulation pattern, indicated in figure 1.10. Coastal circulation in this region

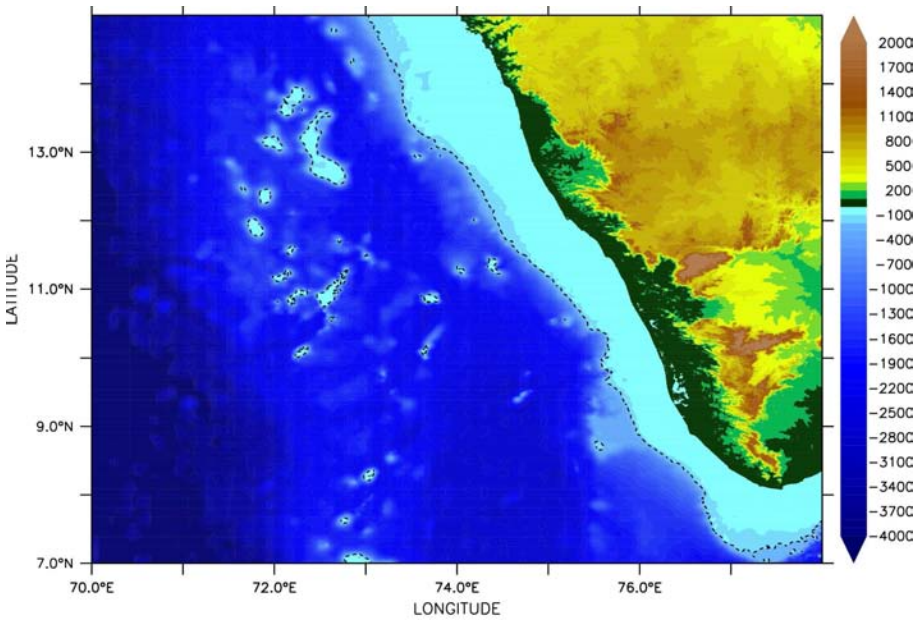

Figure 1.9: Topography of SEAS; the dotted line indicates the 200m isobath

shows a well marked seasonal cycle [Shetye and Shenoi, 1988]. This cycle results in intense air - sea interactions on varying time scales; and this has varied and profound impacts on the upper hydrographic structure including current systems (Hastenrath and Lamb, 1979, Hastenrath and Greischer, 1991). The semi- annual wind field has a maximum during January and July. During the summer monsoon, generally from June through to September, strong winds blow from the southwest forming an intense low-level jet [Findlater, 1977] over the central AS. In response to these winds a clockwise circulation evolves in AS (Wyrtki, 1971, Schott, 1983, Cutler and Swallow, 1984) producing coastal upwelling along the Somalia, Oman and the southwest coast of India [Wyrtki, 1973]. The equatorward eastern boundary of this anticyclonic circulation is known as the West India Coastal Current (WICC) [Shetye and Shenoi, 1988]. To the south of Sri Lanka, this WICC amalgamates with the eastward flowing SMC bending around the Sri Lankan coast and flow poleward into the Bay of Bengal. During winter, generally from November to February, the winds blow from the northeast. Part of this flow bifurcates at the southwest Indian coast and flow poleward to form WICC

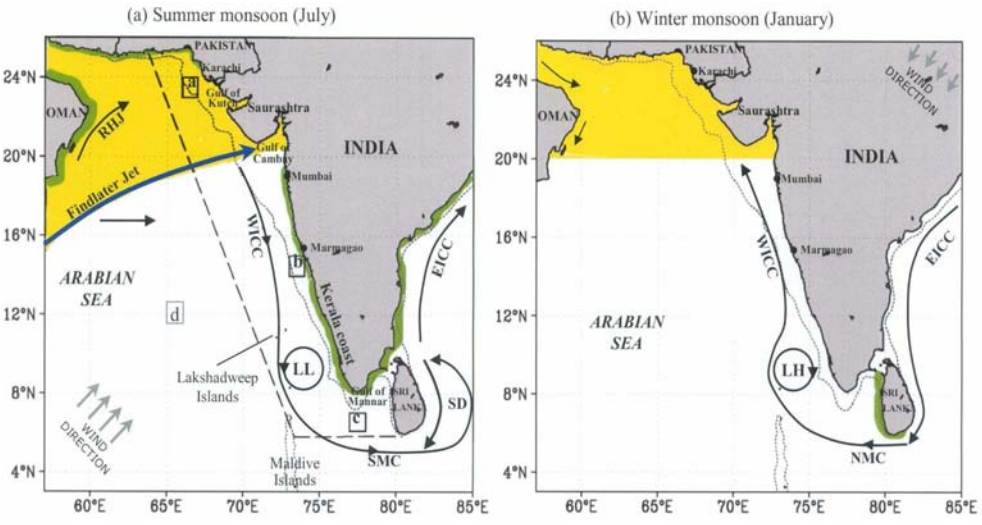

Figure 1.10: (a) Geography of the northern Arabian Sea. Schematics of summer-monsoon circulation are superimposed. Ekman pumping region in the northern Arabian Sea is highlighted in yellow tone. Coastal upwelling promoted by divergence of alongshore wind stress component is indicated in green tone. Current branches indicated are the Ras al Hadd Jet (RHJ), Lakshadweep Low (LL), West India Coastal Current (WICC), Southwest Monsoon Current (SMC), Sri Lanka Dome (SD) and East India Coastal Current (EICC). The Findlater Jet and wind direction are indicated by bold gray arrows. (b) As in (a), but for winter monsoon. Convective cooling region is shown in yellow tone. Additional abbreviations shown are: Lakshadweep High (LH) and Northeast Monsoon Current (NMC). (From [Luis and Kawamura, 2004])

[Shetye et al., 1991]. This poleward flow, which occurs in opposition to the wind field, is facilitated by a density gradient along the west coast of India [Shetye and Shenoi, 1988]. During the inter-monsoon period, from March to April and October to November, weak, highly variable wind regimes ($2 \sim 3ms^{-1}$) occur in the Arabian Sea [Hastenrath and Lamb, 1979] and the basin surface circulation dissipates [Cutler and Swallow, 1984].

Dynamic processes in SEAS are triggered by the local and remote forcing. Wind jets in the equatorial Indian Ocean, between 5°S to 5°N, sets off equatorial Kelvin waves which, upon reflection from the eastern boundary of the Bay

of Bengal, propagate along the perimeter as a coastal Kelvin wave and radiate Rossby waves [Yu et al., 1991]. The coastal Kelvin waves propagate along the perimeter of the Bay of Bengal, bend around the Sri Lankan coast and further proliferates poleward along the west coast of India. The downwelling (upwelling) Kelvin wave radiates downwelling (upwelling) Rossby waves which propagate offshore and promote anticyclonic (cyclonic) circulation in the Lakshadweep Sea during winter (summer) monsoon (Bruce et al., 1994, Bruce et al., 1998, Shankar and Shetye, 1997). The anticyclonic Lakshadweep circulation is also strengthened by negative wind stress curl during the winter monsoon.

To sum up, upwelling along the southwest coast of India is an annually recurring phenomenon that occurs during the SWM (June to September). Though this upwelling phenomenon is less in intensity when compared to the other thoroughly studied upwelling regimes of the Arabian Sea (like those at Somalia and Oman), it has profound impacts on the coastal fisheries of India. While the west coast of India accounts for 70% fish yield of the total Arabian Sea production [Luis and Kawamura, 2004], the southwest coast alone accounts for 53% [Sanjeevan et al., 2009]; hence this region is of considerable importance in the Indian context.

1.8 Past studies and Relevance of the Present work

During the past five decades of oceanography in the Indian Seas, many studies had been carried out to understand the complexity of SEAS starting from the earlier works of Sastry and Myrland [1959], and from the extensive field studies along the southwest coast of India to explore the upwelling phenomenon and bottom trawling of fisheries by Banse [1959] and Banse [1968]. It was from these studies of Banse [1959], for the first time, the reason behind upwelling in SEAS had been attributed to the prevalent divergent current pattern during summer monsoon season. This line of understanding was substantiated by Rao and Jayaraman [1966]. Sharma [1966],[1968] and [1973] had made a comprehensive study on upwelling along the southwest coast of India based on temporal variability in the density structure, horizontal divergence of surface currents, wind

stress component and sea level. He pointed that the depth from which upwelling commences in March was around 90m and the upwelled waters reached the surface by May. Further, the influence of wind direction and speed on the upwelling has been dealt by Subramanyam [1958], Darbyshire [1967], Wooster et al. [1969] and [Sharma, 1968], but could not divulge sufficient information on contribution of wind and this still remains a topic that needs further investigation. However, Mathew [1983], attempted to address some of these issues using temperature, density, surface wind stress and sea level data collected once in a month along the coast. He observed a lag in the upwelling resultant surface cooling between the southern and northern regions of SEAS. Wyrtki [1973], in a classical article on the oceanography of the Indian Ocean has clearly stated that the shoaling of 20°C isotherm was present upto less than 50m from the surface as a result of upwelling. It is understood that upwelling along the southwest coast of India sets in some time during February / March [Johannessen et al., 1987] and could be mapped from sea level anomaly (Shankar and Shetye, 1997, Haugen et al., 2002, Shenoi et al., 2005). Variability of temperature field, influence of along shore winds on the upwelling phenomenon and Ekman transports between 8° and 15°N stands well expounded, by Shetye [1984]; later a thorough study on the circulation and hydrographic pattern of this region was documented, again by Shetye et al. [1985]. Recently the work by Gopalakrishna et al. [2010] has reflected on intra - seasonal to inter - annual variability in upper surface temperature fields. The wind induced mass transports associated with this coastal upwelling regime are comparatively less than the other regions elsewhere [Hastenrath and Greischer, 1991]. Propagation of coastal Kelvin wave from the Bay of Bengal and thus the radiation of Rossby waves and their dynamics in this region and further, their role in formation of Lakshadweep High and Low, both in respect to sea level and SST and their role during the upwelling period is reflected in the works of Shankar and Shetye [1997]. Upwelling as a result of equator-ward alongshore winds lower the SST, which commences at the southern tip of India and propagates northward along the coast with the advancement of monsoon (Madhupratap et al., 2001, Luis and Kawamura, 2004, Rao et al., 2008, Smitha et al., 2008). In spite of all these extensive, elaborated studies, there remains certain areas that needs further research like the contribution of wind component and remote forcing on

the upwelling phenomenon, the spatial extent of upwelling region and the related productivity, the temporal relationship between the forcing factors and the ocean response with respect to upwelling; the role of upwelling towards the heat budget of the region needs special attention and all the above aspects are dealt in this thesis.

1.9 Objective of the Study

This work aims to achieve the following objectives:

1 The spatial and temporal relationship between the forcing factors and the related ocean responses in SEAS.

2 On what time scales does the local and remote forcing influence the upwelling process?

3 Deriving the indices of upwelling based on SST and wind stress.

4 Deriving an index to denote the spatial extent of CHLA in SEAS.

5 Heat budget of the region and influence of upwelling on heat budget terms.

1.10 Scheme of the Thesis

In this thesis, a variety of available satellite data products have been made use of to bring out a synergistic analysis on the upwelling phenomenon in SEAS. Basic concepts of remote sensing, upwelling and linked oceanography topics have been dealt in chapter 1 and auxiliary data products utilized in this study are described in chapter 2. The climatological monthly variability of the upwelling signatures are detailed under chapter 3. Chapter 4 presents the forcing factors that trigger the upwelling process in SEAS. Chapter 5 describes the oceanic response to the forcing factors with respect to the SST cooling and CHLA blooms. Chapter 6 presents the heat budget of the region and the variability of heat budget terms with respect to upwelling. Chapter 7 describes the inter-annual variability of upwelling intensity in SEAS and the influence of climatic events on upwelling.

Concluding remarks are penned in chapter 8.The work concludes with a section on references cited followed by appendix 1 which illustrates the weekly variability of SLA that serves as a signature of planetary wave propagation in the region and appendix 2 provides a list of publications forming part of this thesis work.

2

Data and Methodology

2.1 Introduction

The characteristic features of an upwelling region are low SST, high CHLA, lower SSH and preferably, presence of along shore wind stress, if on the eastern boundaries of the ocean. The vertical motion rotates water in cyclonic (anti clock wise) or anti-cyclonic (clock wise) circulation (in northern hemisphere). Cyclonic circulation leads to upwelling, while anti-cyclonic circulation results in downwelling. To study the relation between above stated parameters and their impacts on upwelling, data has been amassed from various sources. The following are the satellite platforms and the sources from where the data has been accessed / downloaded.

SST data was obtained from the Advanced Very High Resolution Radiometer (AVHRR) on board a series of NOAA satellites (http://poet.jpl.nasa.gov) and the Tropical Rainfall Measuring Machine (TRMM) Microwave Imager (TMI) (http://las.incois.gov.in). Sea Surface Wind data was obtained from QuikScat scatterometer onboard Quikbird satellite (www.ifremer.fr). The SLA data has been obtained from Archiving, Validation and Interpretation of Satellite Oceanographic data (AVISO) that distributes satellite altimetry data of the available altimeters (ftp://ftp.aviso.oceanobs.com). The ocean colour data from Sea viewing Wide Field of view Sensor (SeaWiFS) and Moderate resolution Imaging Spectroradiometer (MODIS) on board Aqua satellite was obtained from ocean colour group at Goddard Space Flight Centre of NASA (http://oceancolor.gsfc.nasa.gov).

Apart from these satellite data products, other auxiliary data products like temperature and salinity profiles to compute mixed layer depth were obtained from CORIOLIS (http://www.coriolis.eu.org), and world ocean atlases 2001 and 2009 were obtained from National Climate Data Centre of NOAA (www.nodc.noaa.gov).

2.2 Principle of Measurement and Processing

2.2.1 Sea Surface Winds

Sea Surface wind is a vector quantity and space-borne microwave scatterometers are the only proven instruments that can measure both wind speed and direction over the ocean under all weather conditions [Wentz et al., 2001]. Scatterometer is one of the active remote sensors used in satellite oceanography that works on the principles of radar. It is an oblique viewing radar pointing towards the sea surface from aircraft or satellites at incidence angles normally between 20° and 70°. Backscattered energy received by the receiver from the field of view of the sensor determines the sea surface roughness and thereby the wind speeds over the sea surface. The backscatter is governed by the in-phase reflections from surface waves where, for a smooth surface the radar receives no return when viewing at an angle [Wentz et al., 2001]. As the surface roughness increases, backscatter occurs as constructive interference of scattering from periodic structures in the surface roughness. The backscatter does not only depend on the magnitude of the wind stress but also the wind direction relative to the direction of azimuth angle of the radar beam. The retrieval of wind speed and direction from the scatterometer measurements requires knowledge on the backscatter variation with wind speed and direction relative to the radar azimuth [Robinson, 2004]. The empirical formula used to derive the winds for a particular frequency of the radar:

$$\sigma_o = \sigma_o(U, \chi, \theta, p) \tag{2.1}$$

where σ_o is the normailized radar back scatter function, (U, χ) are the wind speed and direction relative to the radar azimuth, θ is the radar incidence angle and 'p' is the polarization. Figure 2.1 illustrates graphically the wind speed and

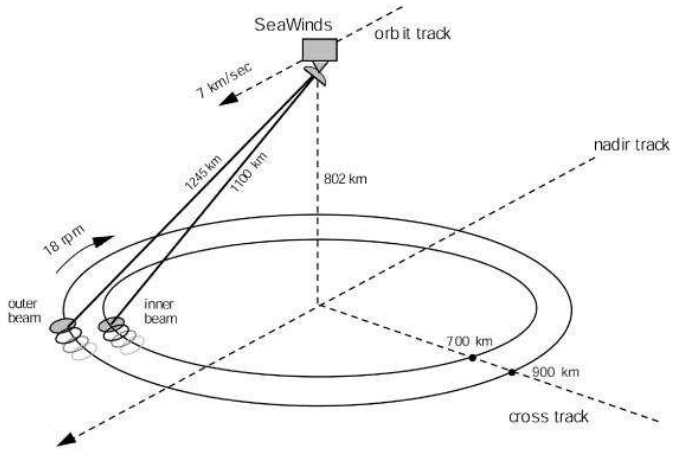

Figure 2.1: Principle of measurement of QuikScat Scatterometer, taken from http://nsidc.org

direction relative to the radar azimuth and the schematic of measurement principle used in QuikScat Scatterometer. QuikScat operates in ku band ($\sim$ 14 GHz) frequency in a sun synchronous near polar orbit with 98.6° inclination angle and an altitude of 803km (Wentz et al., 2000, Wentz et al., 2001). Its revisit time is 4 days. The radar radiates microwave pulses at 13.4 GHz using twin pencil beams at angles 46° (horizontal polarization) and 54° (vertical polarization) with an Instantaneous Field of View (IFOV) for each pencil beam as 30 x 40 km. Thus, each point on the ground is viewed from multiple directions while maintaining constant incidence angle for each of the beams. The overall spatial resolution is 25 x 25 km with an accuracy of 2 ms^{-1} and 20° for wind speed and direction respectively. Scaterrometer data has become a source of real time information regarding global wind pattern for both meteorological and oceanographic purposes. In upwelling studies, the wind stress and curl computed from the scatterometer measurements provide an indirect signal on intensity of upwelling. The signatures of upwelling thus arrived at, from the stresses are the negative (positive) wind stress along the eastern boundaries in the northern hemisphere (southern hemisphere). The curl of wind stress should be positive (negative) in the northern hemisphere (southern hemisphere) to boast of divergence pattern over the ocean surface [Pickard and

Emery, 1982]. Wind stress is computed from QuikScat measured winds using the bulk aerodynamic formula:

$$\tau = \rho_a C_d U^2 \tag{2.2}$$

where τ is wind stress over the ocean, ρ_a is the density of air (1.25 kg m^3), C_d is the wind dependent drag coefficient and U is the wind speed following Smith [1988]. The zonal (u) meridional (v) component of wind speeds in network Common Data Format (netCDF) were obtained from the Asia Pacific Data Research Centre (APDRC). The validation statistics of QuikScat measured winds over the Indian Ocean region were reported by Goswami and Rajagopal [2003] and Satheesan et al. [2007].

2.2.2 Sea Surface height

Sea Surface Height (SSH) is precisely measured using satellite altimeters. These altimeters are radars that transmit sharp pulses toward the Earths surface and receive the return pulse. Height of the satellite above the sea surface is obtained by measuring the time required by the pulse to travel from the altimeter to the surface and back [Robinson, 2004]. Amplitude and shape of the reflected pulse provide additional information about the surface such as sea surface roughness. Basic understanding of altimetry is derived from the knowledge of potential gravity due to Earths atmosphere and the potential gravity due to the solid earth and water along with the centrifugal acceleration due to Earths rotation. Assuming no atmosphere, still water results in an equi-potential surface, and this equi-potential surface is called Geoid. Geoid is a property of gravitational field and responds to global distributions of mass. The displacement of the sea surface from the geoid is known as the sea surface topography. This difference is primarily due to the currents and tides [Stewart, 1985]. In order to attain the sea level deviation from the geoid, one should have detailed knowledge of the global geoid, but this is not available at present, in such cases the long term altimeter measurements of the available altimeter records provide sea surface topography. Essentially geoid is time invariant and thus the long term altimeter records even without the geoid information provide better data of the time varying ocean dynamic topography. At least two altimeters are required to monitor the ocean precisely at very high

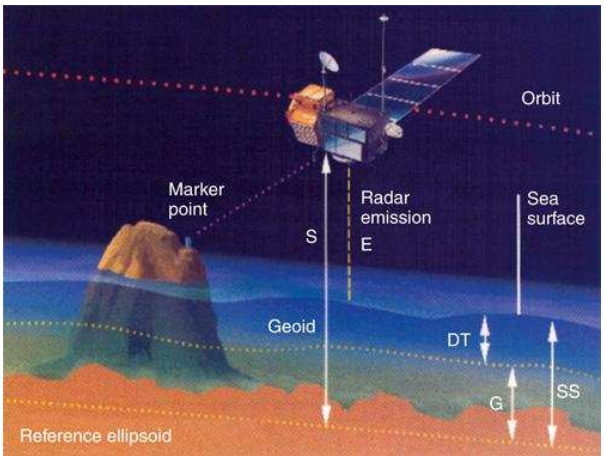

Figure 2.2: Principle of altimetry: Radar altimeters measure the distance between the satellite and the sea surface (E). The distance between the satellite and the reference ellipsoid (S) is derived by using the Doppler Effect associated with signals emitted from marker points on the Earths surface as the satellite orbits overhead. Variations in sea surface height (SS, ie S-E), are caused by the combined effect of the geoid (G) and ocean circulation (dynamic topography, DT), from (www.eohandbook.com/eohb05)

resolutions to understand the mesoscale variability over the ocean [Robinson, 2004]. Figure 2.2 shows the schematic of the principle of altimetry. Of all sensors carried on satellites, the altimeter is most dependent upon its orbit to be capable of successful calibration and interpretation. An altitude over 1300 km is advised for altimeter missions because:

- of the atmospheric drag, there is an order of magnitude less than at 800 km,
- ground stations can much better track the satellite,
- the satellite orbit error resulting from irregularities of the Earth gravitation field at a high orbit is less than at a lower one and
- Air, water vapor, clouds, and rain slow down the return of the microwave signal. A second instrument called a radiometer is used to correct for the influence of water in the atmosphere.

The dual-frequency NASA radar altimeter (TOPEX / Poseidon) works by sending radio pulses at 13.6 GHz and 5.3 GHz toward the earth and measuring the characteristics of the echo [Fu et al., 1992]. By combining this measurement with data from the microwave radiometer and with other information from the spacecraft and the ground, scientists can calculate the height / level of the sea surface. Data from the SLR (Satellite Laser Ranging) and DORIS (Doppler Orbitography and Radio positioning Integrated by Satellite) systems are used to determine the orbit of TOPEX/Poseidon. Together these systems provide all-weather, global tracking of the satellite. There are however, some limitations in land-based systems. Sea level anomaly (SLA) is derived by subtracting the real time observations from the altimeters from the long term mean. The data from different sensors are merged to arrive at better coverage and accuracy of the sea level to less than 4cm www.aviso.oceanobs.com. The sea level anomaly data used for the present study is a merged product of different altimeter missions and is obtained from AVISO data extraction service [LeTraon and Dibarboure, 1999]. The spatial resolution of the data is 0.25° x 0.25°. The temporal resolution ranging from weekly to monthly was selected based on the process to be studied. The geostrophic currents were computed from the sea level anomalies using the geostropic relation:

$$2\Omega \sin(\phi).V = g \tan(i) \tag{2.3}$$

where Ω is the earth's angular velocity, ϕ is the latitude, V is the velocity and tan(i) is the l=slope of the sea surface [Pond and Pickard, 1983]. The geostrophic currents are made use of to understand the circulation pattern in the region of interest during different seasons.

2.2.3 Sea Surface Temperature

Infrared Radiometers Present study makes use of SST data obtained from Advanced Very High Resolution Radiometer (AVHRR) onboard NOAA series of satellites and Tropical Rainfall Measuring Machine - Microwave Imager (TMI). The data products were chosen based on their availability. The AVHRR functions based on infrared radiometry, where the fundamental basis is that all surfaces emit radiation whose strength is in-turn dependent on the surface temperature.

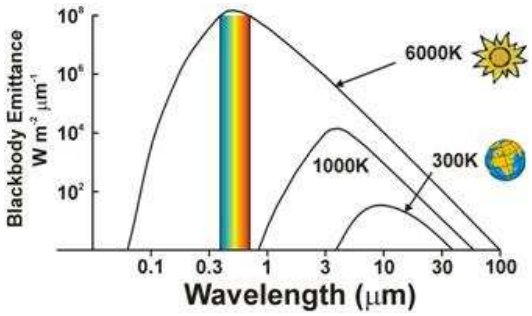

Figure 2.3: Black body emittance spectrum at different temperatures, from http://cimss.wisc.edu

The higher the temperature, the greater is the radiant energy. By measuring the emitted radiation, the temperature can be calculated, provided the physics of the process is well defined Robinson [2004]. The spectral characteristics of thermal emission from body at temperature T in K are determined by Planks radiation law:

$$M(\lambda, T) = \frac{C_1}{\lambda^5}[exp(\frac{C_2}{\lambda T}) - 1] \tag{2.4}$$

where λ is the wavelength in metres, M is the spectral exitance (also called mittance: The radiant flux density of radiation per unit band width centred at , leaving unit area of surface, irrespective of direction), C_1 and C_2 are constants. By integrating over all the wavelengths gives the total exitance of a black body:

$$M = \sigma T^4 \tag{2.5}$$

where $\sigma = 5.669$ x 10^{-8} W m^{-2} K^{-4} (Stefan's constant).The spectral peak of each temperature is found at wavelength:

$$\lambda_{max} T = C_3 \tag{2.6}$$

Figure 2.3 shows the emittance at different wavelengths for different temperatures. The solar emitted energy has a peak in the visible part of the spectrum and typical SSTs emission peak lies between 9μm and 11μm. Thus, the thermal IR is an optimal region for monitoring SST. An IR radiometer can detect the brightness temperature of the radiation at the sea surface. The measured brightness

temperature differs from the actual temperature of the observed surface because of its non-unit emissivity and also because of the intervening atmosphere. The presence of atmosphere restricts the IR radiometry of the sea surface to two spectral windows 3.5 - 4.1μm and 10.0 - 12.5μm. The emissivity of the sea surface in the IR region is approximately 0.98 to 0.99 [Masuda et al., 1988]. The sensor, when viewing the sea surface with an angle zero, the maximum emissivity is 0.992 at 11μm wavelength. However, the sensor monitors the surface from different incident angles during different sea states and thus the emissivity varies with wind speed [Watts et al., 1996]. It could be said that the IR radiance above the sea surface depends not only on the temperature of the surface skin, but also on the surface emissivity, the incident radiation after removing the direct sun glitter. Since the emissivity is ~ 1 in the IR region, the measured brightness temperature is only slightly less than the true SST and thus can be easily incorporated in the atmospheric corrections. The main difficulty in the IR radiometry is the correction for reflection of the incoming solar radiation. Even though the emittance from the sun is greater than the sea surface, it fills only small part of the sky and thus the solar irradiance reaching the top of the atmosphere is about 10^{-5} of its value near the solar surface which is about 1/300 of the radiation emitted by the sea surface (Maull, 1985, Robinson, 2004). At 10μm, the solar reflection is small and thus this spectral window is effective both during the day and night. At 3.7μm, the incoming solar irradiance is of same order as the surface emittance and the diffusion reflection of sunlight contributes an unacceptable error which cannot be corrected. Therefore 3.7μm cannot be used during day time. Thus one can deduce that the spectral windows used for SST measurements are the bands between 3.5 - 4.1μm during night time and between 10.0 - 12.5μm during both day and night. These signals are derived after necessary atmospheric corrections. For IR sensor calibration, a target of known temperature is used. This temperature is measured and transmitted to ground receiving station along with the signal measured by the IR sensor. Atmospheric correction is based on multispectral approach, when the differences between brightness temperatures measured at different wavelengths are used to estimate the contribution of the atmosphere to the signal. For cloud detection, the thermal and near-infrared waveband thresholds are used, as well as different spatial coherency tests. The

accuracy of the IR sensors is high but they cannot see the sea surface through the clouds under overcast conditions. AVHRR is the most successful and widely used IR sensor onboard NOAA series of satellites. It has 5 spectral bands as shown in the following table: The scanner has an IFOV of approximately 1.3m rads

Table 2.1: AVHRR spectral channels and their characteristics, taken from http://noaasis.noaa.gov/NOAASIS/ml/avhrr

Channel No.	Resolution	Wavelength (μm)	Typical Use
1	1.09km	0.58 - 0.68	Daytime cloud and surface mapping
2	1.09km	0.725 - 1.00	Land and water boundaries
3	1.09km	1.58 - 1.64	Snow and Ice detection
4	1.09km	3.55 - 3.93	Night cloud mapping, SST
5	1.09km	10.30 - 11.30	Night cloud mapping, SST
6	1.09km	11.50 - 12.50	SST

and a cross-track scan of $\pm 55.4°$. With a nominal height of 833 km the ground FOV at nadir are 1.1 km and the swath width about 2500 km. The orbit period is about 102 min and 14 orbits are completed per day. The swath of adjacent orbits overlap, ensuring that the whole Earth surface is viewed at least twice a day, once from the ascending (daylight) passes and once from the descending (night) overpasses. The pathfinder SST that is employed in the present study is systematically analyzed AVHRR data from 1985. The data is provided on the public domain on daily, 8-day and monthly averaged scales with a spatial resolution of $\sim$ 9 km. The processing methodology and validation statistics of the Pathfinder project are explained explicitly in Podesta et al. [1995] and Kilpatrick et al. [2001].

Microwave Radiometers To overcome the lack of AVHRR data during the overcast conditions, the data products derived from the microwave (MW) radiometers were made use of. Microwave radiometers are capable of measuring SST independently of the cloud cover. These radiometers are normally operated at wavelengths between 1.5mm and 300mm (200GHz to 1GHz) depending on the parameter to be measured. They observe the thermal radiation emitted by the sea surface in the microwave part of the spectrum under all weather conditions.

At longer wavelengths, there is little or no absorption or scattering by the intervening atmosphere, aerosols, haze, dust or small water droplets in clouds. Only problem is the liquid water in the form of precipitation. But, at longer wavelengths, the thermal emission is weak and thus the signal received is relatively weak. Therefore to maintain the signal strength and overcome the noise levels, the field of view (FOV) must be wider than for IR radiometers. This makes the spatial resolution of MW radiometers coarser than the IR radiometers. The physical principle behind the MW radiometer is the Planks radiation law for non-perfect emitter:

$$L_\lambda(\theta,\phi) = 2hc^2\frac{\epsilon(\theta,\phi)}{\lambda^5}[exp(\frac{hc}{\lambda KT}) - 1] \tag{2.7}$$

where L_λ = spectral radiance at wavelength λ, h = Plank's constant = 6.626 x 10^{-34} Js, c= speed of light, k = Boltzmann's constant = 1.38 x 10^{-23} J K^{-1}, T = temperature of the emitter in degrees K, $\epsilon(\theta,\ \phi)$, θ and ϕ are the zenith and azimuth angles. Following the Rayleigh- Jeans approximation the spectral radiance B_f per unit frequency bandwidth is:

$$B_f = kT\frac{\epsilon(\theta,\phi)}{\lambda^2} \tag{2.8}$$

For a black body at temperature 300k typical of the ocean, the Rayleigh-Jean approximation deviates by less than1% as long as f is less than 117 GHz, corresponding to $\lambda > 2.57$mm. Thus the emitted radiance is directly proportional to the temperature of the emitting surface. Therefore, the emitted radiance is called Brightness temperature while the radiance measured by the microwave antenna is apparent temperature at a certain frequency. But it is typically much lower than the actual temperature of the emitting ocean surface because for the sea water, the emissivity is less than 0.5 at microwave frequencies. The Tropical Rainfall Measuring Mission (TRMM) Microwave Imager (TMI) is a passive microwave radiometer that measures SST [Wentz et al., 2000]. Apart from SST, the other parameters that TRMM measures are the precipitation, Earths radiant energy and lightening. The TMI has five wavebands at 10.7, 19.4, 21.3, 37.0 and 85.5 GHz. The channel at 10.7 GHz is used to measure SST. Its orbit is not sun synchronous and has complete ground coverage between $\pm 40^\circ$ latitude and is

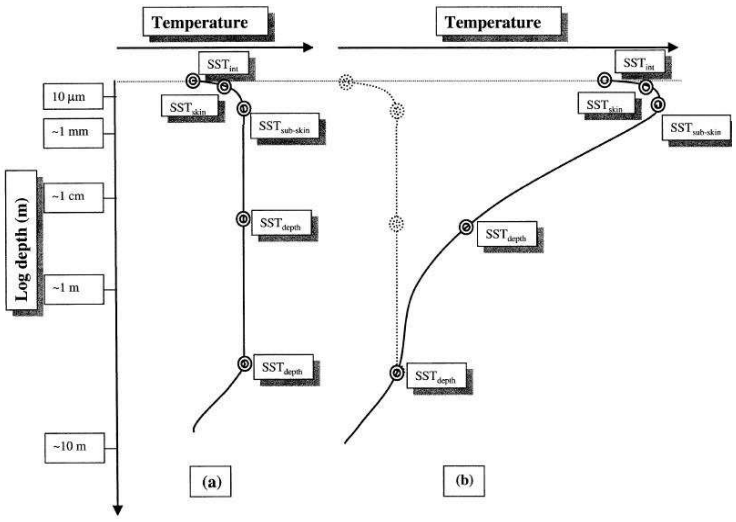

Figure 2.4: Schematic depicting the temperature structure near the sea surface (a) at night and (b) during the day in conditions suitable for diurnal warming. The figure shows where the skin, sub-skin and depth measurements of SST are defined. SST_f represents the foundation temperature at the base of any diurnal thermocline that may be present (after Donlon et al. [2002])

accomplished in 3 days at an altitude of 402 km and an angle of inclination 35°. The spatial resolution at which TMI provides SST is 0.25° x 0.25°. The accuracy of TMI is measured at 0.6°C with the drifter buoys [Wentz et al., 2000]. Figure 2.4 presents the schematic of different SST measurements near the sea surface. Every SST observation depends on the measurement technique, the sensor that is used, the vertical position of the measurement within the water column, the local history of all the component heat flux conditions and the time of the day the measurement was obtained. The vertical structure of SST can be defined [Donlon et al., 2002] as follows:

1 The interface SST, SSTint is the temperature of an infinitely thin layer at the exact air sea interface. It represents the temperature at the top of the SSTskin layer and this cannot be measured using current technology.

2 The SSTskin is the temperature measured by a radiometer at depth within a thin layer ($\sim$ 500 μm) at the water side of the air-sea interface. This

is the basis for measuring the skin temperature using IR radiometers at wavelengths shorter than 5μm [McKeown and Asher, 1997].

3 The SSTsub-skin is the representative of the SST at the bottom of the SSTskin temperature gradient. It could be measured by MW radiometers operating at low frequencies (6 - 10GHz). In this region of electromagnetic spectrum, the penetration depth in seawater is much greater and the resultant measurements depths are greater than 1mm

4 The SSTdepth (also known as SSTbulk) is the temperature beneath the SSTskin, therefore SSTdepth should always be quoted with specific depth in the water column. SSTdepth is measured using traditional temperature sensors mounted on buoys, profilers and ships at any depth beneath SSTsubskin.

The AVHRR SST data products were obtained from Jet Propulsion Laboratory of NASA and the TMI data was obtained from SSMI. The data products were on different time scales ranging from daily, 8-day and monthly. SST (skin) was used to compute upwelling indices and also in synergy with other data products to ascertain the upwelling region. SST obtained from TMI is used for understanding the temporal relationship between the forcing factors and the upwelling response on SST as the AVHRR data is available on 8-day basis.

2.2.4 Chlorophyll-a Concentration

The chlorophyll-a concentration (CHLA) is the primary photosynthetic pigment in phytoplankton that primarily absorbs in the blue and red regions than in green of the visible spectrum of electromagnetic radiation. The measurements of ocean color are based on the electromagnetic energy between 400 and 700 nm. The sunlight is not merely reflected from the sea surface. The color of water surface results from sunlight that has entered the ocean, been selectively absorbed, scattered and reflected by phytoplankton and other suspended material in the upper layers, and then backscattered through the surface. The back scattered energy from the ocean surface progressively shifts from deep blue to green as the concentration of phytoplankton increases [Yentsch, 1960]. Ocean color radiances in

the blue-green can be coalesced from depths as great as 50 m. The transparency of open ocean waters is very high; the upper layer of tens of meters depth contributes to ocean color, this contribution decreasing with depth whereas in the turbid coastal waters, the depth of the upper layers and also the transparency of the water column are very less. Satellite ocean color depends on CHLA, which in turn depends on phytoplankton biomass. Thus the ocean color data provides the practical means for monitoring the spatial and seasonal variations of near surface phytoplankton, oceanic primary production, global carbon and biogeochemical cycles and fishery research. The CHLA is derived from the back scattered radiances using semi empirical algorithms based on the regression of radiance versus chlorophyll [O'Reilly et al., 1998]. The following are the drivers that can change the ocean color:

1 Phytoplankton and its pigments

2 Colored Dissolved Organic Material (CDOM, or yellow matter, or *gelbstoff*) which is derived from decaying vegetable matter (land) and phytoplankton degraded by grazing or photolysis.

3 Suspended particulate matter

- These particulate matter consist of both Organic and Inorganic substances that can alter the ocean color.
- The organic particulates (detritus) consist of phytoplankton and zooplankton cell fragments and zooplankton fecal pellets
- The inorganic particulates consist of sand and dust created by erosion of land-based rocks and soils. These enter the ocean through river run off, deposition of wind-blown dust and wave or current suspension of bottom sediments.

Depending on the density of both dissolved and suspended matter, Morel and Prieur [1977] divided the ocean into *Case 1* and *Case 2* waters. In *case 1* waters, phytoplankton pigments and their co-varying detritus pigments dominate the seawater optical properties and in *case 2* waters, other substances that do

not co-vary with CHLA (such as suspended sediments, organic particles, and CDOM) are dominant. Though the case 2 waters occur in relatively smaller area of the oceans, they are important and optically complex because of their constant interaction with human habitat in the coastal regions, prevalence of large river run off. These optically dominant parameters are retrieved from the ocean color sensor observations depending on their inherent nature to absorb and backscatter the energy in particular wavelengths as shown in the following:

1 Chlorophyll absorption peak is at 443 nm,

2 Measurements must also be made in the 500 - 550 nm range where the chlorophyll absorption is zero and the absorption of other plant pigments (i.e., carotenoids) dominate.

3 CDOM-dominated wavelength is at 410 nm and

4 Suspended particulate matter dominates the red region of the spectrum.

All the ocean color measurements are to be subjected to atmospheric corrections before finally being used. Sunlight backscattered by the atmosphere contributes 80 - 90% of the radiance measured by a satellite sensor at visible wavelengths. Such scattering arises from dust particles and other aerosols, and from molecular (Rayleigh) scattering. Such atmospheric contribution can be calculated and removed by the additional measurements made in the red and near-infrared spectral regions (e.g., 670 and 750 nm). Since blue ocean water reflects very little radiation at these longer wavelengths, the radiance measured is due almost entirely to scattering by the atmosphere. Long-wavelength measurements, combined with the predictions of models of atmospheric properties, can therefore be used to remove the contribution to the signal from aerosol and molecular scattering. The data was obtained by Sea viewing Wide Field of view Sensor (SeaWiFS) radiometer onboard Orbview spacecraft of NASA. It has a sun synchronous orbit with an altitude of 705km with a spatial resolution of 1.1 km at Local Area Coverage (LAC) and 4.5km at Global Area Coverage (GAC). SeaWiFS observes the earth surface using its 8 spectral channels: SeaWiFS Data Analysis System (SeaDAS) is a software tool provided by the Ocean color group

Table 2.2: Spectral channels of SeaWiFS and their purposes,taken from website http://oceancolor.gsfc.nasa.gov

Spectral Channel	Central Wavelength (nm)	Primary Use
1	412 (Violet)	Dissolved organic matter (incl. Gelbstoff)
2	443 (blue)	Chlorophyll absorption
3	490 (blue - green)	Pigment absorption (Case 2), K(490)
4	510 (blue - green)	Chlorophyll absorption
5	555 (green)	Pigments, optical properties, sediments
6	670 (red)	Atmospheric correction (CZCS heritage)
7	765 (near IR)	Atmospheric correction, aerosol radiance
8	865 (near IR)	Atmospheric correction, aerosol radiance

of NASA for processing the SeaWiFS data products, incorporated with necessary correction algorithms. The ocean color data products are obtained in Hierarchical Data Format (HDF) and processed using SeaDAS. The final spatial resolution of the data utilized for this study is $\sim$ 9 km and a relevant temporal resolution of 8-days, monthly is used based on the nature of the analysis. The data obtained from the satellite consists of 4 levels depending on the level of processing as shown in the following figure 2.5 for almost all the sensors:

Tables 2.3 and 2.4 presents thedetails of all the remote sensing platforms used in this thesis.

Table 2.3: Satellite Sensor, Parameters measured, their resolutions

			Resolution		
Sl. No	Sensor	Parameter	Spatial	Temporal	Spectral
1	QuikScat	Winds	0.25 ° x 0.25°	3day running mean	14 GHz (Ku band)
2	TMI	SST	0.25 ° x 0.25°	3day running means	10.7 GHz
3	AVHRR	SST	4 x 4 km	8 day	Thermal IR
4	SeaWiFS	CHLA	9 x 9 km	8 day	Visible
5	MODIS	CHLA	9 x 9 km	8 day	Visible
6	Altimeter	SLA	0.25 ° x 0.25°	Daily and Weekly	13.6 GHz

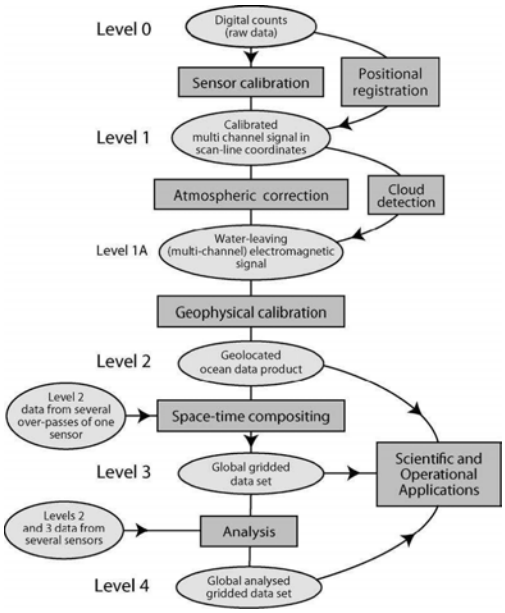

Figure 2.5: Processing levels of satellite data, taken from [Robinson, 2004]

Table 2.4: Satellite data period used for this study and limitations

Sl. No	Parameter	Period	Limitations
1	Winds	2000 - 2009	Cannot measure during heavy rainfall events
2	TMI SST	1998 - 2009	Cannot measure during heavy rainfall events
3	AVHRR SST	1987 - 2007	During Cloud Cover
4	SeaWiFS CHLA	1998 - 2007	During Cloud Cover
5	MODIS CHLA	2008 - 2009	During Cloud Cover
6	SLA	1993 - 2009	Data reliability is less very near to the coast

2.3 Software Tools

To process and analyze the data, suite of software packages were made use of. The following are the list of them:

- Ferret - For major data processing and analysis (www.ferret.noaa.gov/FERRET)
- GrADS - Exclusively used to compute EOF (http://www.iges.org/grads)
- SeaDAS - For retrieving chlorophyll data from SeaWiFS and MODIS level 3 products (http://oceancolor.gsfc.nasa.gov/seadas)
- Origin - For quality line graphs
- Matlab - Exclusively used for wavelet analysis (wavelet analysis toolbox obtained from Colorado University) and Coherence spectra.

2.4 Study Area

By making use of the above mentioned data products and the analysis tools, the spatio - temporal variability of upwelling phenomenon in SEAS (1.9) has been addressed in the present study. This study envisages bringing about an understanding on the upwelling, its generation, forcing factors like wind and remote forcing, heat budget, surface cooling and surface CHLA of SEAS. This region is having immense importance in the climate of India and especially the southwestern coast of India. Through this study, the contribution of satellite data products in effectively understanding the marine environment has been emphasized.

3

Climatology of SEAS

3.1 Sub-surface Signatures

In order to uderstand the sub-surface oceanographic structure during a year in the SEAS region, monthly variability of 20°C and 25°C isotherms are analyzed based on 0.25° x 0.25° world ocean atlas 2001 data [Boyer et al., 2005]. The upliftment of these two (20°C and 25°C) isotherms is considered to be the subsurface signature of upwelling. The representative months of January (winter), April (summer), July (SWM) and October (spring/ Inter monsoon period) are also plotted to understand the thermal structure of SEAS. The monthly climatologies, computed from the available satellite datasets for sea surface winds, SLA, SST and CHLA were analyzed for their monthly and seasonal variability.

3.1.1 Variability of 20°C and 25°C isotherms

Upwelling results in the shoaling of thermocline of the water column; to understand the spatial and temporal variability of shoaling and also to monitor the evolution of upwelling phenomenon as a whole, topography of the 20°C (D20) isotherm in the region is plotted. From figure 3.1 it is observed that during January, D20 was 160m along the coast to the north of 11°N and 130 135m to its south. The depth progressively shoaled towards the offshore regions upto 125m except for the region between 73° to 76°E and 7° to 9°N where the depth was deeper than 150m. In February, the pockets of warmer waters spread offshore

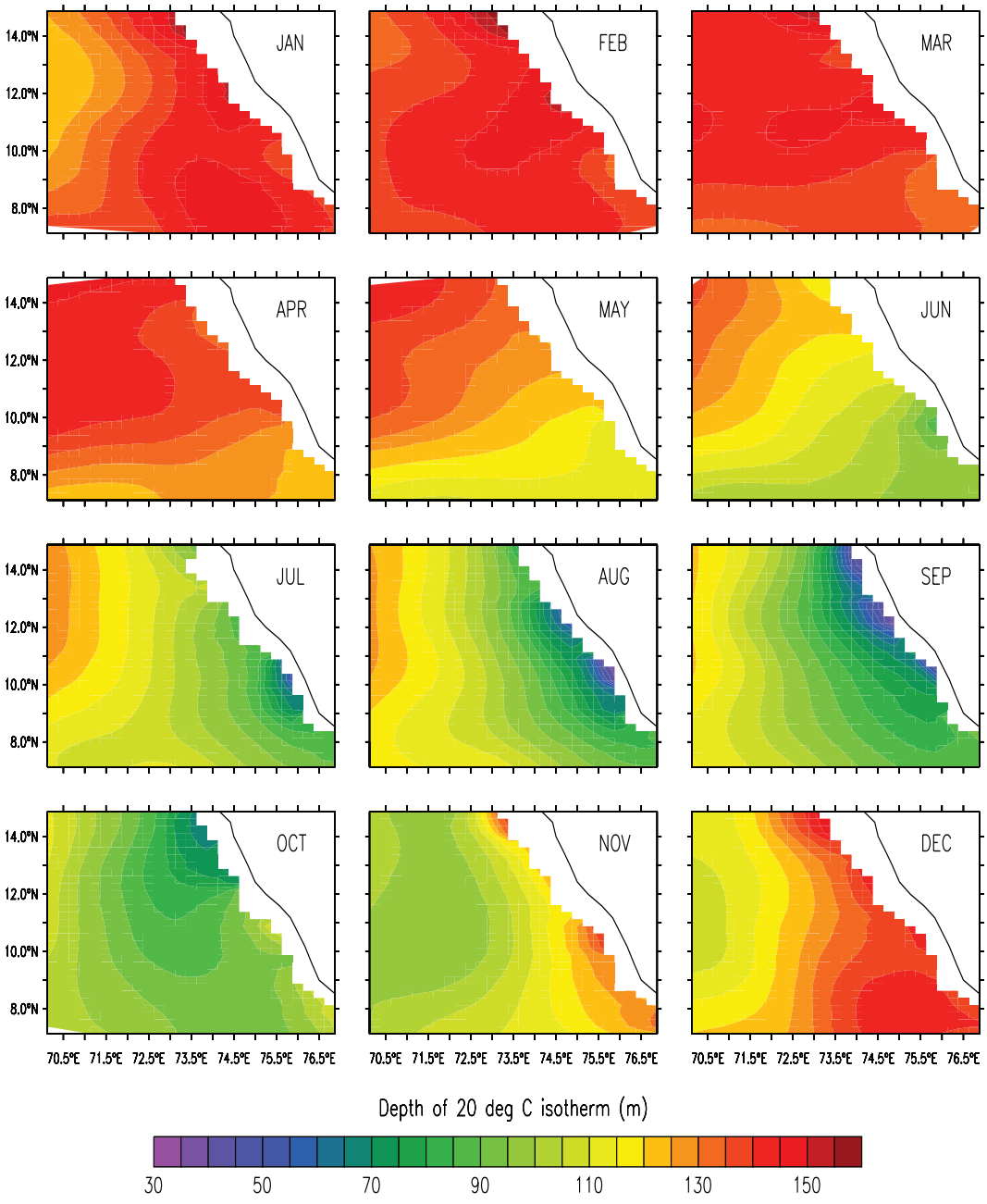

Figure 3.1: Topography of 20°C isotherm

to the north of 11°N, while it shoaled to the south upto 110m. The offshore waters maintained relatively uniform depth between 125 to 135m. A similar uniformity was observed during March too. By the month of April, the orientation of isotherms were seen to be setting perpendicular to the coast. D20 was found to be shallow at the southern region while it deepened towards north. The perpendicular nature of isotherms continued in May with their depth further shoaling to 120m at the north and 95m at the south indicating the beginning of upwelling. By June, D20 shoaled further less than 90m in the southern region whereas the depth was 110m in the north. The isotherms changed their orientation becoming parallel to the coast by July and all along the coast, the D20 was less than 70m and it progressively deepened upto 130m towards the offshore. Further shoaling was noticed in the months of August and September near the coast where D20 was less than 60m. A noticeable fact is the shifting of the shallowest depth or in other words, the centre of upwelling towards north by September. This phenomenon is maintained in the northern region in October which indicates the existence of upwelling while the southern regions were marked by warmer waters with deepening of the isotherms upto 100m; this indicates the withdrawal phase of upwelling in the region. In November, the coastal regions were prevailed by warmer waters where D20 was observed to be greater than 130m and the offshore regions were shallow at 85 to 95m. By December, the D20 in the whole region was greater than 100m with deeper values along the coast. The pattern of variability for 25°C (D25) isotherm (Figure 3.2) was following the D20 for all the months except for November, where the northern part of the region was still maintaining shallow depths while D20 had sunk deeper.

To summarize, January, February, March, April and December are the months where, the D20 was at its maximum depth along the coast; among these months, the presence of shallow D20 when compared to the coast, was observed in the offshore region between 72° to 70°E during January and December. The signature of upwelling, i.e., the shallow D20, was spotted at the southern tip of the coast during April and this feature further progressed northward in the subsequent months. By June, upwelling was well established at the southern coast and in October, it was limited only to the northern part of the region. July, August and September are the months when upwelling was present all along the coast

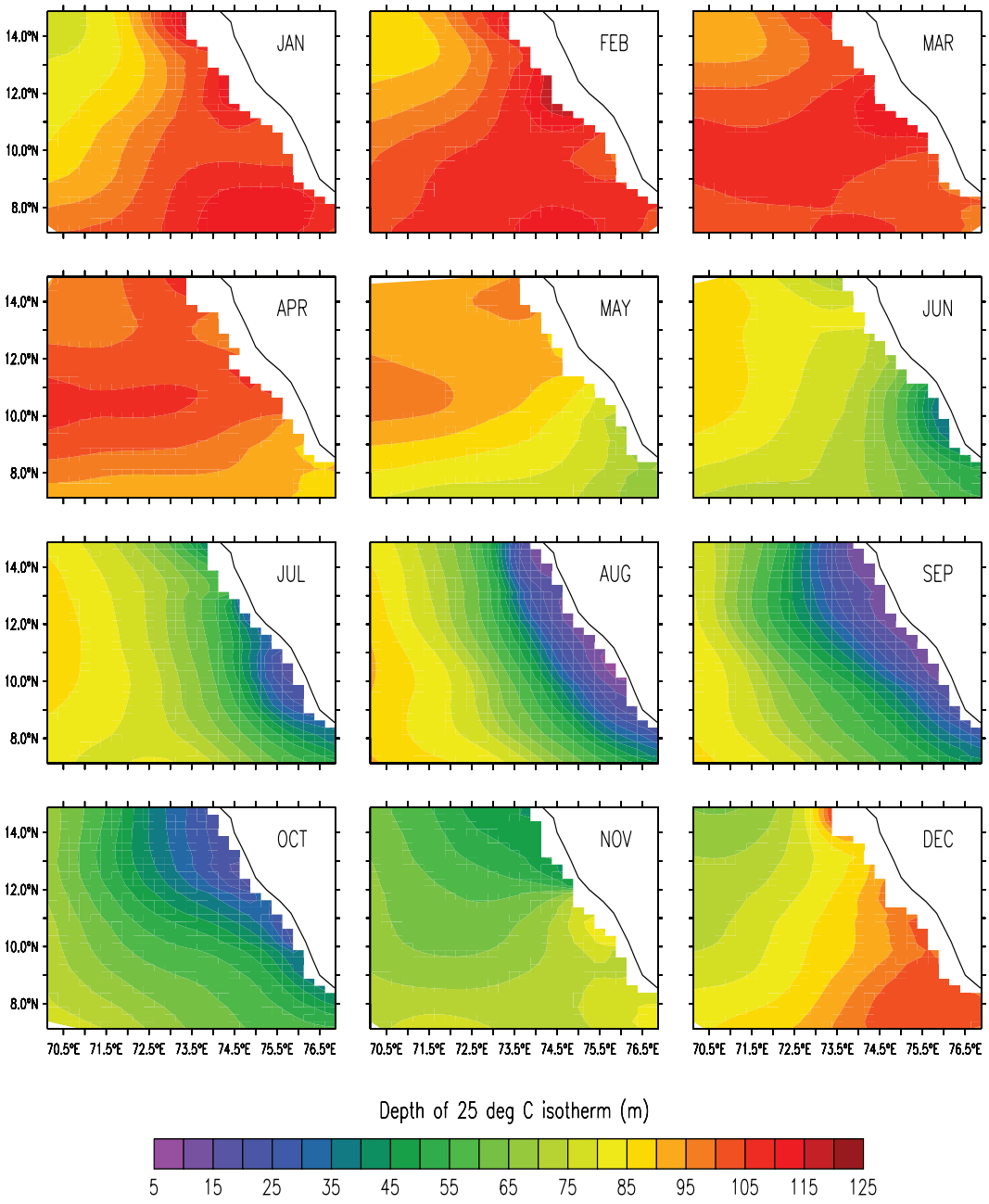

Figure 3.2: Topography of 25°C isotherm

extending upto 72.5°E. May and November are the periods of transition between upwelling and non-upwelling phases.

3.1.2 Thermal Profile of the region

The climatological temperature profiles for the representative months of different seasons obtained from the WOA 200l within the study region are plotted at three stations along 8°, 10°, 12° and 14°N latitudes (Figure 3.3). The representative months of January (winter), April (summer), July (SWM) and October (spring/ Inter monsoon period) are considered here to understand the temperature structure of the upper 200m during a year. Along 8°N, the stations were plotted at 76°, 73° and 71°E. At 76°E; during January, the temperature of upper 80m was observed to be $\sim$ 28°C that decreased with depth to 15°C at 200m. The thermocline depth during this season was approximately around 100m. The summer temperature was observed to be warmer around 30°C and lowered to 27°C at 80m which also is the thermocline depth for this season. The temperature further dropped to $\sim$ 14.5°C at 200m. July registered the coolest of all the months with surface temperature being observed around 27.5°C and theremocline depth at 40m; this indicates the presence of upwelling in the region during SWM period. By spring, the surface temperatures rose higher than 28°C indicating the termination of upwelling phase with the arrest of upwelling phenomenon at the surface waters while the thermocline depth still observed to persist as in the case during SWM.

The coastal location along 10°N at 75°E showed similar profile as that along 8°N during January and April with near surface temperature during April slightly greater than 30°C. The thermocline during July to October was observed to be very near to the surface around 20m. The temperature during October was warmer than July in the upper 100m and thereafter, up to 200m, the profile during both the months was observed to be approximately the same.

Along the 12°N latitude, the coastal station was considered on 74°E longitude. Here, the surface waters during January were observed to be $\sim$ 28°C. A slender rise in temperature with depth was noticed up to 60m which later decreased with depth. The thermocline depth was found to be around 80m. In summer, the

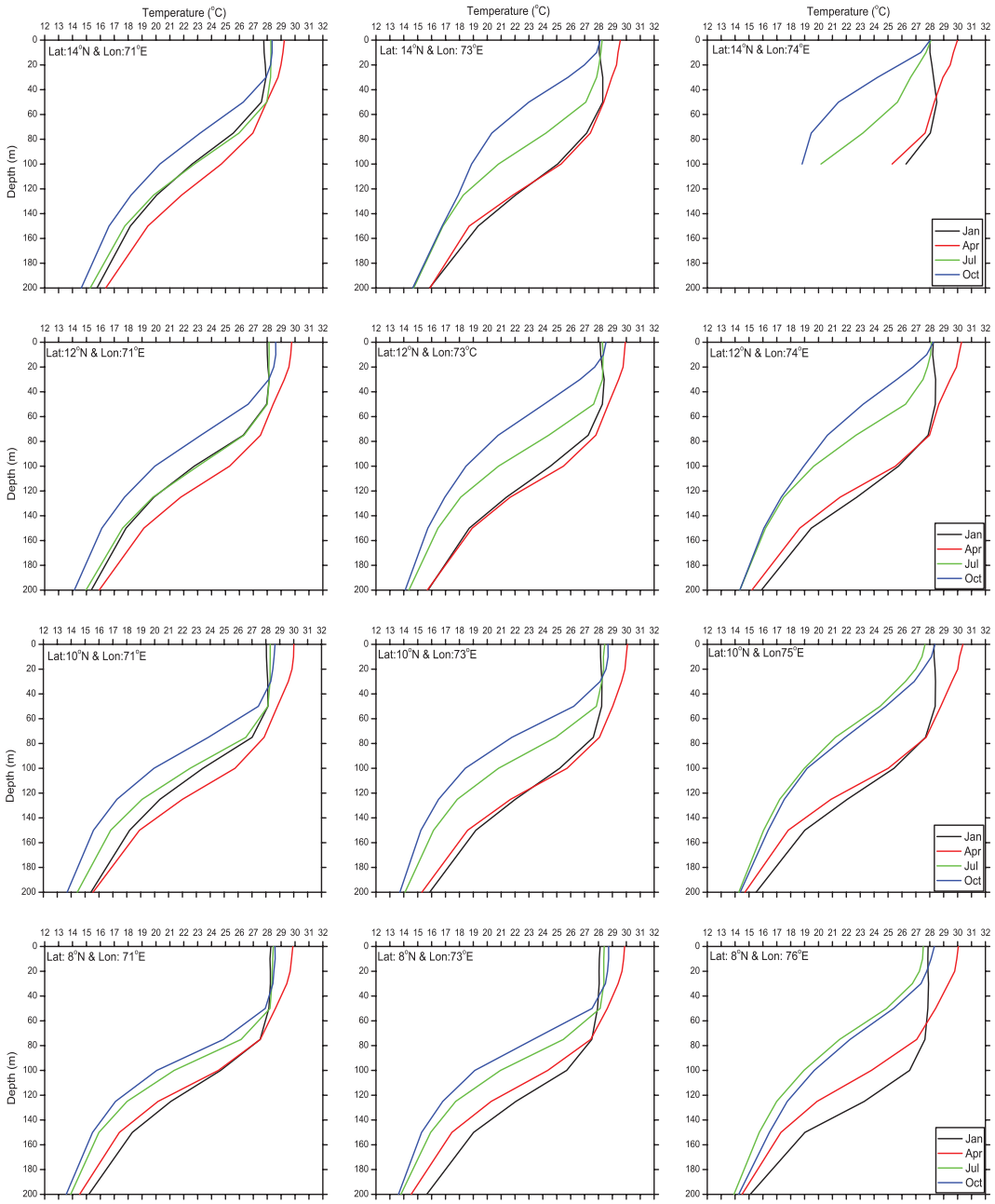

Figure 3.3: Temperature profile during different seasons of a year derived from WOA 2001

surface temperature was greater than 30°C whereas during the summer monsoon, surface temperature was ∼ 28°C inferring the presence of cooler upwelled waters at the surface. The thermocline shoaled to 50m during upwelling from 80m depth that was observed during summer. The post monsoon / spring period was found to be the coolest of all the seasons in this region with the surface temperatures noticed to be less than 28°C and the thermocline almost tapping the surface. Similar conditions were encountered along 14°N near to the coast during all the seasons.

The (central) station along 8°N selected at 73°E had temperature values in the upper 40m observed as ∼ 28°C during January with a thermocline depth of 80m. The temperature at the 200m was ∼ 15.5°C. The temperature profile throughout the summer was analogous to that of the station near to the coast for the same season. During the summer monsoon (July), the surface temperature was less than 28°C upto 50m and subsequently an abrupt slump was observed indicating that the thermocline shoaled as a result of upwelling in the region. During post monsoon, though the waters in the upper 40m were warmer than July, below this depth, the water column was observed to be the coolest of all seasons. This anomalous cooling of the subsurface waters even after the collapse of SWM winds could be linked either to the presence of upwelling induced cooler waters at the subsurface. Along 10°N at 73°E, the temperature profile for all seasons was similar to that along 8°N. Along 12°N, at 73°E, the surface temperature during January was 28°C which slightly increased with depth up to 50m and thereafter fell to 16°C at 200m. During summer, the surface temperature was warmer around 30°C due to the presence of the Arabian Sea warm pool [Kurian and Vinayachandran, 2007] reflecting conditions of pre monsoon season. The temperature below 120m was similar to that during the winter monsoon (January in this case from the figure 3.3). For the summer monsoon period, the temperature in the upper 60m was around 28°C and dropped consistently to 14°C at 200m. The thermocline depth was observed to be around 50m. The surface temperature during post monsoon was warmer than that during January and April but cooler below the depth of 15m. The absence of thermocline indicates the presence of strong upwelling in this region even after the weakening of summer monsoon. Along 14°N and at 73°E, conditions were similar to that near the coast along the same latitude with

the exception during April when the surface temperature was greater than 30°C. These warmer surface temperatures were due to the prevalent warm pool.

Offshore stations along each of the latitudes were considered at 71°E. Along 8°N, the thermal structure at 71°E was similar to that across 73°E. Along 10°N, during January, April and July, the profiles were same as at 73°E but during post monsoon, the thermocline was deeper when compared to that at 73°and 75°E. Along 12°N, the thermal structure during both the monsoons was identical upto 150m and thereafter, a feeble rise was observed during July. During post monsoon, the surface temperature was slightly greater than that during the monsoon season but below the thermocline at 30m, the thermal structure in this season appeared the coolest of all the seasons. Along 14°N, at 71°E, the temperature for the upper 30m was found to be least during January with the thermocline depth approximately around 60m. The temperature gradually fell to $\sim$ 16°C at 200m. During summer, a temperature of 29°C near the surface decreased to 27°C at 80m and thereafter gradually dropped to 16.5°C, at 200m depth. The temperature during the summer monsoon, in the upper 50m is slightly higher than that during winter monsoon is 28°C and below the thermocline, the profile was approximately similar to that of January upto 130m and thereafter indicated decreasing trend. The temperature profile during October was again similar to that at 12°N.

To summarize, from figure 3.3, it was observed that the surface temperatures at all the stations during all seasons varied between 27.5° to 30.5°C. In the coastal sections, along 8° and 10°N, thermocline was observed to be near to the surface during July and October indicating the presence of upwelling. Intense upwelling during summer monsoon could be identified from the presence of cooler waters at the surface. In the northern region, existence of upwelling was observed during October. Thus it can be stated that the upwelling commences in the southern regions during SWM and advances northward, with time. In the northern regions, upwelling prevails well after the collapse of SWM, till October and subsides later; thereby inferring the difference in the temporal evolution of upwelling along the coast and the spatial distribution away from coast.

3.2 Satellite Observations

3.2.1 Monthly Variability in Wind pattern

In order to appreciate the evolution of upwelling based on forcing factors and the associated response, satellite derived products are made use. From the above analysis of the hydrographic conditions of the region, it is surmised that the upwelling in the region is not entirely wind dependent but also related to another factors such as the complex circulation pattern prevailing in the region (and its reversal in direction), which may play a vital role. These factors and their monthly variability has been explained in detail in the following sentences. The monthly variability of the wind pattern in the region was obtained for ten years (August 1999 - July 2009) – as per the quality data record of QuikScat measured sea surface winds (QuikScat ceased to function from November 2009). The 3 day running averaged wind products were used to compute the monthly mean wind and thereby the long term average of all the corresponding months for every year. The resultant 25km x 25km resolution monthly climatological product (Figure 3.4) was utilized to ascertain the mesoscale variability of the wind for the region.

On inspection of the figure 3.4, it was observed that the direction of wind in SEAS was northerly irrespective of the season. Wind speeds are high during the summer monsoon months, especially during June, July and August compared to other months. This implies that the region was dominated by only summer monsoon and there is only a feeble impact of winter monsoon. In January, wind speed near the coast was 3 m/s in the southern region except near the southern tip where it is higher than 6m/s. In the open ocean region between 70° - 72°E, the wind speed was observed to be 6 m/s. The wind direction was northerly upto 11°N and north-northeast, down south. In February, the least wind speed region was limited to 7° - 9°N, while the rest of the region had wind speeds between 5 - 6 m/s. A minute change in the wind direction was observed near to the coast from January. Here, in February, the wind direction all along the coast was north - northwesterly. Rest of the region, the open ocean, was prevailed by northerly winds. High wind speed greater than 6 m/s is maintained at the southern tip

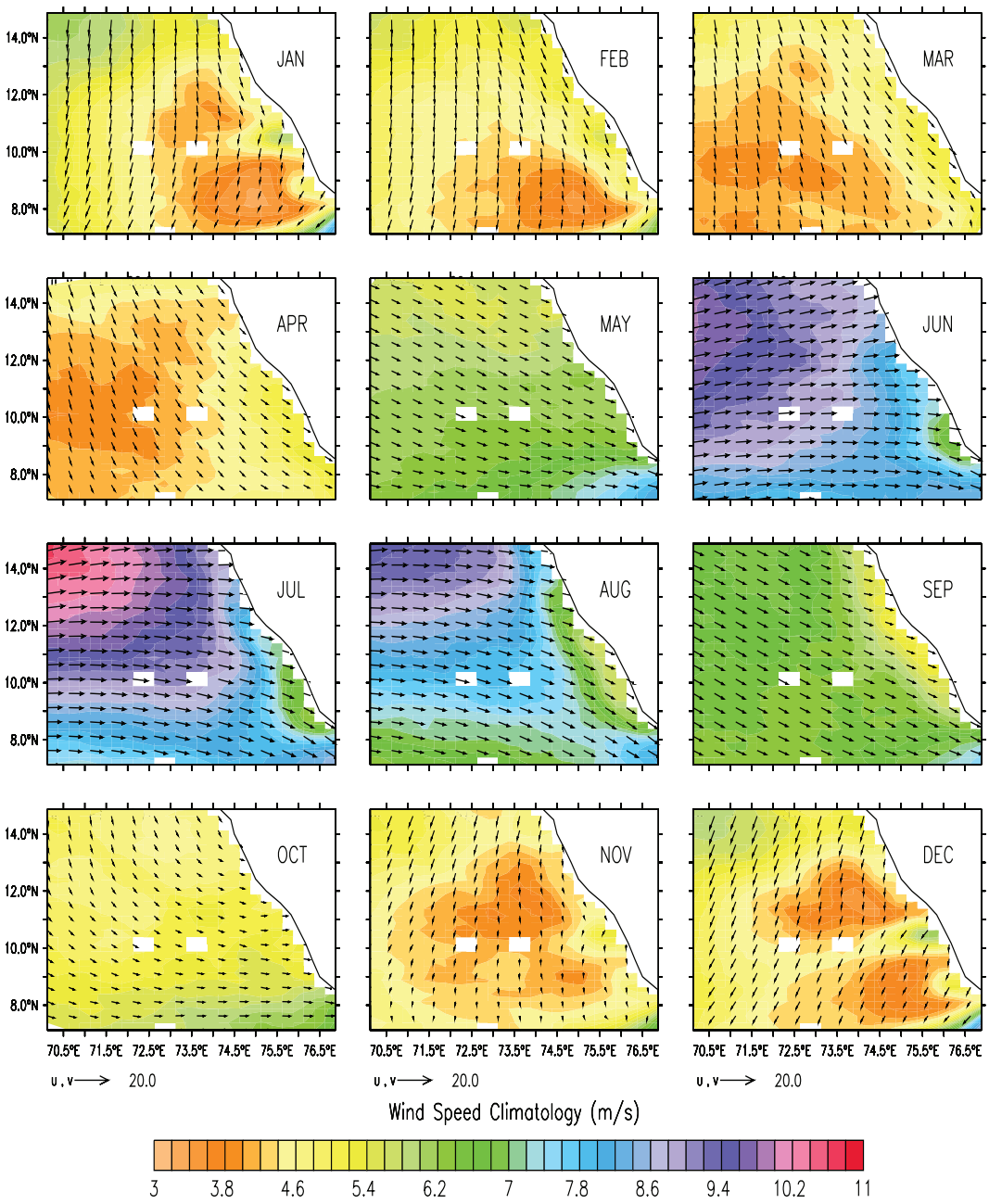

Figure 3.4: Monthly variability of Wind Speed and Direction over SEAS

of India. In the inter monsoon period of March, the wind speed, except near to the coast, was less than 4 m/s. Along the coast, the wind speed was $\sim$ 5.5 m/s. The wind direction was north - northerly from coast to 72°E; beyond that it was absolute northerly. By April, the entire region was prevailed by northwesterly winds though the strength was very less. During May, the direction prominently turned north westerly along with increase of speed. Wind speed all over the region was greater than 6 m/s and near the southern tip of India, the wind speed was greater than 7 m/s. By June, the SWM regime was set over the entire region and a significant rise in wind speeds (greater than 8 m/s) was observed; that it was $\sim$ 9m/s in the northwestern corner of the region. An interesting feature observed was the development of a low wind pocket very near the coast between 8° and 10°N with speed less than 7 m/s. During July, which is also the peak monsoon time, the speeds were greater than 10 m/s in the northwestern corner and rest of the region indicated 8 m/s. The low wind pocket observed during June spread offshore and northward. The wind direction to the south of 8°N was predominantly zonal (westerly), and near the coast, it was northwesterly and in the open ocean region, it was southwest. The low wind region further elongated up to 13°N parallel to the coast during August. Wind speed reduced in the NW corner to 9 m/s and a possible change in the direction to northwest was observed at 72°E. During the receding phase of SWM, in September, the wind direction was completely northwest and speeds all over the region were 7 m/s, while a further drop to 5 m/s was observed along the coast. During the inter monsoon period of October, the wind speed reduced to 5 m/s all over the region and direction was northwest to the north of 8°N, while to the south, it was perfect westerly (zonal component) which dominated the region. In the initial phase of northeast monsoon, during November, the wind speed was observed to be less than 4.5 m/s with a strong low wind region centered on 11°N and 73°E. Wind direction was northerly all over the southern region and northeasterly up to 12°N. Later, the low wind region observed during November split into two eddies and extended towards the coast. The speed within these regions was 3 m/s and direction all over the region, indicated northeast.

In summary, it can be stated that the wind direction near the coast was northerly (equatorward) irrespective of season. Despite this fact, coastal up-

welling in the region was taking place only during the SWM. This is because the alongshore winds that were prevailing during the northeast monsoon does not have adequate strength to drive Ekman transport away from the coast, also the absence of divergent circulation pattern to generate upwelling. Another important fact to be reckoned is that the zonal component of the wind varies once a year i.e., during SWM, while the meridional component has bi- modal variability and this component of wind functions importantly in coastal upwelling for the region and this fact is dealt in chapter 4.

3.2.2 Monthly Variability of Sea Level

On observing the sea level anomaly (SLA) derived from merged altimeter measurements, distributed by AVISO, the monthly climatology showed a distinct annual cycle (Figure 3.5). On a broad scale, the SLA was positive during winter monsoon months and negative during summer monsoon. From figure 3.5, it could be observed that two eddies were forming, one on the southern region between 73° - 75°E and 7° - 9°N, and another along the coast between 11° - 13°N. These eddies were anti cyclonic during winter monsoon and cyclonic during summer monsoon. The presence of cyclonic eddies is an indication of divergence of the sea surface and thence upwelling favorable. In January, SLA all over the region along the coast was positive with values greater than 16 cm. Negative anomalies were observed in the northwest corner of the region. In February, the twin eddies showed dissipation and spread westwards, the whole region is prevailed by positive anomalies. By March, both these eddies were completely dissipated and a flow westward was observed. During April, the entire region does not show noticeable variability. In May, a patch of negative SLA was observed along the coast indicating the initial phase of upwelling in this region. By June, negative anomalies spread upto 72°E from the coast, with high intensity along the coast, and this clearly indicates the establishment of upwelling along the coast. During, July, two cyclonic eddies could be observed at the exact location where, anti cyclonic eddies were located during winter monsoon and negative anomalies prevailed in the whole region, leading to infer the spatial spread of upwelling,

off the coast. Similar conditions were observed during August too. In September, the two eddies showed dissipation, but negative anomalies still prevailed in the region. During October, negative SLA showed reduction in magnitude along the coast while in the open ocean region, strong negative anomalies continued to dominate.

This indicated the start and dissipation of coastal upwelling. The coastal region was prevailed again by positive anomaly by November. The positive anomalies spread upto 72°E from the coast and the formation of twin anti cyclonic eddies could be again observed, thus completing one full annual cycle.

3.2.3 Monthly Variability of Sea Surface Temperature

The response of the ocean towards upwelling can also be understood in the form of cooler SST. For the present study, AVHRR - Pathfinder SST data from 1982 - 2009 was used to ascertain monthly variability of the SST. The 8 day temporal with 4 x 4 km spatial resolution data was averaged for every month; this monthly data was made use of to arrive at the climatology. From the scrutiny of figures on SST (Figure 3.6), for each month in the study region, it was understood that March, April and May are the warmest months in the region. Similarly, July, August and September are the coolest. During January, the SST in the region varied between 27.5°C at the southern tip of India and northwest corner to 29°C for rest of the region. In February, a patch of warmer waters was observed along the southern coast between 8° - 10°N up to 75°E. The northwest corner of the region remained cooler between 27.5°C and 28.5°C. During March, coastal regions up to 73°E were found to be at $\sim$ 29.5°C with a warm patch of 30°C between 9° - 10°N. April and May recorded almost uniform temperature all over the region with temperature above 30°C. The warm patch between 9° and 10°N that was observed during March further rose to 31°C in April and moved offshore in scattered patches by May. The surface cooling signatures were observed in June at the southern tip of India with temperatures less than 28°C upto 10°N along the coast extending up to 75°E from coast. Apart from this, cooler temperatures are also observed between 70° - 71°E and 11° - 12°N. Coastal region to the north of 11°N were maintaining values around 29.5°C. During July and August, the whole

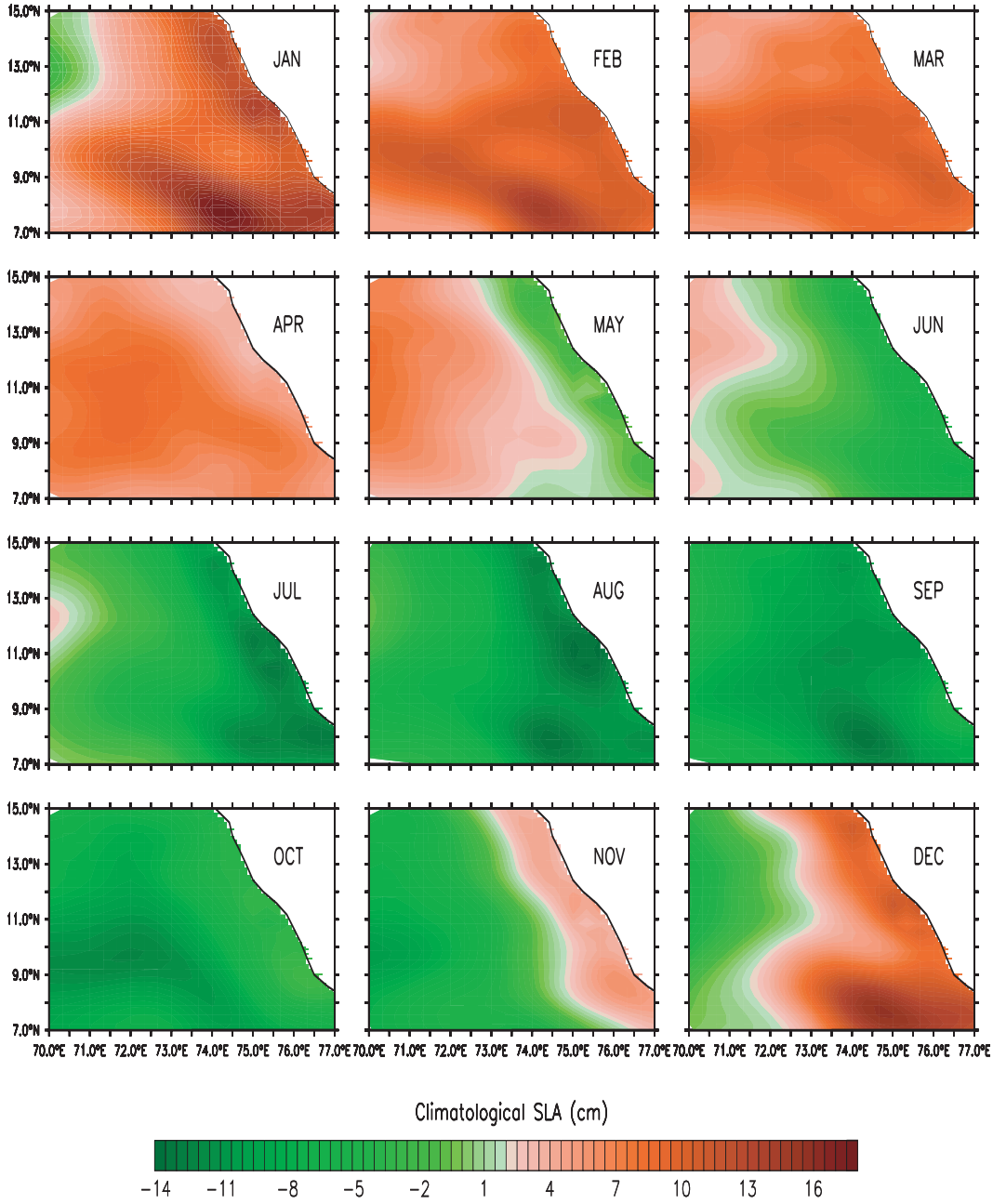

Figure 3.5: Monthly variability of Sea Level Anomaly over SEAS

SEAS was covered by SST less than 26°C. By September, these cooler temperatures turned slightly warmer to greater than 28.5°C in open ocean region, while the coastal regions remained cooler, less than 28°C. This transition indicated the terminal phases of upwelling. With the seizure of SWM, the region turned warmer by October with SST above 29°C. This warming further intensified in November and uniform temperatures of above 29°C were observed all over the region. A warmer patch of temperature greater than 30°C was observed along the coast between 11° - 14°N. By December, these warmer waters spread further up to 72°E with further reduced the surface temperatures. Cooler SST $\sim$ 28.5°C was observed at the southern tip of India.

To summarize, the surface temperatures are warmer than 28°C in the SEAS region from January to May and upwelling resultant cooler temperatures are observed in the satellite measured SST near the southern tip of India in June and thereafter with the advancement of upwelling, the entire coast indicated cooler temperatures all over the region by July and August. The receding phase of upwelling began in September and its influence on SST was limited only to the coastal regions; upwelling ceased to exist by October. One noticeable fact was the drop of SST by nearly 4.5°C in the coastal regions from April / May to July / August. Concurrently, the open ocean temperatures dropped by 2° - 3°C. Thus it could be clearly concluded that upwelling in SEAS is an annual phenomenon that occurs during SWM period.

3.2.4 Monthly Variability of Chlorophyll-a Concentration

The growth of phytoplankton occurs in the layer where both light and nutrient concentrations are sufficient. With increase of the upwelling nutrient flux the conditions of phytoplankton growth becomes better and the maximum of its vertical distribution moves to shallower layer. When nutrient flux is very intensive and phytoplankton biomass is high, the maximum of vertical distribution of phytoplankton is located at the surface. The result is a direct correlation between total phytoplankton (or chlorophyll) concentration in water column (or within the euphotic layer) and in the thin surface layer. Hence, both the surface

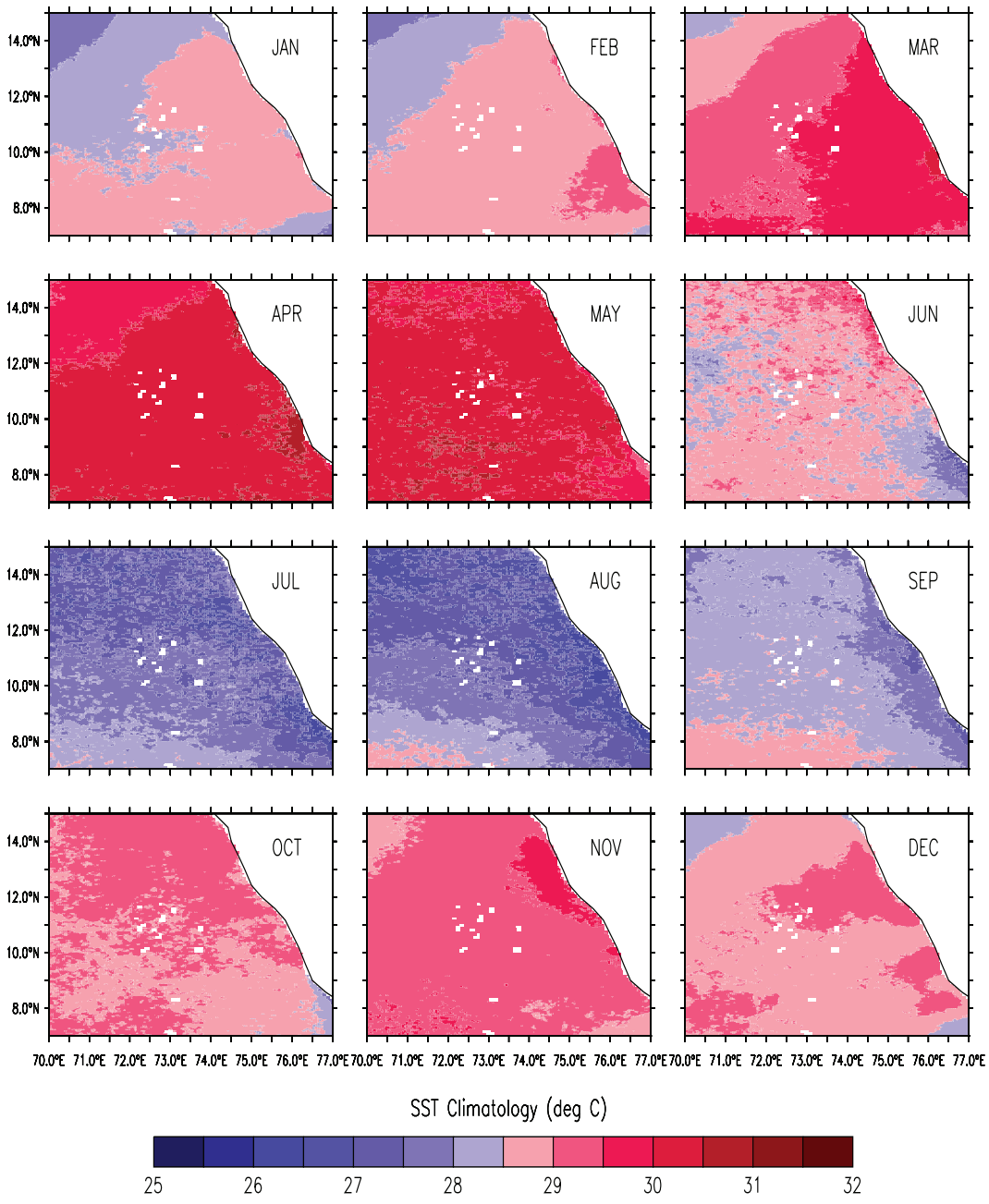

Figure 3.6: Monthly variability of Sea Surface Temperature over SEAS

CHLA and the chlorophyll above the penetration depth can be used as a measure of water productivity, i.e., phytoplankton biomass. Therefore, the satellite measured surface CHLA provides an estimate on the biomass of the region of interest. Figure 3.7 shows the monthly variability of CHLA for the study area. Monthly averages were arrived upon computing the long term mean of respective months in each year from 1998 to 2007. On examination of the CHLA monthly climatology, it is observed that similar to SLA, CHLA too has a distinct annual cycle. The region shows feeble variability with respect to the CHLA during non upwelling months. For this period, CHLA remained less than 0.5 mgm^{-3} all over the region except very near to the coast during the months of January, February, March, April, November and December. For May and October, i.e., during the initial and terminal phases of upwelling, CHLA of 2 - 3 mgm^{-3} was observed all along the coast. By June, a strong patch of 5 mgm^{-3} CHLA was observed at the southern region of the coast and which spread about $\sim$ 100 km from the coast. This patch extended further north by July coinciding with the peak phase of SWM and the resultant upwelling, northwards. These highly productive waters spread $\sim 200 - 300$ km offshore, while a maximum concentration was noted between 8° - 10°N during July - September. Two distinct productive fronts can be noticed: one, between 8° - 9°N and the other between 11° - 12°N. These are also the regions of high river run-off during the rainy SWM season. By August, the frontal regions were subdued and rather uniform CHLA content was observed all over the coast. In the entire open ocean region, CHLA up to 1 mgm^{-3} was observed during this period. The same scenario prevailed in September too but with depleted offshore values to the west of 72°E and south of 12°N. The CHLA content reduced considerably by October, all over the region, and was present only very near to the coast. The entire region stands deprived of measurably productivity by November and December based on CHLA.

3.3 Temporal Cycle of the signatures

In order to get an understanding on the temporal structure, over a year, three representative regions (Box1: Lat: 7.5° - 8°N, Lon: 76° - 76.5°E; Box2: Lat: 10.5° - 11°N, Lon: 74.5° - 75°E; Box3: Lat:13.5° - 14°N, Lon: 73.5° - 74°E) as

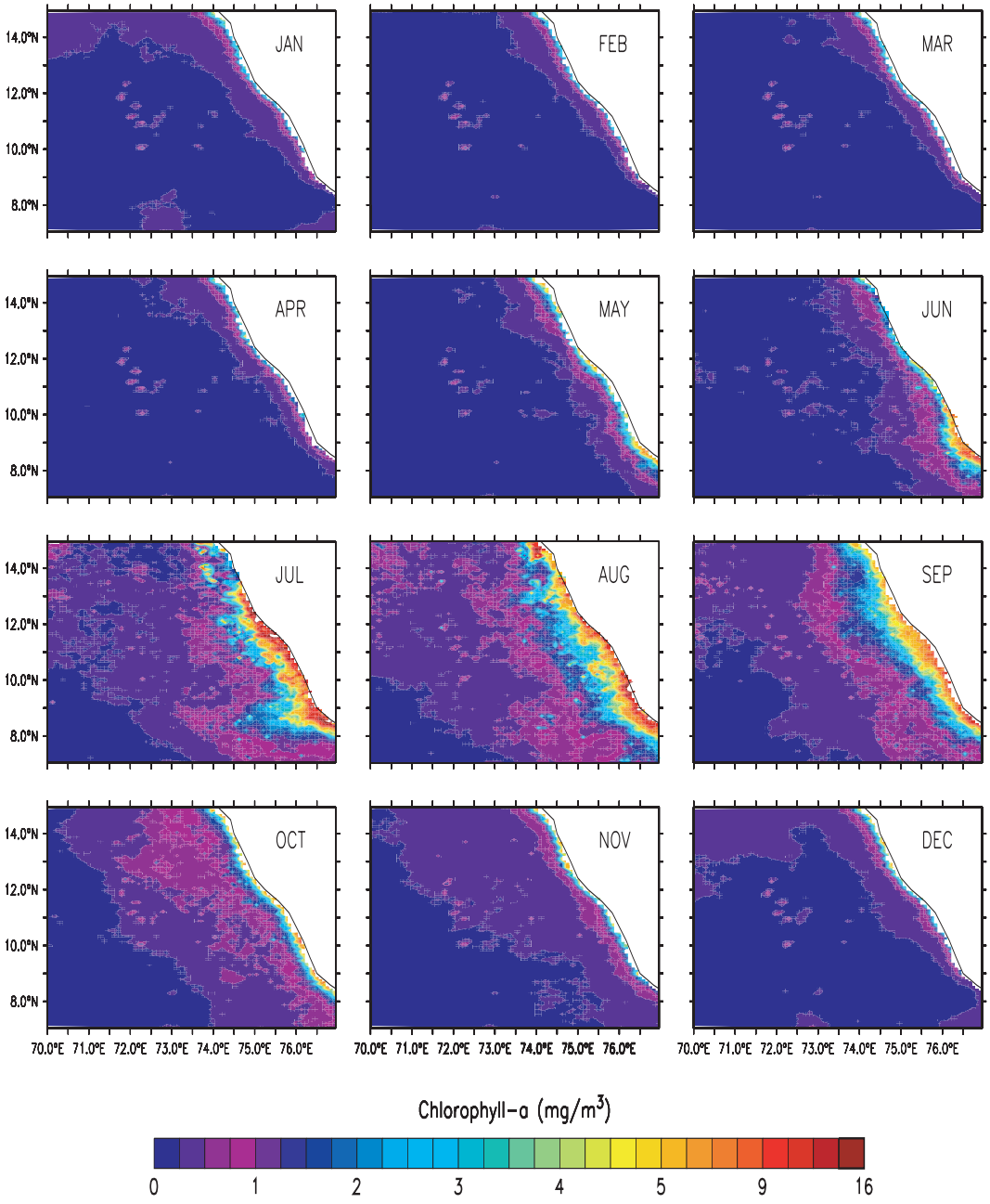

Figure 3.7: Monthly variability of Chlorophyll- a Concentration over SEAS

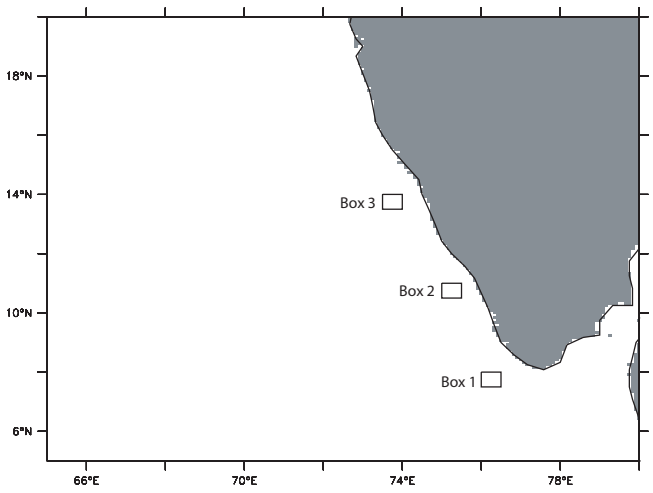

Figure 3.8: Figure showing locations along the coast considered for understanding the temporal variation of signatures. (Box1: Lat: 7.5° - 8°N, Lon: 76° - 76.5°E; Box2: Lat: 10.5° - 11°N, Lon: 74.5° - 75°E; Box3: Lat:13.5° - 14°N, Lon: 73.5° - 74°E)

shown in figure 3.8 along the southwest coast of India were selected. The area average of the long term monthly mean at these regions for all the four parameters discussed in previous sections aid the presentation of upwelling signatures as plotted in Figure 3.9. The long term averages through box 1 to box 3 indicate a wide range of perturbation(s) during SWM season coinciding with the upwelling phenomenon. The wind speeds at all the three boxes showed increase during the SWM season with the highest in box 3 among all the three regions, followed by box 1 and then, box 2. The wind speed initially showed decrease from January to April indicating the receding phases of winter monsoon and commenced to peak sometime during May to reach their maximum by July and later receded to pre - monsoon speeds by October. A slight built up was observed during November signaling the onset of winter monsoon. To summarize, this shows that the semi-annual cycle of wind pattern in the region is bestowed with summer monsoon winds that blow sturdily during June to September having a dominating influence on the processes of our concern.

As expected, during seasons of upwelling, lowering of sea level, already re-

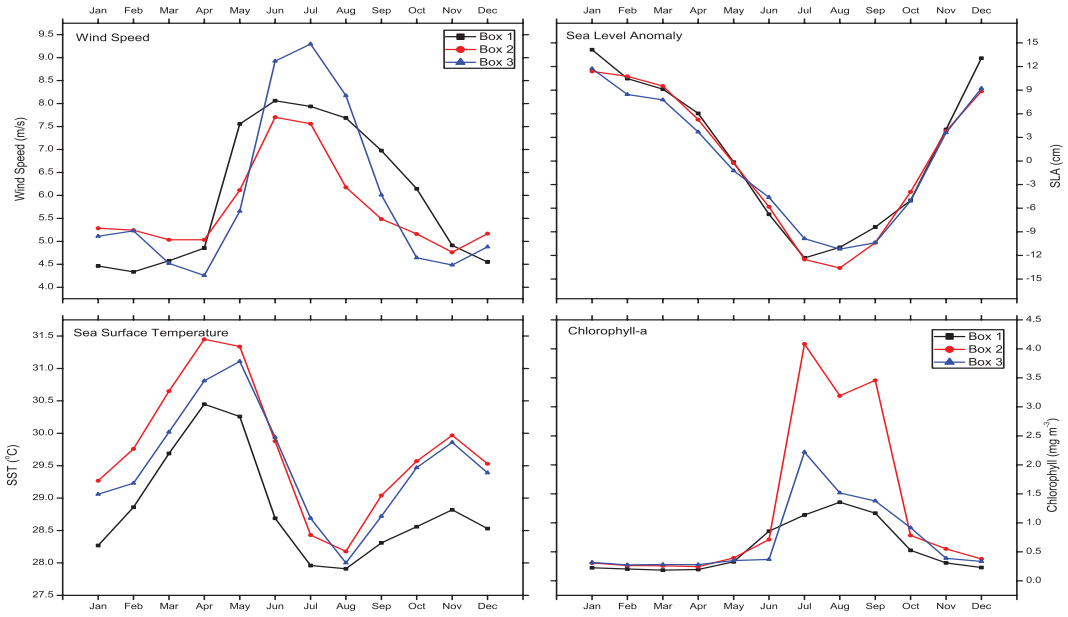

Figure 3.9: Monthly variability of the signatures at selected regions along the coast

ported for these parts of the ocean [Shankar and Shetye, 1997] stands once again, re - confirmed. Though minor variations of 2 to 3 cm was observed between the 3 boxes, the overall features in the figure suggest a gradual decrease from start of the year to the lowest levels during July, August and thereafter follows by a rapid increase towards the year end. It is deduced that SLA has an annual cycle for this part of the ocean and further that, the commencement of retraction from lowering to increase in SLA starts from the southernmost areas of the study region followed by the adjacent regions in box2 and later in box3.

The results pertaining to SST, though following a similar pattern, as above, however differ in actual values. The long term averages in box 1 exhibited lowest SST values; the low, coincided with the annual upwelling. During most of the months, maximum SSTs were noted in box 2, being the central region of the study area which inadvertently also exhibited the maximum fall in SST values from a high of $\sim 31.4°C$ in April to a low of $\sim 28.3°C$ in August. All along the coast, a secondary peak in SST was very evident, centered on November due to water temperature inversions in the region [Nisha et al., 2009].

From January to June and later from November to December, the coastal water indicated near homogeneous values of CHLA, around 0.3 to 0.5 mgm^{-3}. With the advent of monsoon, predominant land run off to the coastal regions bring about large nutrient inputs to near shore; meantime, ocean subsurface processes promote upwelling and the combined affect resulted in moderate buildup of CHLA up to 1.2 mgm^{-3} in the southern most box 1, whereas slightly higher values 1.5 - 2.0 mgm^{-3} dominated the waters in box 3, which was located in the northernmost section. The most significant enhancement in CHLA occurred in and around box 2, where values as high as 4.5 mgm^{-3} should contribute to good primary productivity.

Thus, from the monthly variability of signatures, one can state that the wind and SST have semi-annual variability, while SLA and CHLA have annual mode of variability in SEAS. This provides a unique setting to distinguish the forcing and arrive at the responses of upwelling in this region.

4

Role of Forcing Factors

4.1 Introduction

It is common knowledge now that wind plays an important role in coastal upwelling processes. Theory says that upwelling occurs along a coast (with ocean on its western side) when the wind stress has an equator ward alongshore component or in the case of open ocean, it is positive (negative) wind stress curl in the northern hemisphere (southern hemisphere) [Stewart, 2005]. Also, coastal divergence of the seaward Ekman current is augmented by the alongshore equator ward wind stress, whereas Ekman pumping results from the wind stress curl. In the Indian Ocean, with the onset of SWM, a strong low level wind jet known as Findlater Jet [Findlater, 1977] is established across the Arabian Sea. On either side of this jet, the changing curl of wind stress would produce a region of divergence. The upwelling along the west coast of India is an illustration of an eastern boundary upwelling that is driven both by divergent currents and also, the alongshore equatorward wind stress. Many studies had been published in the past on the seasonality of the upwelling phenomenon based on various *in-situ*, modelled and other observational data sets (Chavez and Messie, 2009, Boe et al., 2011). With the availability of QuikScats ten year long fine resolution dataset from 1999 to 2009, it is possible to find the periodicity of wind forcing over the region during upwelling season. Apart from atmospheric forcing, in the form of SWM winds, there exists another forcing which is a manifestation of oceanic conditions driven

from elsewhere, termed here in this case as remote forcing on the coastal upwelling regime of SEAS. Kelvin waves, generated on the western African coast travelling along the equatorial wave guide reaches the eastern Indian Ocean and split north and southwards. The northern arm of the wave orients itself along the coast thus turning into a coastal Kelvin wave. This coastal Kelvin wave travels along Myanmar and east coast of India, finally reaching SEAS [Rao et al., 2010]. It is stated that Kelvin wave results in altering the East Indian Coastal Current (EICC) to turn around Sri Lanka and join the West India Coastal Current (WICC) [Shankar and Shetye, 1997]. McCreary et al. [1993] observed that winds along the eastern boundary of India generated similar Kelvin wave and thence influence WICC. Satellite altimetry provides the best observational platform to study the changes influenced by these Kelvin Waves and the subsequent Rossby waves that play a role vis-a-vis coastal upwelling in this region. The periodicity of these waves has been well established by many earlier studies (McCreary et al., 1993, Bruce et al., 1994, Rao et al., 2010). In this study an attempt has been made to understand the role of remote forcing on the SST [cooling] and upwelling related phytoplankton blooms in the SEAS.

4.2 Wind Forcing

4.2.1 Wind Stress

SEAS is a typical eastern boundary upwelling system where winds blows equator ward, along the southwest coast of India. Along shore and across shore wind stresses were computed separately from QuikScat measured winds between years 2000 and 2009. Monthly climatology was computed from the wind stress as illustrated in Chapter 3, whose variability is shown in figure 4.1. The sign convention is such that, negative sign indicates southward (Equator ward) for along shore wind stress and westward for across shore wind stress and vice - versa.

It is observed that meridional wind stress was predominantly southward near to the coast all most throughout the year. During January and February, the

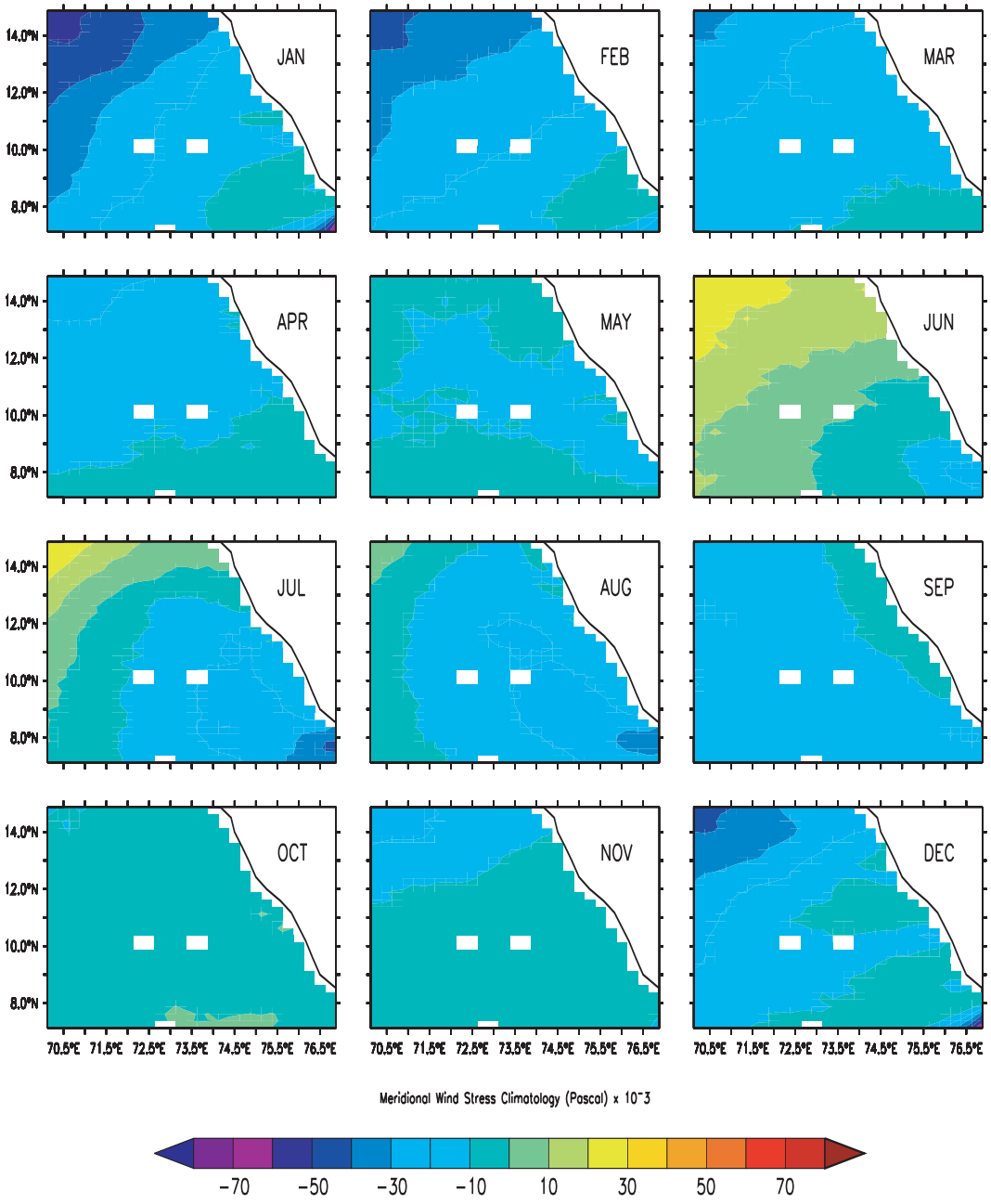

Figure 4.1: Monthly variability of meridional wind stress over SEAS

meridional wind stress had a similar pattern with only slight variability in magnitude; maximum northerly stress was noted at the northern end of the region. A small patch of higher order stress was observed near to the coast between 8° and 10°N extending up to 73°E. In March, all SEAS region was prevailed by stress ranging between -10 x 10^{-3} and -30 x 10^{-3} Pascal. By April, the direction of stress had shifted northward. Significantly, in May, northern and southern parts of SEAS were prevailed by positive stress with a large negative field of wind stress, extending from the coast to 71°E. This is a clear indication of changes that occur in atmospheric setting(s) which suit the onset of SWM. This scenario was further strengthened by June, when an intense southerly wind patch 11°N - 73°E from the coast was observed of the order of 10 x 10^{-3} Pascals. This confirms results from previous studies (Rao et al., 2008, Smitha et al., 2008) that upwelling commences from the southern tip of India and extends northwards along the coast. During this period, the northerly patch was observed up to 9°N with an offshore extent of approximately 150km. This northerly patch extended up to 12°N by July and further, extended up to 72°E indicating the peak phase of wind setting that results in intense upwelling. These northerly wind stress signatures extended all along the southwest coast of India and by August, brought the entire area under the influence of wind induced upwelling. During September, only a feeble northerly wind stress was observed all along the coast (extending approximately 100km from the coast). This is considered as a signature for the start of retreating phase of the SWM winds. Based on above and other results, a detailed discussion on the oceanic response with respect to upwelling to the receding SWM is presented in chapter 5. The wind structure during October was one that of an inter-monsoon phase where one can observe a lull in the winds. By November, with the onset of northeast monsoon, strengthening of northerly winds was observed and it further continued in December also.

To summarise, the meridional (alongshore) wind stress, very near to the coast, was northerly for a significant part of the year. However, the strength of such an along shore wind stress was relatively weak unlike in other places of notable eastern boundary upwelling zones around the world. To state in advance, it had two peaks associated with both the monsoons. The accurate periodicity of the wind stresses are deduced from the continuous wavelet transforms in the

following sections. The maximum extent of upwelling favourable wind stress was observed to be around 300 - 400 km from the coast. From the along shore winds, it is implicit that the upwelling starts at the southern tip of India and extends northwards along the coast. Figure 4.2 shows the monthly zonal (across shore wind stress) in SEAS. On close inspection, it is understood that unlike meridional wind stress which has a bimodal variability, the zonal wind stress has only an annual variability. The sign convention adopted for zonal wind stress, as stated earlier, is such that, the positive sign indicates westerly wind stress and vice - versa. Note that, January and February showed easterly shear due to the influence of northeast monsoon.

During the inter-monsoon periods of March - April and October, the region was observed to be under the influence of calm winds and hence feeble wind stress. Intense zonal winds were observed during the SWM period (the months: June, July, August and September). During August, the wind stress was observed to be as high as 200 x 10^{-3} Pascals. With the onset of northeast monsoon, the direction shifted easterly by November. Additionally, the periodicity of zonal wind stress along the coast was studied using continuous wavelet transform, based on 3 day running mean of the stresses. The influence of wind stress had not been properly explained by the earlier researchers and this aspect is dealt explicitly in chapter 5 in an attempt to quantify the weightage of each of the forcing factors on the upwelling phenomenon in the region.

4.2.2 Wind Stress Curl

As per the classical upwelling theory, positive wind stress curl causes divergence in Ekman layer and act as a catalyst for upwelling; on the other hand, negative wind stress curl results in convergence in the Ekman layer and downwelling is expected in the northern hemisphere. The monthly climatology of wind stress curl (Figure 4.3) showed positive curl all along the coast during the summer monsoon months of June, July, August and September. It first starts as a small speck towards the southern tip of India in May and extends northward with progress of time and is well distinguishable all along the coast by August. A point to be noticed is the presence of negative wind stress curl away from the coast during the June, July

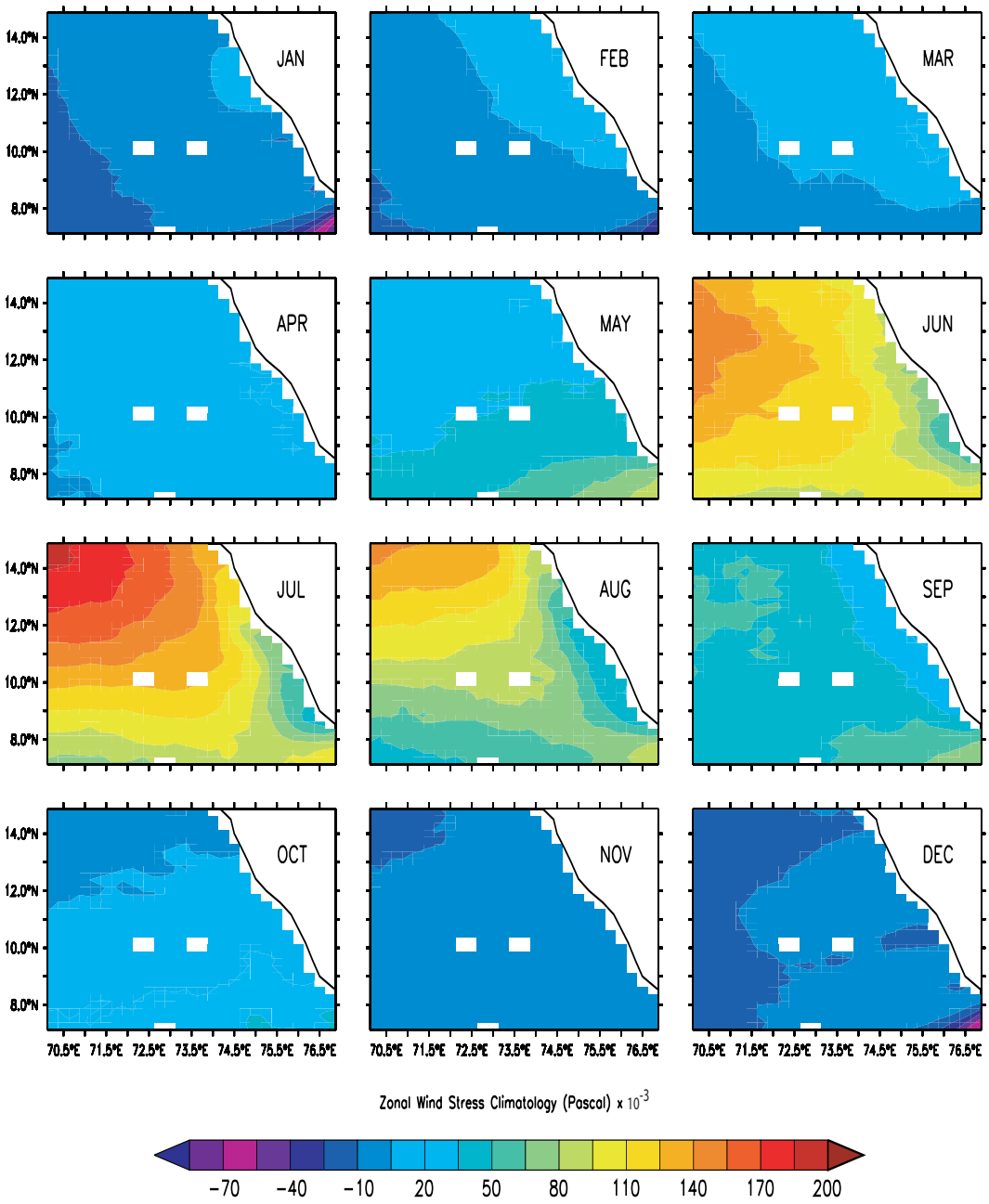

Figure 4.2: Monthly variability of zonal wind stress over SEAS

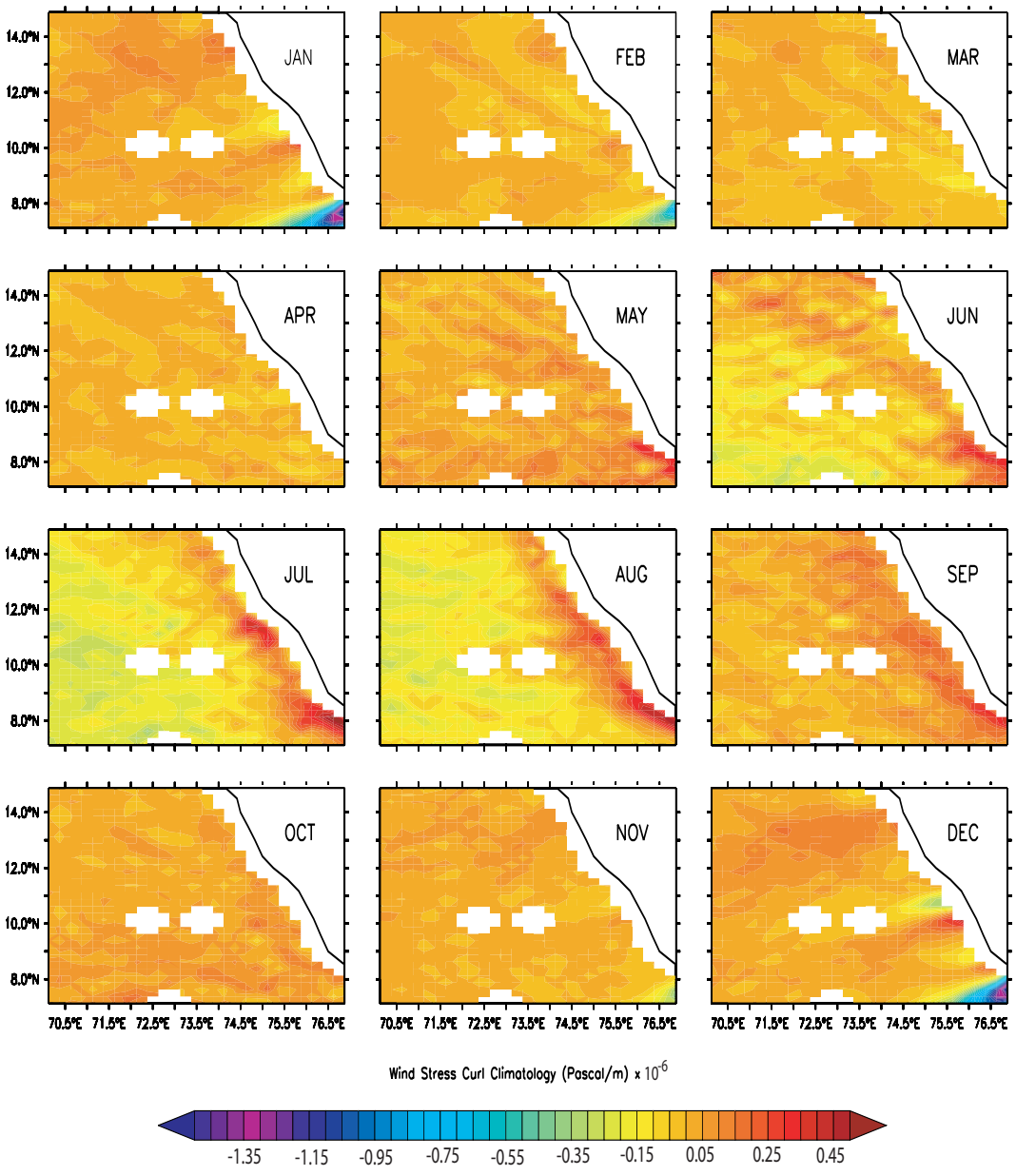

Figure 4.3: Monthly variability of Wind Stress Curl over SEAS

and August. Negative curl was also observed at the southern tip of India during the winter monsoon season from November to February, indicating the presence of downwelling and this confirms the model studies of Rao et al. [2008]. For rest of the months in a year, wind stress curl over the region was uniform and does not show any variability.

4.2.3 Ekman Transport

Upwelling intensity can be estimated from Ekman mass transport which is perpendicular to the direction of the wind in the region. Ekman mass transport (M_e) for the southwest coast India was computed from the bulk aerodynamic formula as used for satellite derived wind stresses by Koracin et al. [2004] and Petit et al. [2006] and the references therein:

$$\tau_y = \rho_a C_d W_{mag} V \tag{4.1}$$

where τ_y is the meridional wind stress, ρ_a is density of air which is 1.29 kgm^{-3}; C_d is wind dependent drag coefficient calculated using Smith [1988] method, W_{mag} is the magnitude of wind speed and v is the meridional wind speed. Ekman transport M_e is obtained as:

$$M_e = \frac{\tau_y}{f} \tag{4.2}$$

where f is the Coriolis paramter $2\Omega \sin\phi$ (s^{-1}), Ω is the angular frequency of earth (s^{-1}) and ϕ is the latitude.

Ekman transport was computed for 1 x 1 degree grid box along the 200 isobath line (Figure 4.4). Ekman transport was dependent on the direction of the wind prevailing in the region. Along the southwest coast of India, wind direction was equator-ward i.e., meridional, irrespective of the season. During SWM, wind was north-northwesterly and in northeast monsoon, it was north-northeasterly [Shetye et al., 1985] very near to the coast. The alongshore component during SWM season decreased from 8° to 10°N and again increased up to 14°N. Between 10° and 14° N, wind built-up from May to July and later showed a decrease in speed with time till the end of monsoon [Muraleedharan et al., 1995]. As wind was meridional in both the seasons, Ekman mass transport will be offshore along most parts of the coast line.

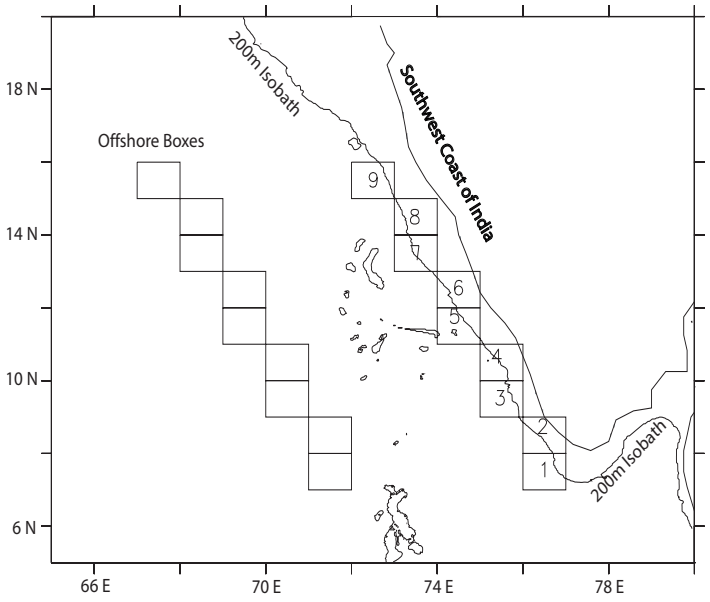

Figure 4.4: Southwest coast of India showing 200m isobath line and the boxes considered for computing Ekman transport along the shelf break

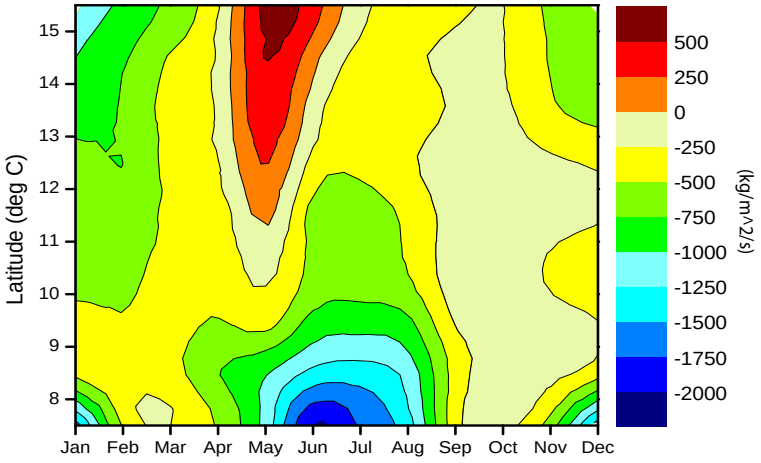

Figure 4.5: Ekman transport along the southwest coast of India

Climatology (Figure 4.5) computed from the QuikScat wind products show the pattern of Ekman transport prevalent in the region. Onshore transport was observed during the pre-monsoon months of April and May from 12° to 16°N. Mild offshore transport observed between 9° and 10°N latitudes during winter monsoon is due to the wind blowing parallel to the coast for that period at this region. Maximum offshore mass transport was observed for the summer monsoon period between 8° and 10°N latitudes ranging from 500 to 2000 kg/m^2/s. Intense offshore Ekman transport was observed off 8°N during winter monsoon which is also in toe with the prevailing wind direction near the southern tip of India (Luis and Kawamura, 2000, Luis and Kawamura, 2001).

4.3 Temporal Variability

In order to understand the temporal variability and its frequency, three locations were selected along the coast as shown in figure 3.8. The boxes were selected such that they are located at southern, central and northern portions of the southwest of India where the coastal upwelling is prevalent. Climatology of zonal and meridional wind speed computed from the 3 day running mean for the period 2000 to 2008, was plotted to elucidate the daily variability in direction and speed along the coast. On minute inspection, it was observed that, wind speed in box 1 was equatorward (northerly) [Figure 4.6] for most months of the year, but north - northwesterly during summer monsoon. The winds changed their direction north-northeasterly by the end of October. In the central box (box 2), the trend was similar to that observed in box 1, with slight variations in the magnitude of the wind speed. But in box 3, winds were north-north easterly till March and then northwesterly upto October. Change in direction towards northeasterly, was observed in November. It is noted that the direction of wind was oriented northerly in box 3 during summer monsoon, while in the remaining two regions; winds were oriented more northwesterly during the same season. This indicates that the SWM winds are influenced by the orographic effect of the Western Ghats present along the coast and thus the winds are oriented along the coast and are equatorward thereby resulting in an apt setting for an eastern boundary upwelling regime in SEAS. Within the SWM season, intra-seasonal

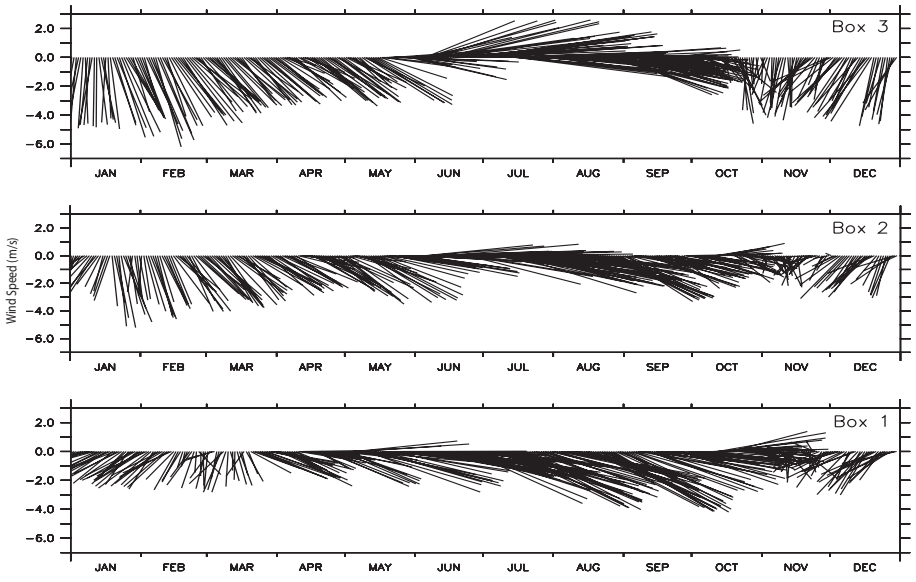

Figure 4.6: Wind Speed and direction at three different locations along the coast (Box1: Lat: 7.5° - 8°N, Lon: 76° - 76.5°E; Box2: Lat: 10.5° - 11°N, Lon: 74.5° - 75°E; Box3: Lat:13.5° - 14°N, Lon: 73.5° - 74°E)

variability was observed which can influence the upwelling related responses from the ocean on those time scales. The definite temporal variability is deduced by applying continuous wavelet transform at these three boxes using the wind stresses derived from 3 day running mean for all the years considered for this study.

4.3.1 Wavelet Transforms

Meridional (Along Shore) Wind Stress To ascertain the periodicity of wind stresses along the coast, daily wind data from the selected boxes were subjected to continuous wavelet transform with Morlet wave as mother wavelet as followed in Torrence and Compo [1998]. Figure 4.7 shows the wavelet transform for along shore wind stress in Box 1 near to the southern tip of India. The figure has three sub figures: a. time series of the meridional wind stress for the entire time period of 2000 to 2008; b. shows the power spectrum of the stress. [In figure 4.7, x-axis indicates the total days and y-axis indicates different frequencies of

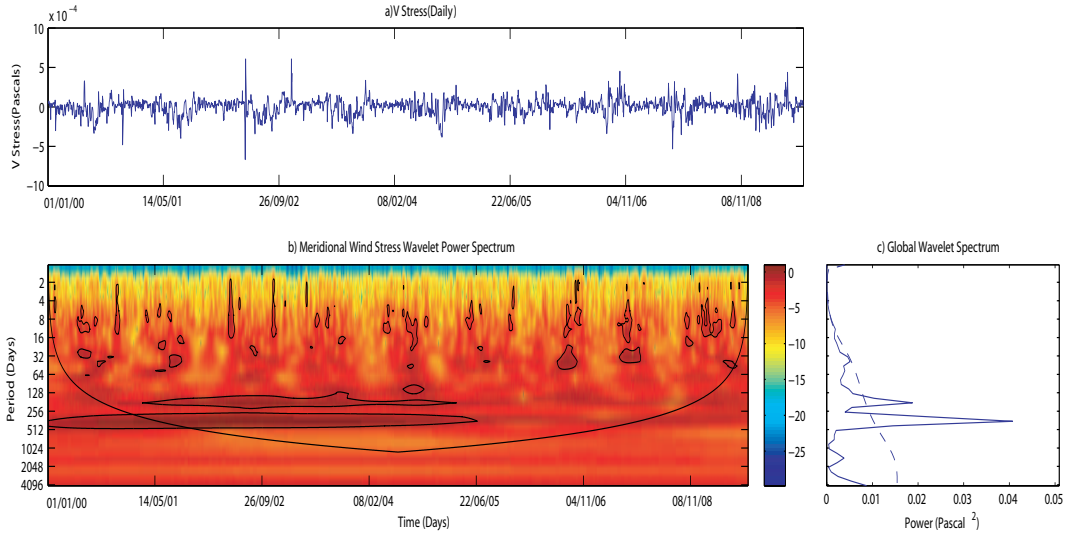

Figure 4.7: a. Time Series, b. wavelet power spectrum and c. Global wavelet spectrum of Meridional Wind Stress in Box 1

variability with a cone of significance set at 95%]; c. presents the global wavelet spectrum. From power and global wavelet spectrum, the predominant frequencies were observed at 4, 8 - 16 days, 32 - 64 days, semiannual and annual modes. The modes which were significant are 32 - 64 day band (Madden - Julian Oscillation), semi annual and annual. Post 2005, the annual and semi annual modes seem to be reduced in intensity while the other modes were still prevalent. This is directly attributed to the decrease in the meridional component of wind speed during that period [Jayaram et al., 2010a].

In the central portion of the southwest coast of India (Figure 4.8), the significant frequencies of variability observed to be were semi-annual and the MJO. Apart from these, there existed other minor frequencies also like 8 - 16 days and annual variability. Within a short distance of 2 degrees ($\sim$ 200km), a factual change was observed in the frequency of variability. Again further, towards the northern region (box 3), the annual mode of variability was observed to be significant while the semi annual mode was completely absent (Figure 4.9). The other dominant frequencies like seasonal (64 - 128 day), MJO were also observed, though not significant. Thus it can be deduced that even though the region

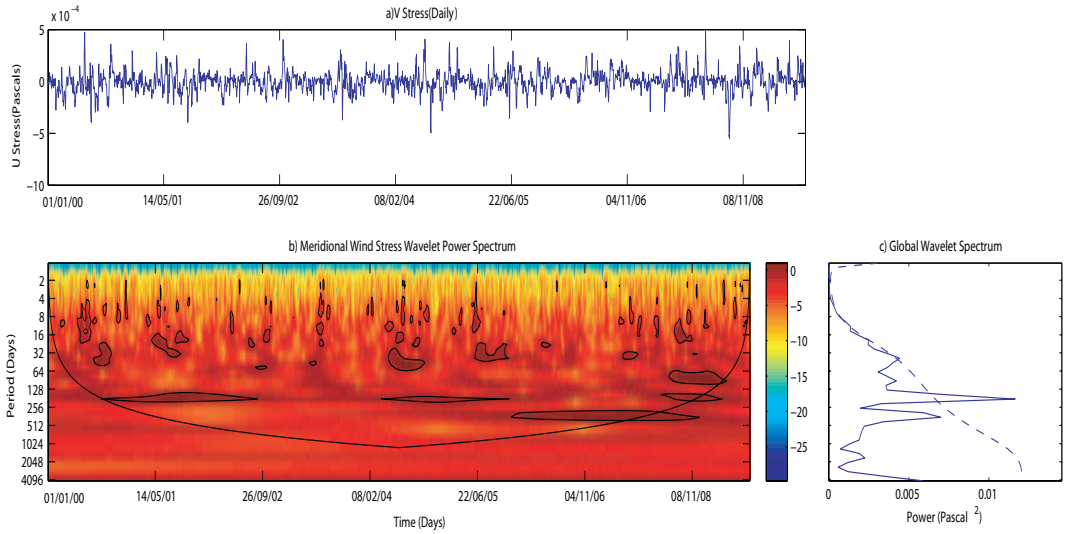

Figure 4.8: a. Time Series, b. wavelet power spectrum and c. Global wavelet spectrum of Meridional Wind Stress in Box 2

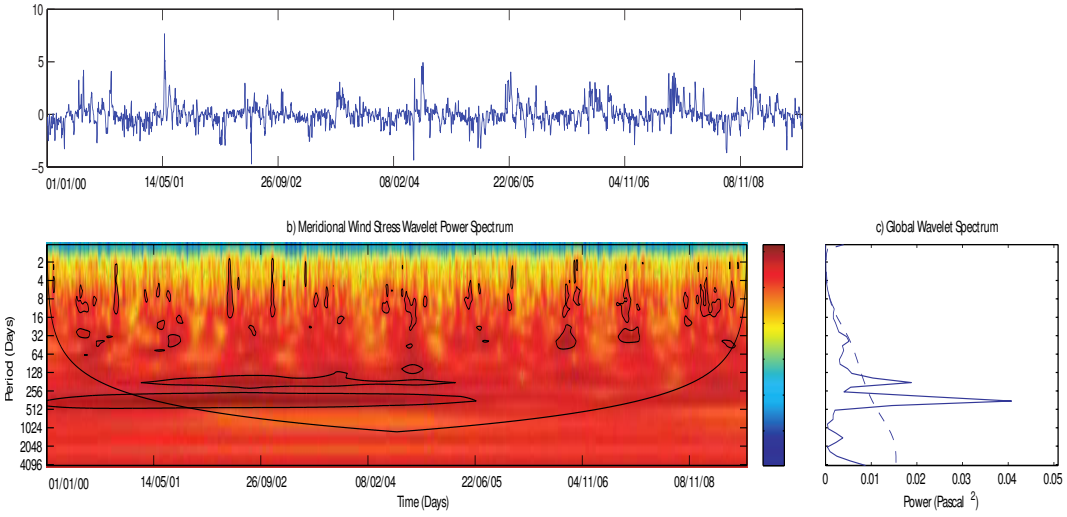

Figure 4.9: a. Time Series, b. wavelet power spectrum and c. Global wavelet spectrum of Meridional Wind Stress in Box 3

is small, there seems to be spatial variations in the wind structure all along the coast. These spatial and temporal variations of the along shore (Meridional) wind stress do have implications on upwelling. It can also be stated that the availability of quality, high resolution remote sensing data products on wind alone can deduce these minor oscillation, that have great potential to affect the upwelling intensity in the region for any given year. A similar wind pattern was noticed in the northern region (box 3) also (Figure 4.9). Thus it can be summarised that the differences in the wind stress structure along the southwest coast of India implicitly modulate the upwelling pattern in the SEAS.

Zonal (Across Shore) Wind Stress Though the zonal wind stress does not have influence on triggering of upwelling, it does have a certain role to modulate the after effects of upwelling, like cooling in SST and changes to primary productivity of the region. In order to ascertain the role of zonal (across shore) wind stress, the zonal component of wind stress for the above selected boxes was subjected to continuous wavelet transform. From the figure 4.10, it can be observed that the annual mode was significant and rest of the minor frequencies were located between 8 - 16 days and less. A noticeable fact was the absence of MJO in the zonal wind stress in this region. Zonal wind stress in box 2 was analogous to that of box 1.

A similar pattern to that of box 1was observed in box 2 also (Figure 4.11). But in the box 3, both semi annual and annual modes were significant. From the time series graph (Figure 4.12), it was observed that there was a peak in each SWM season and during rest of the year, zonal wind stress was minimal while there many many number of minor to major oscillations in the meridional wind stress.

To abridge, on the role of wind in triggering the upwelling in SEAS, it can be stated that the meridional (along shore) wind stress is the main contributing parameter. Meridional wind stress showed different periodicities within the region, though the extent of SEAS being small. The dominant modes of variability are observed to be MJO at 40 - 60 days, semi annual and annual modes. There are other minor frequencies with a time period less than 15 days and these can modulate the upwelling related productivity within the upwelling regime of SEAS.

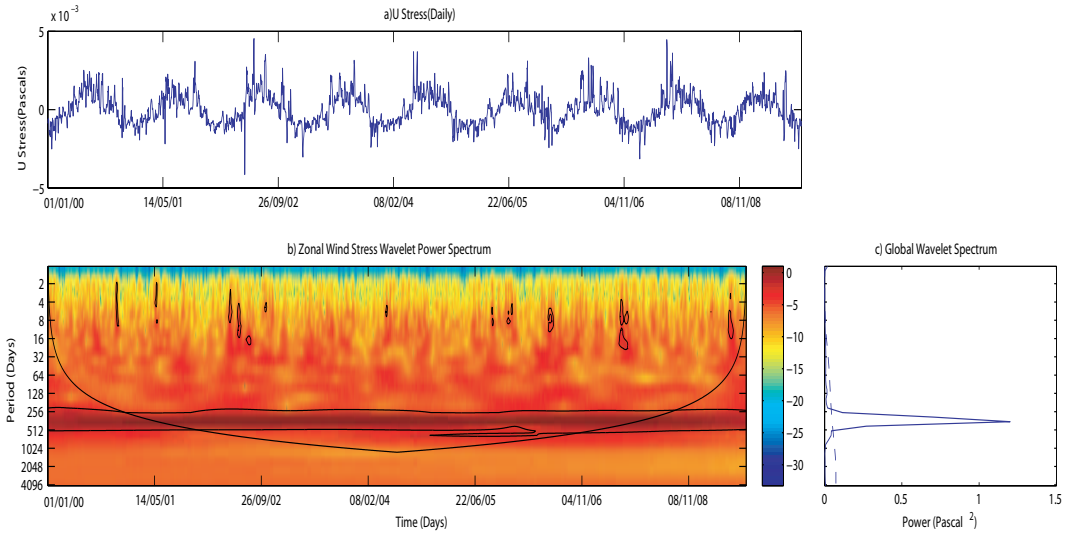

Figure 4.10: a. Time Series, b. wavelet power spectrum and c. Global wavelet spectrum of Zonal Wind Stress in Box 1

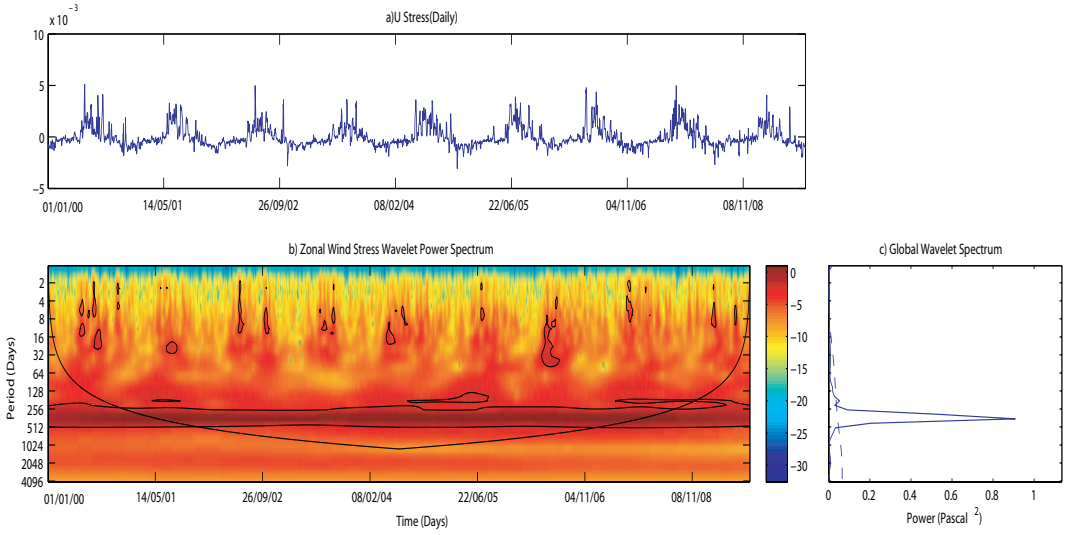

Figure 4.11: a. Time Series, b. wavelet power spectrum and c. Global wavelet spectrum of Zonal Wind Stress in Box 2

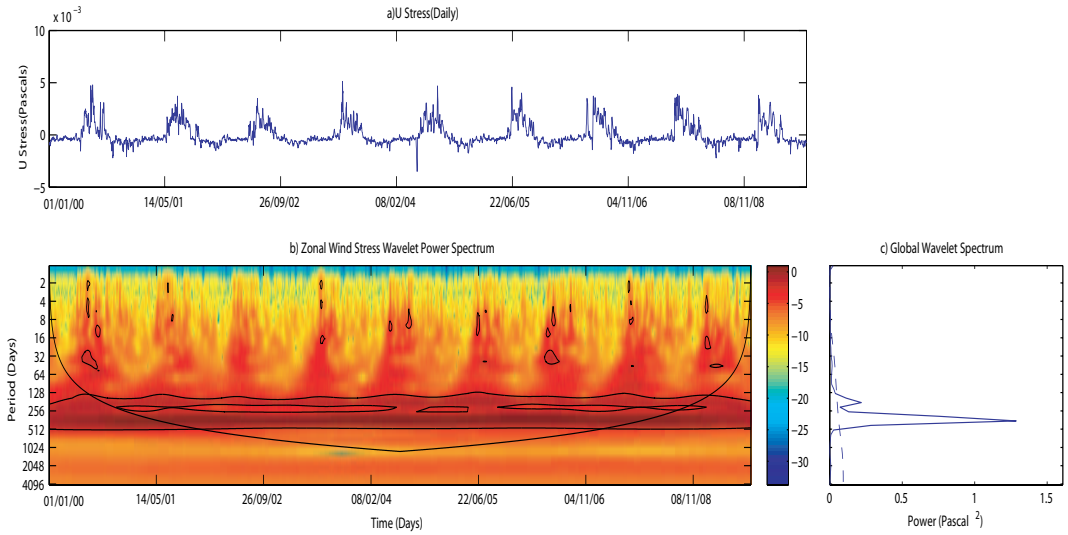

Figure 4.12: a. Time Series, b. wavelet power spectrum and c. Global wavelet spectrum of Zonal Wind Stress in Box 3

In the zonal (across shore) wind stress, the dominant mode of variability is the annual mode. There are minor frequencies on the scales of less than one week. In the zonal mode, the MJO are absent. The role of major and minor frequencies on modulating the upwelling is to be investigated in chapter 5.

4.4 Remote Forcing

The Sea Level Anomaly (SLA) derived from altimeters characterises dynamic topography pertaining to circulation and density field of the entire water column. Also, SLA reveals information on steric effects and the effects of stationary and planetary waves [Fu et al., 1992]. Planetary waves like Kelvin, Rossby and Yanai waves are manifested due to surface wind and buoyancy flux and these will influence the near surface circulation through local and remote forcing, as reported for the tropical Indian Ocean (McCreary et al., 1993, McCreary et al., 1996, Bruce et al., 1994, Schott and McCreary, 2001, Schott et al., 2009, Rao et al., 2010). Altimeter records have made possible the mapping of these planetary waves propagation and their influence on coastal circulation. During SWM

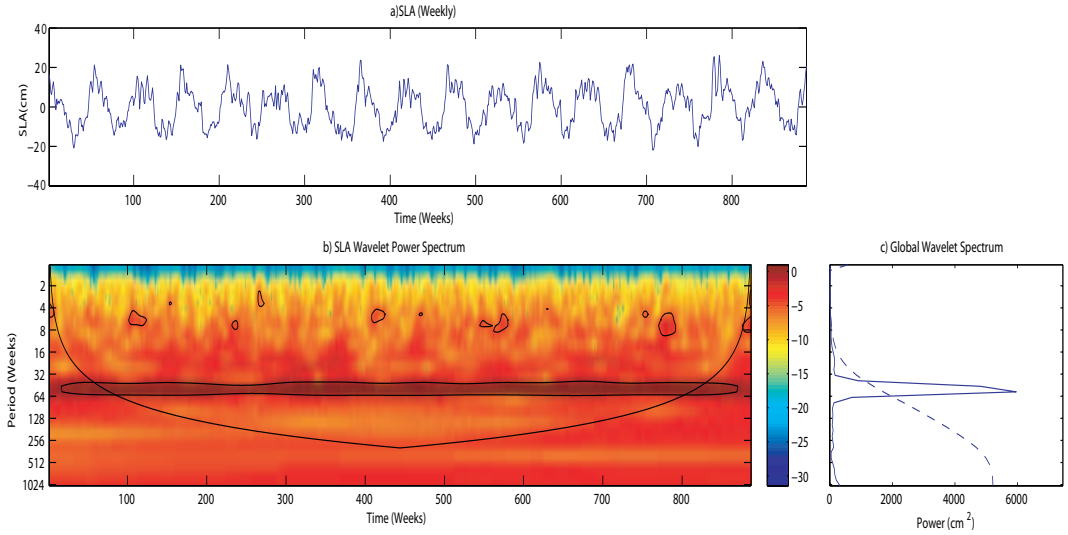

Figure 4.13: a. Time Series, b. wavelet power spectrum and c. Global wavelet spectrum of SLA for Box 1

season, the westward propagating upwelling Rossby waves are triggered off the southwest coast of India and are further strengthened by local wind stress forcing and result in large negative SLA [Shankar et al., 2004]. Thus SLA can be used to index the strength of upwelling and downwelling [Florenchie et al., 2004]. Figures 4.13, 4.14 and 4.15 show the temporal variability, wavelet power spectrum and global wavelet spectrum of SLA along the southwest coast of India. The data used here is the merged weekly SLA for the three boxes (following figure 3.8)selected along the southwest coast of India. The X-axis of these figures shows the number of weeks starting from 1993 to 2009.

Kelvin waves reach the SEAS by early April / May after turning around Sri Lanka. The signatures of Kelvin wave propagation can be observed from altimeter data. In the present work, the periodicity of the SLA along the coast was deduced using wavelet transforms. It is understood from the figures (Fig No: 4.13, 4.14 and 4.15), that the dominant mode of variability is annual. Minor frequencies are observed in box 1 and 3 during 4 - 8 weeks. In order to establish the spatial variability, Emperical Orthogonal Function (EOF) has been computed and presented in Figure 4.16. The first principal component has a variance of

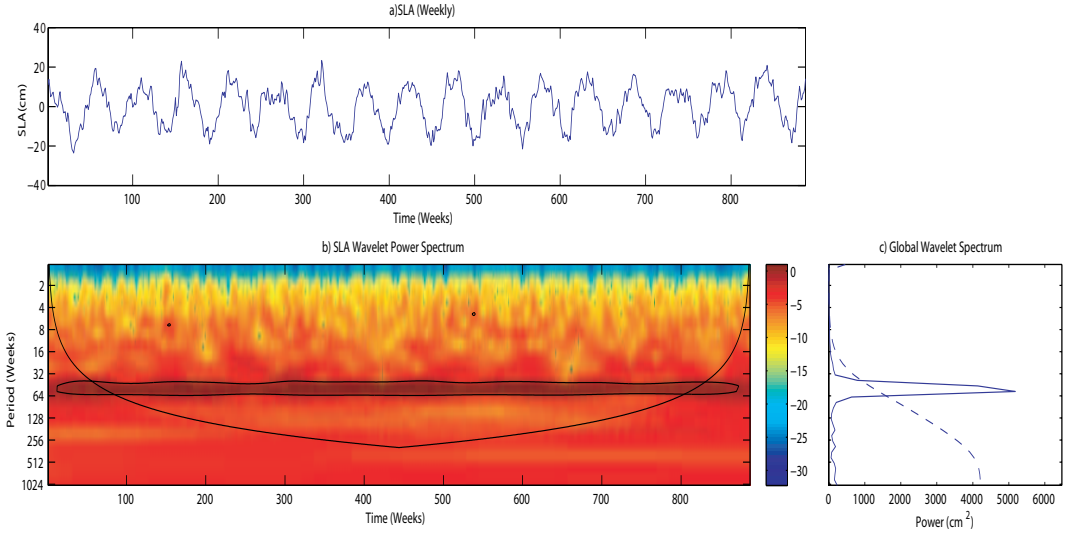

Figure 4.14: a. Time Series, b. wavelet power spectrum and c. Global wavelet spectrum of SLA for Box 2

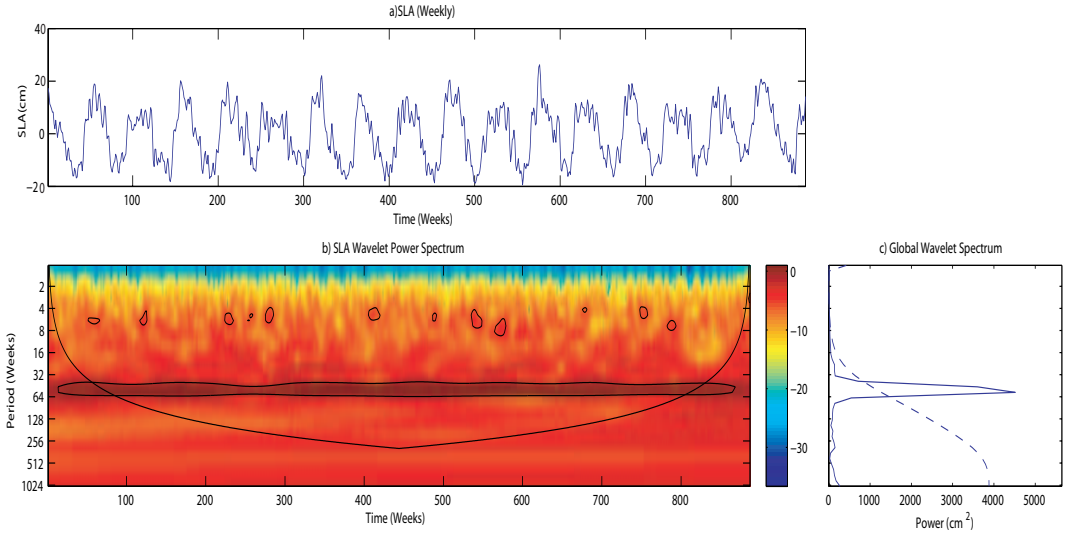

Figure 4.15: a. Time Series, b. wavelet power spectrum and c. Global wavelet spectrum of SLA for Box 3

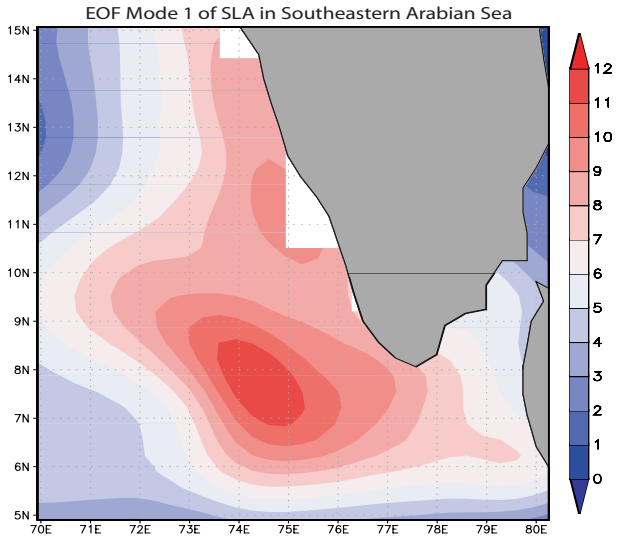

Figure 4.16: Empirical Orthogonal Function(First Mode) of SLA in SEAS

64%, and EOF shows maximum variability between 74° - 75°E and 7° - 8°N. This is the same region of the Lakshadweep High and Low. Westward propagation of the planetary waves is also observed from the EOF mode 1 of SLA in figure 4.16. Thus it can be inferred that maximum variability of SLA in the region is due to Rossby waves.

Long term weekly data plotted along the southwest coast of India as a Hovmuller like diagram with latitude on y-axis and time on x-axis as per the boxes chosen along the coast (Figure 4.17) aids the understanding of the spatial and temporal propagation of Kelvin / Rossby waves. The locations along the coast were selected such that they are parallel to the coast line and situated away by 0.5° from the coast as altimeter data are prone to errors near to the coast. The figure (Figure 4.18) well captures the downwelling / upwelling Rossby waves in this region. During January, positive anomalies were observed all along the coast from 7° to 15°N. By February, the intensity of these positive anomalies had reduced to the north of 10°N whereas, intense positive anomalies were persisting to the south of 10°N. A sort of balanced state prevailed by March with SLA observed to be near zero. By late April, the sea level began to fall and was prevailed completely by negative anomalies by the end of May; this, indicating the arrival

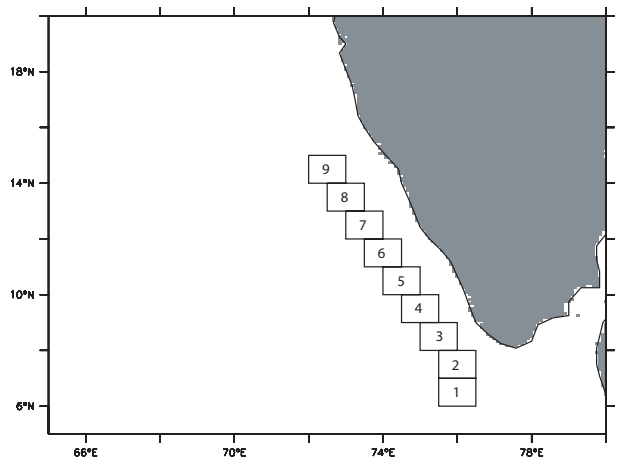

Figure 4.17: Location map of SLA boxes considered along the southwest coast of India

of upwelling Rossby waves in the region. Intense negative anomalies were observed up to 14°N during July and August. Less intense negative anomalies were observed between 8° and 12°N during September and this aspect was observed to be intensifying for a brief period. The positive anomalies were noticed from November which further intensified by December, completing an annual cycle of SLA in the region.

4.4.1 Weekly Evolution of SLA in the northern Indian Ocean

From the long term averages of SLA computed using altimeter data between 1993 and 2009, weekly SLA was plotted to map the propagation of Kelvin waves and the resultant Rossby waves all along the coastal wave guide of the Bay of Bengal and into SEAS (Figures are included in Appendix 1). From the weekly figures the following inferences are derived:

1 1 - 12 weeks: Negative anomalies are prevalent all along the BoB coast indicating the evolution of first upwelling Kelvin wave. During this period, positive SLA was observed in SEAS indicating downwelling phenomenon in the region.

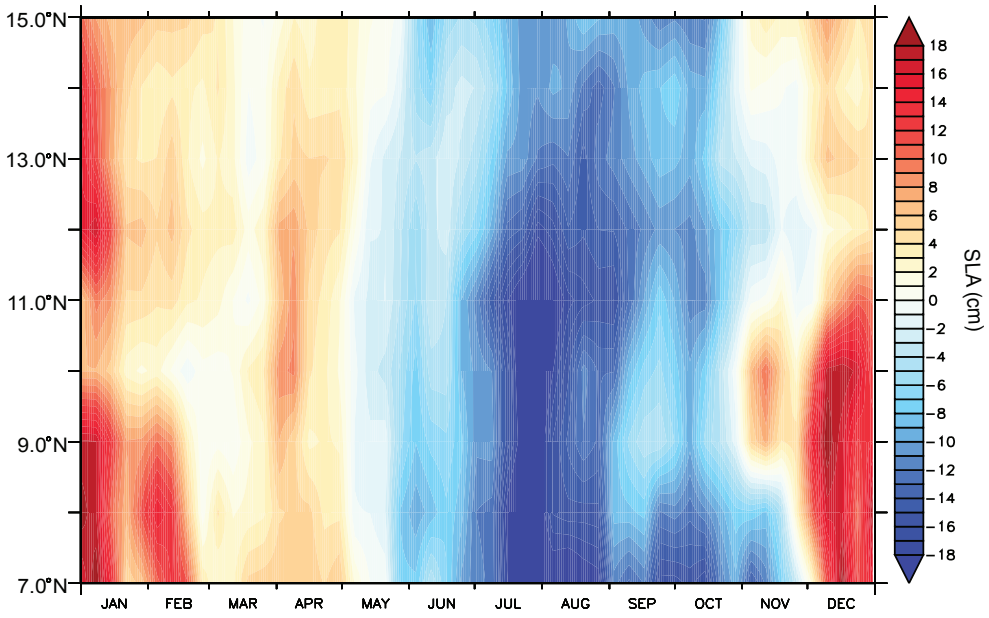

Figure 4.18: Sea Level Anomaly along the coast during a climatological year

2 13 - 24 weeks: During 13 - 18 week period, positive anomalies were observed but with decreasing intensities indicating the gradual shoaling of thermocline in the region. By 19th week, negative SLA was observed along the coast up to 20°N and these negative SLA was found to be heading westward, indicating the westward propagating upwelling Rossby waves. By 22nd week, two distinct eddies were observed, one at the southern tip of India and the other centred on 74°E and located between 8° - 10°N. By this time, upwelling was well established in the region.

3 25 - 36 weeks: The upwelling phase of westward propagating Rossby waves stood enhanced by the wind induced upwelling in this region, thereby, shoaling the thermocline. This is well resembled by the intense negative anomalies. By the 29th and 30th weeks, the Rossby waves were spreading further westward. The first downwelling wave signatures are observed in the BoB as reflected by the positive anomalies. By 35th week, the negative anomalies along the coast were observed to be nearing zero; however they persisted away from the coast.

4 37 - 48 weeks: The westward propagation of negative SLA was present till the 41st week and was replaced by positive SLA by 42nd week indicating the conclusion of the upwelling phase. The positive SLA indicated downwelling in the region, as observed by 47th week. Apart from this, evolution of a second upwelling Kelvin wave was observed in the coastal BoB during this period.

5 49 - 52 weeks: The manifestation of Lakshadweep High can be clearly identified during this period. A well developed high sea level is maintained off the southwest coast of India centred between 74° - 75°E and 7° - 10°N, and it was found to be moving westward. This completes the full cycle of downwelling - upwelling - downwelling phase of sea level in SEAS during a year.

To sum up, on the forcing factors of upwelling in SEAS, it is discerned that the main contributing factors for the generation of upwelling are the along shore wind stress and remote forcing. The present study concentrates on the modulation of upwelling vis-a-vis these forces. The intra-seasonal variability of the wind stresses and the strength of coastal Kelvin wave have the potential to modulate the after affect of upwelling, say, the biological productivity. Thus it is on these minor frequencies that one needs to concentrate upon - this aspect is dealt in chapter 5. From the wavelet transforms of both the components of wind stress, it is observed that the meridional (along shore) component of the wind stress showed variability within the basin and has both significant semiannual and annual modes of variability along with other minor frequencies like the MJO. The zonal component of wind stress has only annual mode of variability and the MJO are absent. Wind stress curl is positive near to the coast during the SWM season indicating the presence of upwelling. Wavelet analysis of SLA along the coast showed significant annual mode of variability. To discern the region of variability, the SLA data was subjected to Empirical Orthogonal Function on spatial scale. The resultant first mode was having 67% variance and has been located between 74° and 75°E longitudes and 7° and 9°N latitudes, which is the region of Lakshadweep High and Low. The propagation of these waves results in high and low in winter and summer monsoon seasons, respectively. Since these offer

maximum variability in this region, they are reflected in the first mode of EOF of SLA. Hovmuller diagram of SLA along the coast indicated the northward limit of these waves and also the strength of upwelling as obtained from SLA studies. The response of ocean to these external forces will be discussed in the next chapter.

5

SEAS Response to Forcing Factors

5.1 Introduction

The impact of upwelling is often perceived as the presence of cooler SSTs and heightened surface CHLA in its region of occurrence. Reversibly, satellite products such as SST and surface CHLA throws light on the extent of upwelling region. In SEAS the forcing mechanisms that trigger upwelling are remote forcing of planetary waves and atmospheric forcing due to the SWM winds; it has been established in the previous chapters that these forces influence upwelling on different time and space scales. In order to determine how the ocean has responded through upwelling, induced by above mentioned forces, on different space and time scales, a detailed analysis has been carried out with respect to the signatures of responses.

5.1.1 Relation between Wind Stress, SLA and SST

The annual variation in the local SST near to the coast in the upwelling regions is associated mainly with annual variations of local equatorward along shore wind stress and solar radiation. Another process (say, remote forcing) on longer and shorter time scales may also influence SST. Thus, SST can indirectly serve as a measure of upwelling and its intensity. Also, coastal upwelling lifts the nearshore

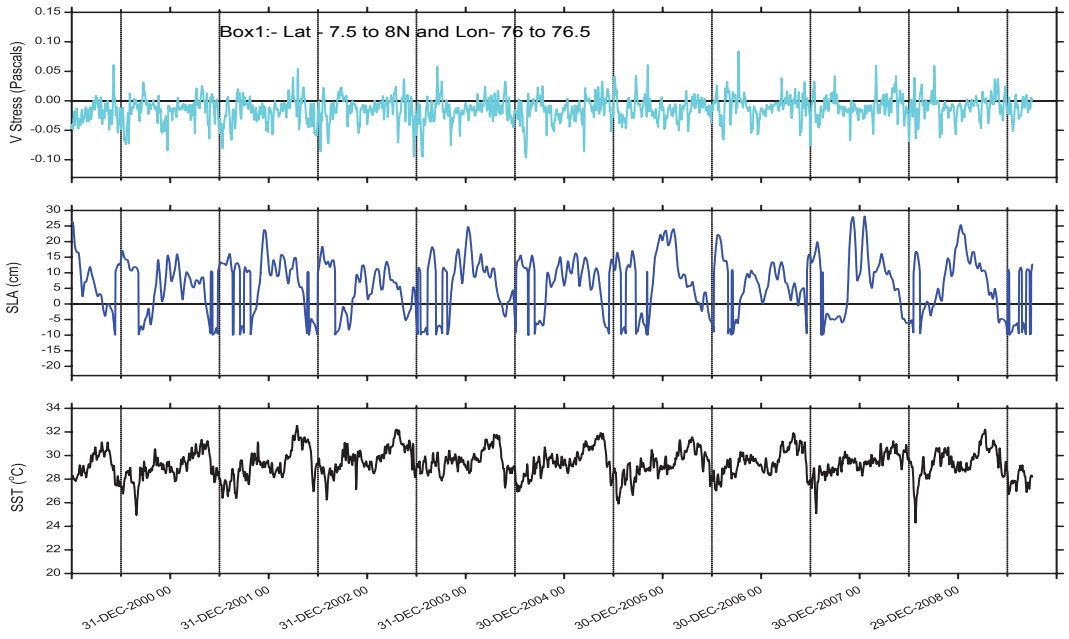

Figure 5.1: Time Series of Wind Stress, SLA and SST in box 1

thermocline and brings about a drop in sea level due to increased mean density in the water column. These sea level fluctuation(s) are associated with poleward propagating coastally trapped Kelvin waves in the ocean [Hormazabal et al., 2001]. In order to ascertain the relationship between external forces and the response of SST variation on time and space scales, an analysis involving, TMI measured SST, wind stress derived from QuikScat measured winds and merged altimetry data from AVISO was conducted. Daily and monthly climatological means were computed from relevant satellite observations for the common period of data availability which was between 2000 and 2009. SST, along shore wind stress and sea level anomaly for the above ten years were plotted at three different regions (Figure 3.8) along the southwest coast of India as followed in Chapters 3 and 4. The time series data was filtered using a triangle filter for smoothing. This smoothing was done in order to eliminate the influence of extreme winds and any other spikes so as to arrive at a conclusion for a normal upwelling event. Figures 5.1, 5.2 and 5.3 show the time series of along shore wind stress, SLA and SST in box 1, 2 and 3, respectively. From these figures, it was observed that

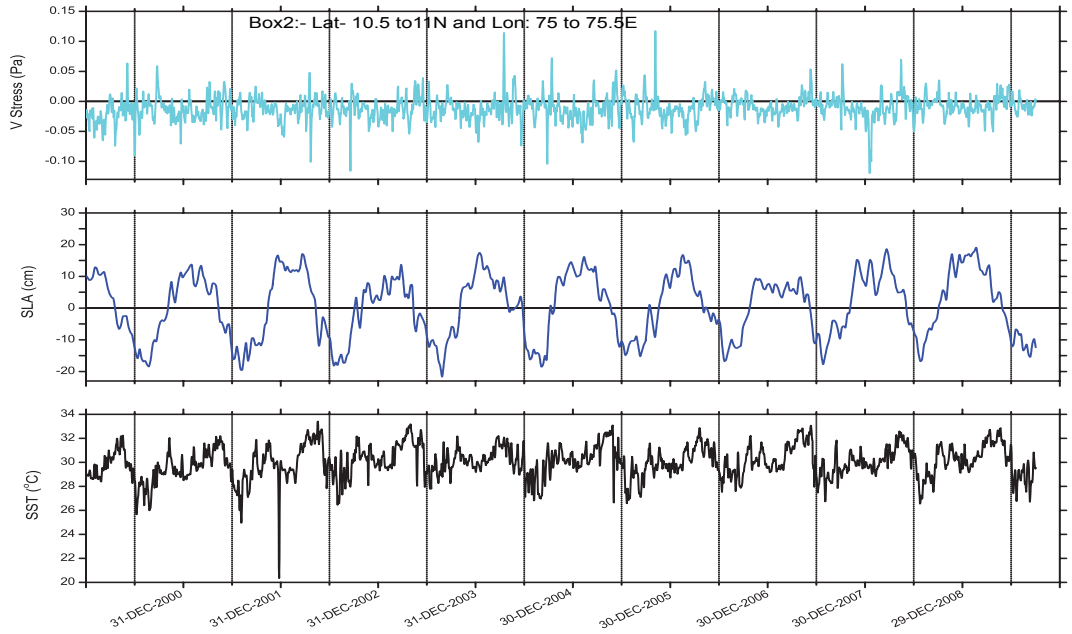

Figure 5.2: Time Series of Wind Stress, SLA and SST in box 2

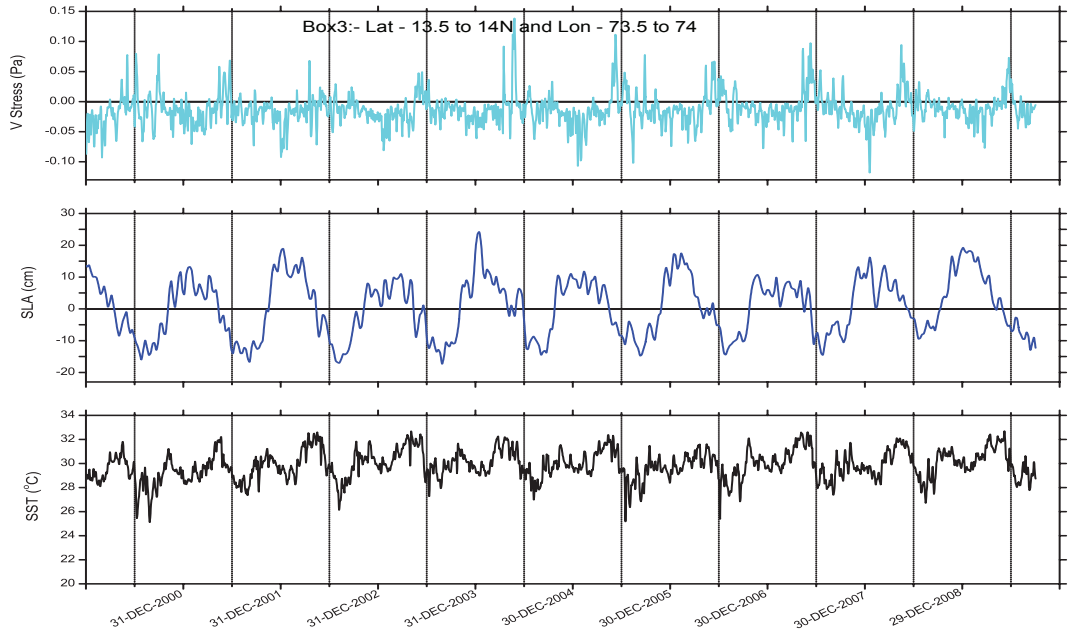

Figure 5.3: Time Series of Wind Stress, SLA and SST in box 3

wind stress was equatorward for most of the year except during the pre-and post summer monsoon. Interannual and intraannual fluctuations too were observed at all the locations. These fluctuations would then force variable Ekman transport and that lead to SST variability. The interannual fluctuations of wind stress and SST reflect the influence of changing monsoon intensity and the resultant features in the Indian Ocean region. Maximum equatorward wind stress was observed in box 1 during 2003 and was not present in other boxes. The pattern of wind stress in boxes 2 and 3 was almost similar for all the years. Sea level anomaly also showed distinct pattern in box 1 when compared to the other two boxes; in box 1, intra annual fluctuations were more evidently dominant. It is known from the literature (Bruce et al., 1994, Shankar and Shetye, 1997) that this region is more volatile with respect to the surface circulation due to the impact of westward moving Rossby waves that are being radiated from the coastally trapped Kelvin waves. The seasonal and intra-annual variability was rather weak in box 2 and box 3 regions. The sea level changes were showing more of annual variability than intra-annual variability, inferred as a wave like structure, apart from oscillations with minor frequencies. The magnitude of positive SLA was greater in box 1 while negative anomalies were greater in boxes 2 and 3. The sea level fluctuations found along the coast was a combined result of remote forcing and wind induced upwelling. SST exhibited inter-annual as well as intra-annual fluctuations at all the boxes, mostly in annual and synoptic scale.

To investigate possible links among along shore wind stress, SLA and SST along the southwest coast of India, coherence spectra for these variables were computed. Statistics showed vital results on time and space scales between forces and the resultant SSTs. Figure 5.4 shows the coherence spectrum between along shore wind stress and the SST in all the three boxes along the southwest coast of India. From this figure, it was understood that in box1 (southern region), the dominant peaks are at 4 - 7 days and again at 70 to 100 days. It is well known fact that the 70 to 100 days oscillations are pertaining to seasonal variations. The peak at 4 - 7 days is due to the influence of synoptic variations in wind on SST. Therefore it is understood that in this region, the variability in SST is due to the winds and thus can be inferred that cooling of SST takes place after 4 - 7 days of wind action in the region depending on wind intensity. Other smaller peaks

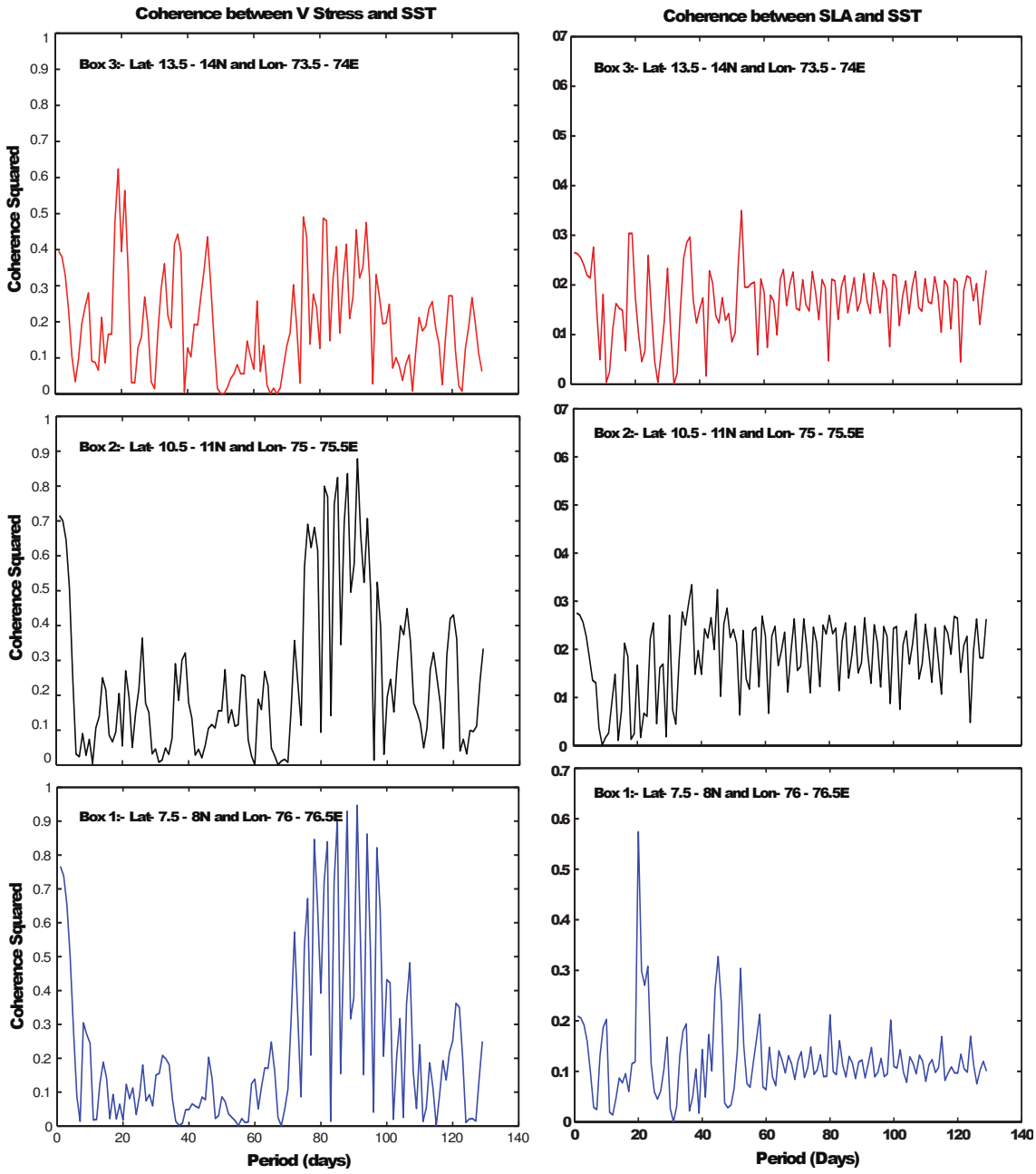

Figure 5.4: Coherence between SST and V Stress (left panel); SLA (right panel) over SEAS; These three boxes correspond to the boxes shown in figure 3.8

are not dominant and thus can only be summed up as synoptic variations on a day-to-day scale. In box 2 also, a similar pattern to that of box 1 was noticed in the 4 - 7 day scale followed by a notch higher intensity in the 20 - 60 day region and again distinct seasonal signature (within 70 - 100 days). In third box, the 4-7 day period, signal was weak whereas there was a strong indication of another signature at the 20 - 30 day band as well as the seasonal fluctuations occurring in the 80 - 100 day periods. This indicates that the wind structure along the coast is varying and thereby varying the influence on the local SST. Figure 5.4 shows the coherence between SLA and SST for all the three boxes along the coast. From box 1, two prominent peaks, one at 20 days and the other at 45 days were observed and the rest were mostly subdued. In the other two boxes, there were no prominent peaks except randomly at 20 - 40 - 55 day periods; however, such seasonal signatures were not observed in SLA.

Detailed analysis to deduce cause-effects between wind forces, remote forcing (SLA) and SST leads to infer the following: for the southernmost and central regions of the southwest coast of India, the region clearly defines impacts due to wind forces in the order of 4 - 7 days leading due to a reduction in SST, coincident with the upwelling season. Such impacts are not prominent towards the northern sector. Referring to figure (5.1), the SST reduction occurs during the SWM season or otherwise during the upwelling regime wherein the remote forcing of planetary waves often fall in the period of 20 days, which stands out most distinct in the box 1 region.

As previously discussed, associated with upwelling, the surface features indicated cooling in SST, and concurrently, the analysis of the above figures indicates the link to such cooling events, wherein the wind stresses can be attributed to bring about a reduction in SST and such wind impacts do occurs in a 4-7 day cycle. Thereafter, in the absence of such periodicities, except for seasonal signatures, the resultant SLA has a peak around 20days which refers to the influence of planetary waves (remote forcing), mainly prevalent in the southernmost regions. To the contrary, box 3 located towards the northern sector; evidence a composite impact on SST which is brought about probably by identical combination of wind stresses and SLA of varying orders, falling within 20-60 days (multiple peaks). Further, based on magnitude of coherence, the impact of planetary waves does

not bring about good influence on upwelling, inferred through SST. Likewise, for the central coastal regions, though remote forcing of variable periods less than 40days are inferred through SLA variation, the lower order 4-7days period wind stress appear much dominant in bring about SST variability. Another important conclusion that could be drawn from this analysis is that the peak in SLA in 40day band was due to remote forcing of planetary waves, generated elsewhere and next, that in 20day band are due to the locally generated Kelvin and Rossby waves.

5.2 Upwelling Index derived from SST

5.2.1 Latitudinal Temperature Gradient [LTG]

Direct measurement of upwelling is often difficult due to logistical reasons and harsh ocean status during SWM. A method to quantify upwelling is by making use of 'upwelling indices' as a proxy for the same. SST can be made use of to deduce an index of upwelling. One of the characteristics of coastal upwelling is that the coastal surface water is of lower temperature than that of the surrounding offshore waters. The coastal upwelling index based on SST is defined as the temperature difference between the coastal waters and of those waters which are five meridians offshore, along the same latitude. In some of the previous studies of similar kind, by [Naidu et al., 1999], Smitha et al. [2008] and Munikrishna [2009], the offshore limit for computing temperature gradients were taken as three degrees and mid ocean, respectively. In yet another study on the inter-annual variability of upwelling along the North African coast by Nykaer and Camp [1994], the five meridians distance was selected as the outer limit of offshore box and results were found to be fruitful. A detailed account on the offshore limit of coastal process along with upwelling was presented in Antony et al. [2002]; *in-situ* and altimetry measurements had shown the offshore limit of coastal processes along the west coast of India is approximately 350 to 400kms. The method of selection of three degree meridian and mid-ocean difference, as applied to the present study region, say, off 10°N and down south, cooler SSTs were observed as far as 72°E meridian which is approximately four degrees offshore from the coastline – and this reflects

on the drawbacks of these methods. Following Antony et al. [2002] observations and also in order to have uniformity all over the study region, yet retaining similar oceanographic conditions, five degree meridian distance was taken as a benchmark for computing temperature gradients for coastal upwelling index for southwest coast of India. This upwelling index is referred to as Latitudinal Temperature Gradient (LTG), which is a function of temperature difference along given latitude and time. The geographical positions (8° to 15°N) for which LTG have been computed were selected on the middle of the shelf region, i.e., along the coast at 200 m depth contour which was taken as the offshore limit of the coast line [Shetye et al., 1985] as shown in figure 4.4. Spatial resolution of the data being very fine and also different from that of wind products, it was cumbersome to compute LTG for every grid point. In order to get a meaningful result, LTG has been computed for a 1 x 1 degree box averaged SST along the coast and a box of similar size, five degrees offshore.

With the onset of summer monsoon, upwelling starts from the southern tip of India with cooler SST and propagates northward along the coast. From SST climatology, progressive cooling of the ocean surface with each passing month can be observed from June to August (Figure. 5.5). This cooling event began dispersing by September and will be completely replaced by warm waters by October. During all the four months [June - September],a patch of warmer waters was observed between the coastal and mid ocean. The cooling of mid ocean to the north of 10°N is because of the open ocean upwelling during the summer monsoon [Muraleedharan and Kumar, 1996]. This justifies the selection of 5 degree spacing between the coastal and open ocean waters to compute the LTGs.

The climatology of SST upwelling Index computed between 1988 to 2007 data presents an insight into the spatial distribution of the temperature gradients along the coast. From figure 5.5, the maximum postive gradient was observed from 8° to 10°N during the period April to December, highrer positive gradients greater than 0.5°C were observed from June to September up to 12°N latitude.

The same results are obtained from the World Ocean Atlas of 2001 with slight variations in the northern latitudes of the region; confirming the indices computed from satellite measurements to be correct. The correlation obtained between these two climatologies is 0.85. The increase in temperature gradients during June to

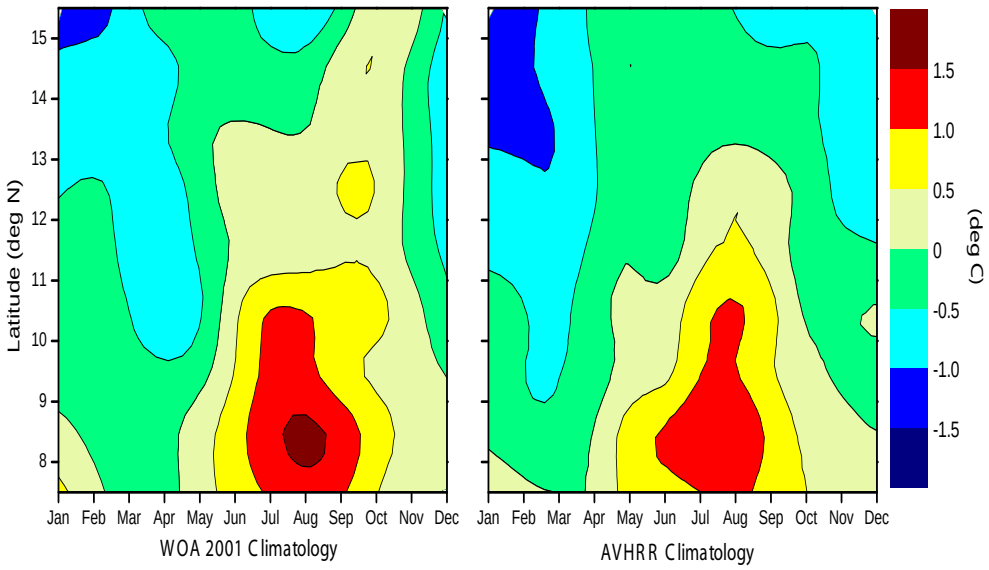

Figure 5.5: LTG along the southwest coast of India derived from World Ocean Atlas 2001 and AVHRR Climatology

September coincides with the SWM winds and the intensification of upwelling. We attribute the decrease in the temperature well before the onset of SWM winds to the presence of remote forcing induced by the upwelling Kelvin wave that sets in the actual process of upwelling in the region (Johannessen et al., 1987, Haugen et al., 2002, Shenoi et al., 2005). North of 13°N, negative LTGs were observed all throughout the year within the range of 0° to −0.5°C. A downwelling process was observed between 13° and 16°N latitudes from January to February with LTGs ranging from −1.0° to −1.5°C. The offshore cooling of the Arabian Sea during the northeast monsoon to the north of 15°N is attributed to the impact of convective cooling taking place in the northern Arabian Sea. Thus negative LTGs were observed as offshore waters are cooler than the coastal waters. A mild downwelling process was observed till 12°N latitude from November to the end of March.

5.2.2 Correlation between Wind and SST based Upwelling Indices

In the previous chapter (Chapter 4), an index of upwelling based on Ekman transport, was presented for quantification of upwelling. The indices based on SST follows a different set of parameters and platform; an intercomparison of these is necessary to build up confidence on the index for this region, where SWM (upwelling periods) and non-monsoon (non-upwelling periods) cycles recur. Cross correlation was computed between the two indices for each month and in each degree box and are represented spatially (Figure 5.6). Positive correlation was observed in the winter months alone for the latitudes north of 12°N and also between 8° and 9°N (February and March). Also, the entire coast line had negative correlation values, mostly prevailing during March, April and May. This period (non-upwelling) coincided with the event(s) when SST was very high and SWM winds had not set in for initiating upwelling. Positive correlation was observed between the two indices off 8° and 11°N during July only and from 14° to 15°N in the months of August and September, which is, of course, the upwelling period. Another interesting observation was the negative correlation during August and September between 8° and 10°N. The reason for this form of correlation is due to the fact that wind speeds will be higher during the initial stages of monsoon, till July and thereafter, will retreat, slowly towards the end of monsoon phase (i.e., by end of September). But the memory of the ocean with respect to SST cooling is retained for longer duration, which had been observed during late monsoon months of August and September [Muraleedharan et al., 1995]. Thus the study based on cross correlation between the climatologies of both the indices enhances our present understanding on the upwelling along the west coast of India [Jayaram et al., 2010a].

5.3 Upwelling Induced Productivity

A major impact of upwelling in the ocean is that the region turns out to be the most productive compared to the neighbouring non - upwelling regions. Parts of the Arabian Sea are some of the important productive zones in the Indian

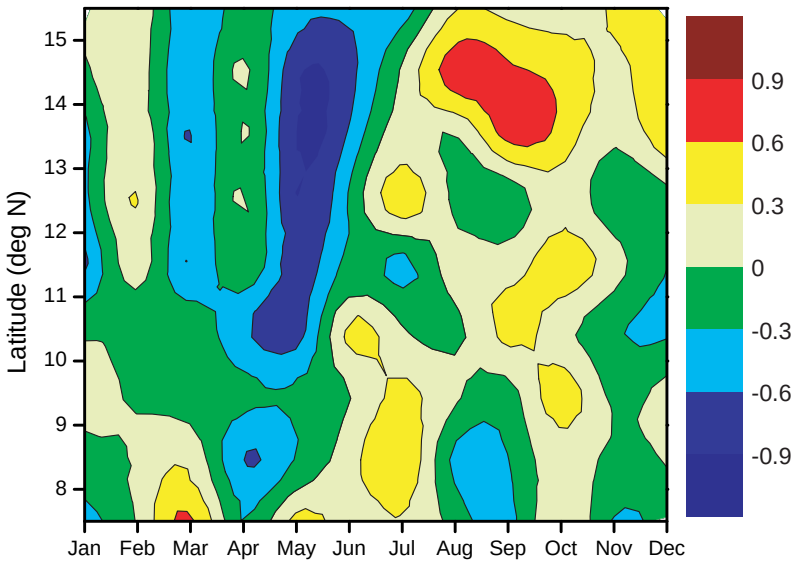

Figure 5.6: Correlation between indices based on Ekman Transport and LTG

Ocean. The state of productivity is often well inferred by satellite remote sensing by making use of the visible spectrum, which inturn quantitatively accounts for the presence of chlorophyll. In other words, CHLA measured by remote sensing techniques helps us to delineate the upwelling regions from non-upwelling. In this context, SEAS which is a productive zone exhibited prevalence of CHLA predominantly during upwelling season. The seasonality and the spatial extent of the chlorophyll blooms have been well demonstrated by both model simulations and *in-situ* observations (Levy et al., 2007, Vimalkumar et al., 2008). Even though the SEAS region is productive for a lesser part of the year compared to the northern part of the west coast of India, it contributes to 52.9% of annual fish yield while the northeast coast contributes to 47.1% [Sanjeevan et al., 2009]. These differences in productivity are influenced by diverse physical forcing(s). Upwelling in the region starts in the subsurface well before the onset of SWM but the resultant primary productivity signatures like heightened surface CHLA starts to emerge only after the onset of SWM winds [Smitha et al., 2008]. These winds churn the ocean and thereby increase the extent of mixing. Eventually, the mixing paves way for the subsurface nutrients to upwell towards the surface and

thereby increase the surface productivity. A detailed analysis has been carried to ascertain the relation between wind, mixed layer and productivity in terms of CHLA, on both time and space scales.

5.3.1 Relationship between Wind and CHLA

Global climate change research is primarily successful only when one can identify and quantify the factors controlling the primary productivity and the related responses [Falkowski et al., 2000]. Environmental forcing modulates the spatial and temporal changes for the profusion of phytoplankton and their communities by affecting the mixed layer light availability and other key determinants of the photosynthesis [Milutinovic et al., 2009]. To study and understand the variability and distribution of the upwelling in SEAS, the satellite measured surface wind stress products along with ocean color and MLD, which are affected by the availability of light in the ocean and thereby productivity of the region, were analyzed for their spatial cross-correlation, inter-annual variability for a period of 9 years (2000 - 2008).

Temporal Variability Over the oceans, wind plays an important role in determining stratification and de-stratification processes that could determine the bloom timing in waters. The stirring of upper layers by convective overturn and winds are the major mechanisms regulating the phytoplankton growth (Cushing, 1975, Kim et al., 2007). The timing of blooms is often related to wind speed; though there exists a relation between wind stress and the initiation of blooms, the mechanisms that link them are not very clear [Kim et al., 2007]. In order to understand these mechanisms, area averaged weekly wind stress; CHLA and MLD are considered for the period between 2000 and 2008 to understand upwelling and related processes in the region.

To obtain a clear understanding on the temporal relationship between wind forcing, MLD and CHLA and thereby the upwelling system in SEAS during 2000 to 2008, further analysis has been carried out as penned in the following lines. Wind data is filtered using an 8-day moving average to match the temporal resolution of CHLA. A hypothesis is put forward that, the CHLA begins to bloom

as and when wind stress starts weakening. Kim et al. [2007] hypothesized similar relation for Japan/East Sea. The rationale behind this hypothesis is that, gradual decrease in wind stress stabilizes the water column, thereby upwelling the nutrients, which are utilized by phytoplankton in the presence of sunlight resulting in enhancement of productivity. In this whole chain of events, there should be a time lag between the decrease in wind stress and increase in CHLA which allows phytoplankton cells to grow up to a measurable density. To reveal the functional time lag, 8day CHLA and wind stress were normalized with the maximum value for that particular year and was plotted as a time series graph for each year individually (Figure 5.7).

The picture depicts singular annual occurrence of strong wind stress and CHLA during the SWM but generally with a time lag. A time lag of approximately 2 - 3 weeks is observed between the decrease from the peak wind stress and enhancement of CHLA. Only exceptions being the years 2004 and 2006 where there is a lengthy gap between the decrease of wind stress and the sighting of peak CHLA concentration. Years 2007 and 2008 were observed to be abnormal years with respect to chlorophyll concentration. It is observed from the data that the average CHLA remained very low for the region but there were some unusual spurt in the concentration for a week in both the years which resulted in vast decrease in the normalized values for the rest of the year. In-case if it was observed for only one particular year, it could be treated as an error in the data and could have been flagged, but this unusual spike was observed in the subsequent year of 2008 and therefore had to be considered not as an outlier. Extensive quality check had been undertaken to confirm the values obtained using data from SeaWiFS, MODIS onboard both Terra and Aqua and it is confirmed that the increase in chlorophyll concentration for a short period is indeed correct value and not an outlier. Another noticeable fact in CHLA pattern in all the years is that there existed two peaks resulting in bimodal variability during SWM, however during 2006 and 2008 primary peak is not prominently observed which need to be backed up with continuous *in-situ* biological data sets.

A close scrutiny of results from these figures explicitly reveals the existence of intra-seasonal oscillations within this small region (which is a subset of Arabian Sea) and with in a short span of 4 month encompassing the SWM period.

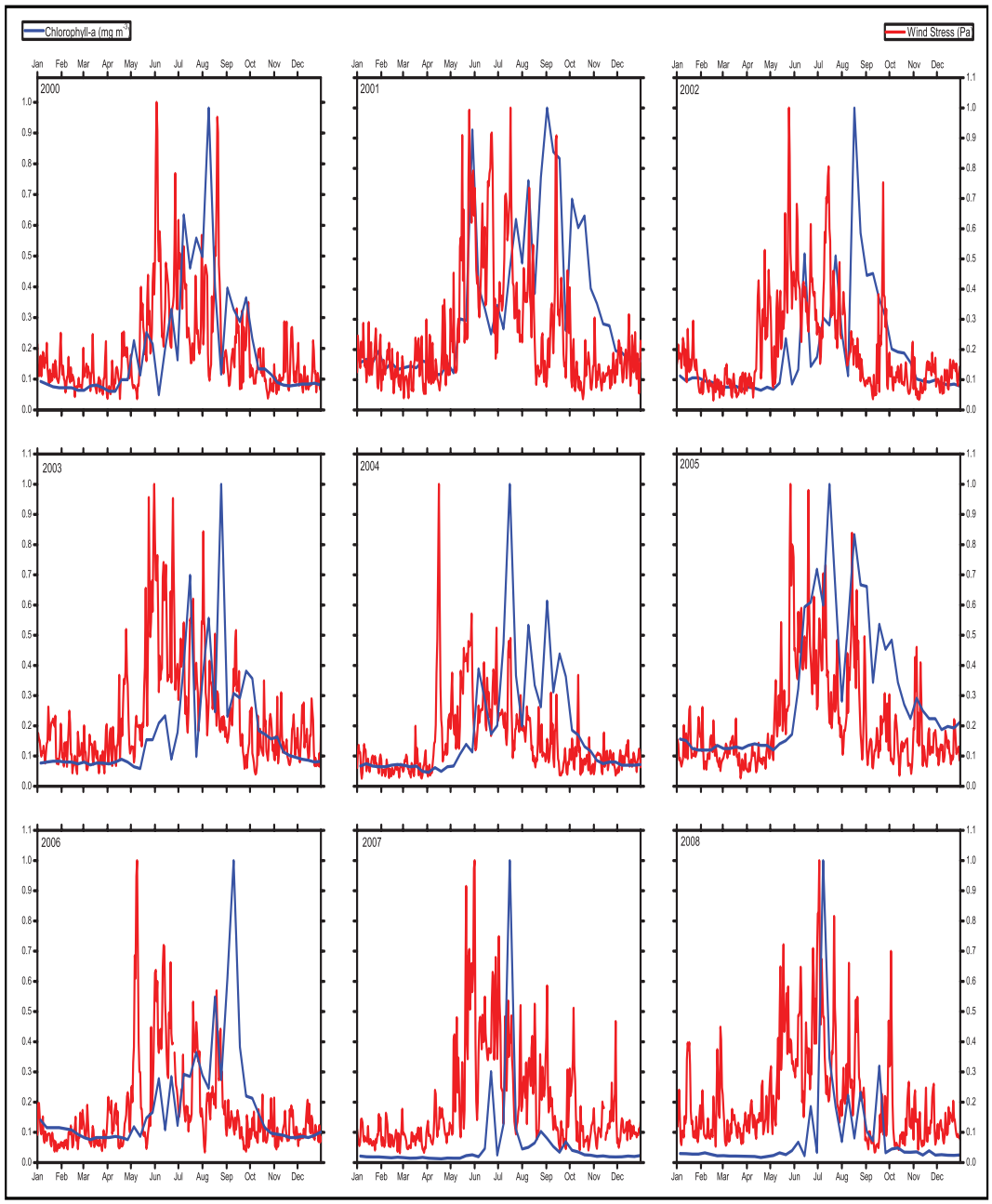

Figure 5.7: SeaWiFS mean chlorophyll (blue curve); QuikScat 8-day moving average filtered daily mean wind stress (red Curve)

These limitations however do not hinder the SEAS influencing fisheries and local climate. In order to further understand the processes that relate wind stress, MLD and CHLS, especially during the upwelling, time series is plotted for the SEAS during the SWM season in the following section (except 2008 for absence of data pertaining to the mixed layer depth). Wind stress, CHLA and MLD are normalized with the maximum value for that particular year and plotted for the SWM season as shown in figure 5.8.

It can be noticed that during all the years, whenever the wind stress was high, the subsequent CHLA was less. Similarly, whenever there is an increase in the wind stress, then the MLD deepened during the subsequent weeks and shoaled when a drop in the wind stress is observed. This proves our earlier hypothesis that CHLA increase should be feasible with a drop in wind stress, following a thorough mixing and upwelling of nutrients to the surface. In other words, it can be stated that upwelling is pronounced when wind shows a decrease or lull period of the monsoon which is an important observation of this study and could influence the future of monsoon and upwelling based studies. From the figure (5.8), it is noticed that CHLA content was appreciable in the region during 2000, 2001 and 2005. 2007 was least productive among all the above years. The interannual variability of the upwelling phenomenon will be discussed in chapter 7.

5.3.2 Spatial Distribution of CHLA

Figure 5.9 shows the mean and standard deviation of CHLA in the region between 1998 and 2007 obtained from SeaWiFS measured CHLA records. From the figure, it is observed that the offshore extent of CHLA is approximately 250 - 300kms from the coast. The region of maximum variability is observed to be between 8° - 10°N and 76° 77°E where the intensity of upwelling is utmost [Jayaram et al., 2010a], as read from the standard deviation plot. Empirical orthogonal function (EOF) was computed for CHLA in SEAS. First mode of EOF (Figure 5.10), showed 69% variance and the second mode showed 8%. It can be observed that the maximum variable region of CHLA in SEAS is between 8° and 10°N, which is marked in red colour.

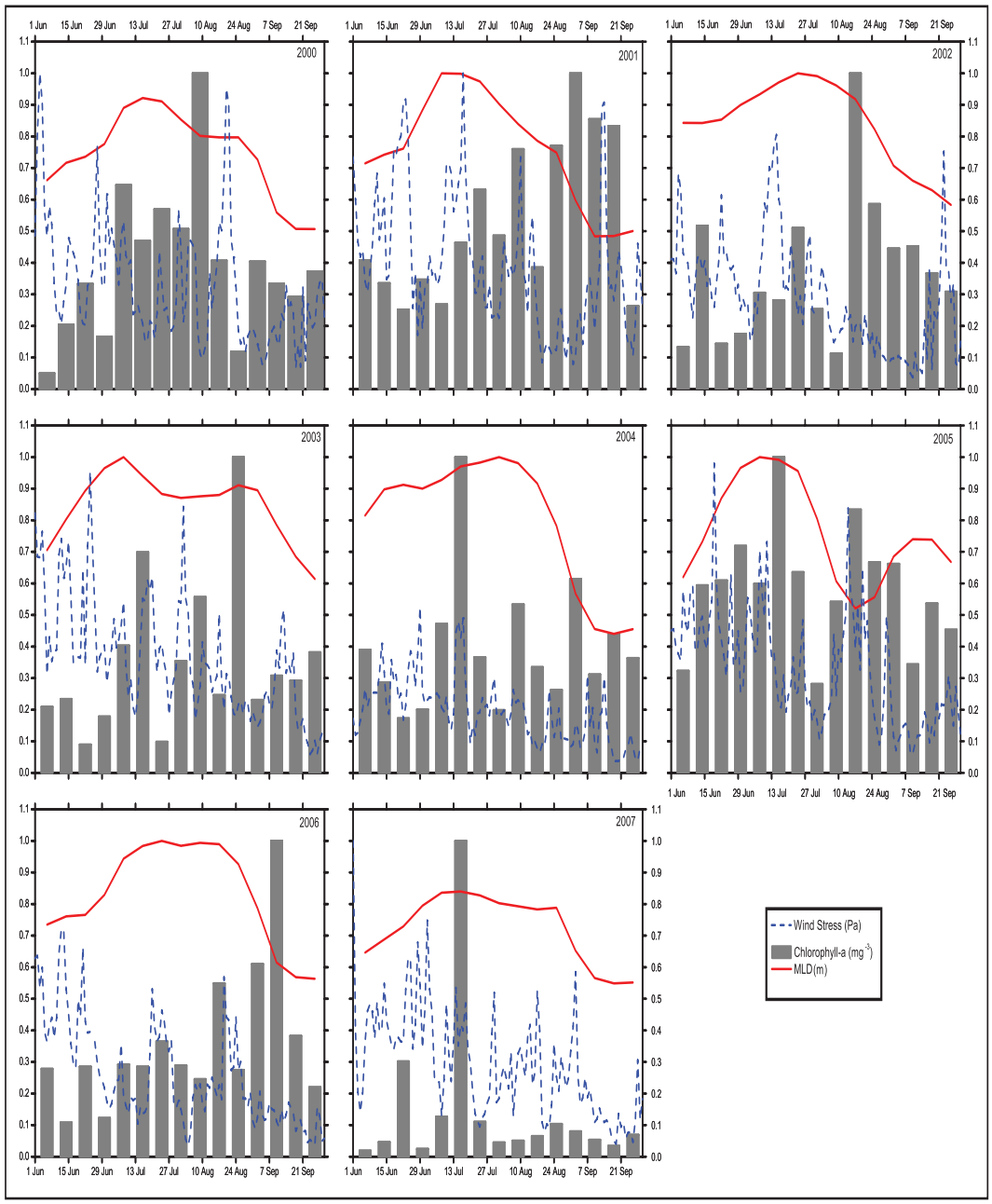

Figure 5.8: Wind Stress, CHLA and MLD in SEAS during SW monsoon

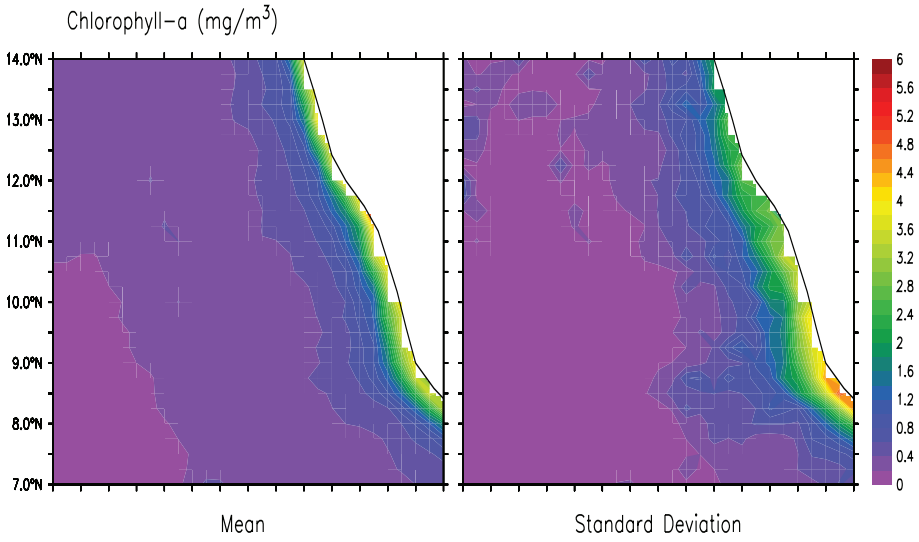

Figure 5.9: Mean and standard deviation of CHLA between 1998 and 2007

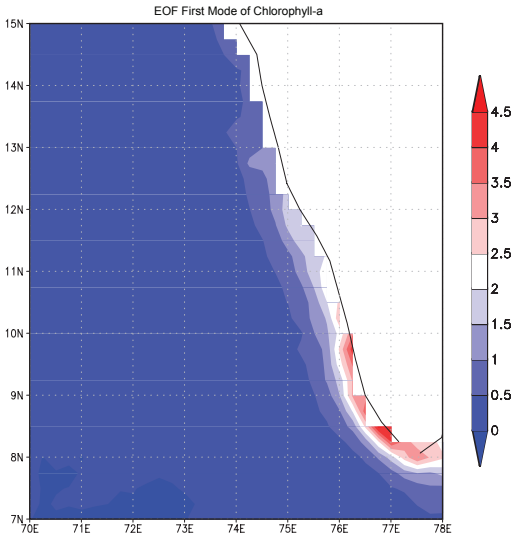

Figure 5.10: Empirical Orthogonal Function First Mode of CHLA

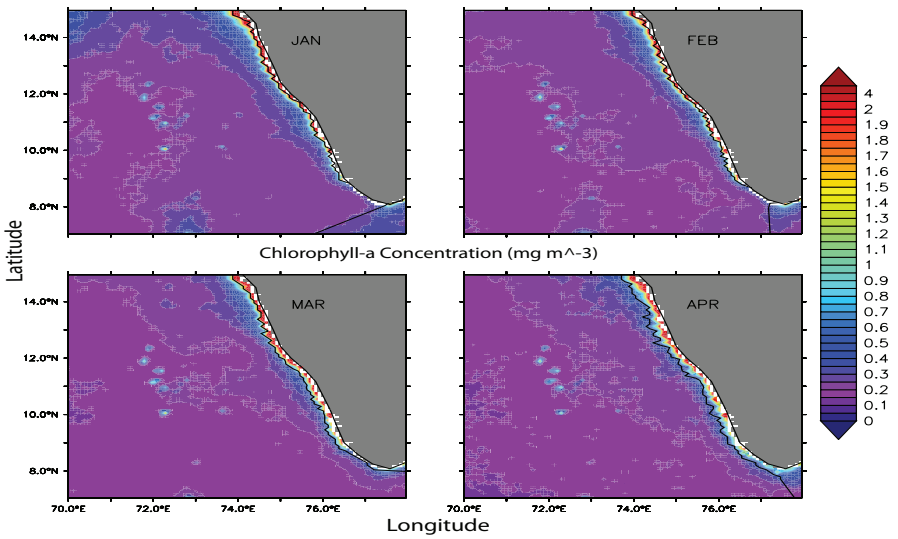

Figure 5.11: CEI for the months of January, February, March and April. The black contour line indicates the extension of Chlorophyll along southwest coast of India

5.4 Chlorophyll Extension Index [CEI]

To establish the offshore extent of CHLA during a year in different seasons, a measure of its concentration is to be understood over a period of time. In order to interpret biological variability within the upwelling region, surface CHLA data from SeaWiFS is used. An index is defined to estimate the spatial extent of CHLA away from the coast during upwelling. From the climatological mean computed with SeaWiFS CHLA data years 1998 to 2007, the mean CHLA in SEAS during the upwelling period is observed to be 0.95 mgm^{-3}. In this context, an index is defined based on the spatial limit where the surface CHLA drops below 0.95 mgm^{-3} as chlorophyll extension index (CEI). A similar index was defined for the north African coast by [Lathuiliere et al.,, 2008] and found concurrent with the *in - situ* observations. Figures 5.11, 5.12 and 5.13 shows the CEI for each month of the climatological year constructed from the SeaWiFS chlorophyll data between 1998 and 2007.

CHLA extension during January, February, March and April is located very near to the coast and the contours with concentrations up to 0.5 mgm^{-3} spreads

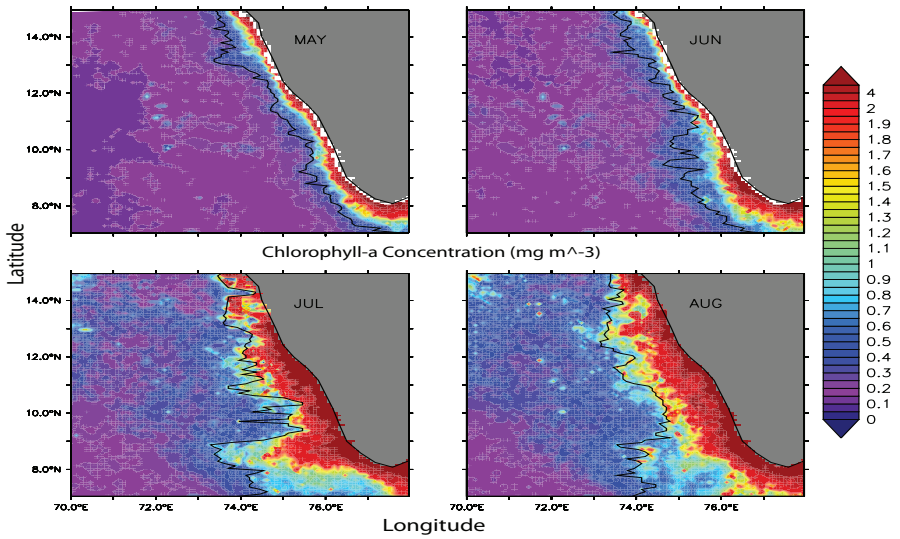

Figure 5.12: CEI for the months of May, June, July and August. The black contour line indicates the extension of Chlorophyll along southwest coast of India

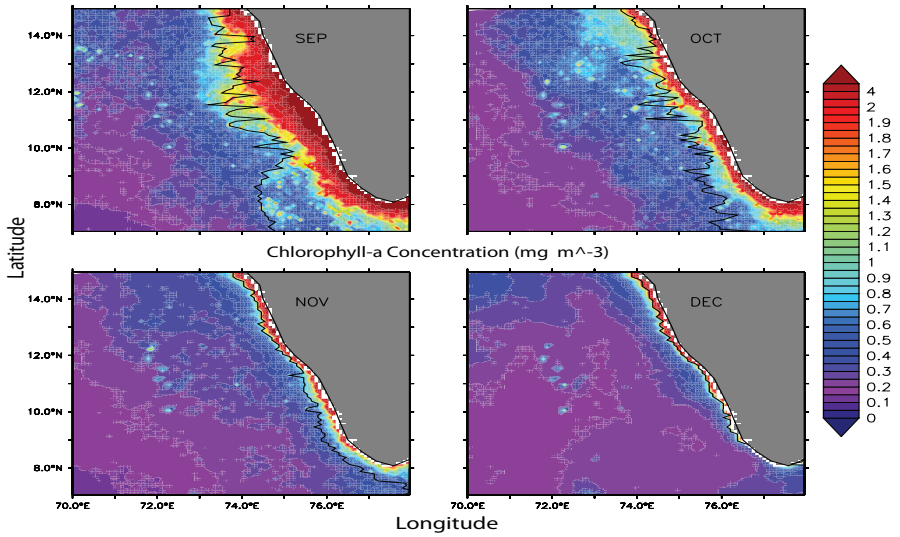

Figure 5.13: CEI for the months of September, October, November and December. The black contour line indicates the extension of Chlorophyll along southwest coast of India

approximately up to 50 - 60 km from the coast. In the southern region, during the months of JFMA, the southern region is practically devoid of any surface CHLA. From May onwards, the CEI showed evident increase towards the southern tip of India and narrowed down northwards. By June, the spatial extent of CHLA increased all along the coast and further got enhanced offshore by July. In July, the CEI extended nearly 300- 400 kms offshore between 8° and 9°N; between 9° and 10°N, this offshore extension subdued and gradually increased towards north. CEI along the coast during August is uniformly spread throughout upto 300 - 350 km from the coast. During September the spatial extent is greater in the northern region while it decreased mildly down south. By October, the CEI is very much limited to the coast with an approximate extension upto 50kms. In November, this index further decreased and by December, it cycled back to prevailing conditions as in January.

From the foregoing based on the newly proposed scheme of indexing solely based on CHLA, valued information as to the spatial extent in an upwelling region will abundantly serve the purpose of identifying and demarcating productive zones. In the case of SEAS, all throughout the year, a narrow band of approximately $\sim$ 50km coastal space is decorated by CHLA exceeding the mean. In the backdrop of prevailing upwelling conditions as expected during the months of June to September, such an analysis has helped to identify the broad zone of enriched CHLA which often exceeds 300kms from the coast.

Environmentally and biologically, significantly for these parts of the ocean a CHLA of 4 - 5 mgm^{-3} is critically regulated and serves the purpose of protecting and maintaining parts of large marine ecosystems. Evolving a criterion in this regard helps to regulate marine fishing activities as well as would serve as a biological indicator in protecting coastal waters.

SEAS is a region of multitudinal features exemplifying multiple ocean responses to basically wind stress and remote forcing. These responses are captured as signals in SST and CHLA. A detailed analysis on available remote sensing data has paved the way to establish the linkages between wind stress, SLA and SST on one hand whereas, the sub regional productivity in the upwelling zone is explored by understanding the relation between wind and CHLA. The above analysis was partially supported by data on mixed layer depth. By adopting this approach,

by selectively locating three representative areas, it has been possible to deduce the impact of wind stresses on SST followed by extracting time bands. In continuation of the above, the upwelling index based on LTG divulges the intensity of upwelling along the coast at more number of transects. An exercise on correlating the two upwelling indices also proved beneficial to unmask the memory of the ocean with respect to SST, followed by a well quantified exercise to understand the relationship between wind and CHLA. The work in this area provides information on time lags in occurrence of peak activities and so also provides insight into the stabilization features of the ocean responding to the drop in wind stress and consequently the results on CHLA for SEAS. This enhanced knowledge has prompted to prepare monthly maps on chlorophyll extension index which should support ocean operations in the field of fishery activities and aid the demarcation of potential fishery zones.

6

Heat Budget of SEAS

6.1 Introduction

Heat is the amount of thermal energy transferred from one body to another because of the temperature differences between those bodies [Sears and Zemansky, 1970]. In the environmental context, about half the solar energy reaching the earths surface is absorbed by oceans and land. Of the energy absorbed by the ocean, most part of it is released locally to the atmosphere by evaporation and infrared radiation [Stewart, 2005]. And heat lost by the tropical oceans is the major source of energy needed for driving the atmospheric circulation. It is also known that the solar energy retained in the ocean from summer to winter influences the earths climate to a large extent [Laing and Evans, 2010]. For these reasons it is imperative to understand the heat budget even at a regional level, in order to understand local climatic features and its variability on different space and time scales.

Upper layers of the ocean are in constant interaction with the atmosphere above, and undergoes incoherent input-output of heat energy at its surface and over a time, this imbalance changes the energy stored in those upper layers; the transfer of heat through the surface is named heat flux. The total flux of energy into and out of the ocean must be balanced (zero), otherwise the ocean as a whole would get heated up or cool down. This sum of heat fluxes into and out of the ocean is termed as the heat budget of the ocean. The flux data used in this study was obtained from Woods Hole Oceanographic Institute under the International

Satellite Cloud Climatology project (ISCCP). The gridded temperature profile data was obtained from CORIOLIS IFREMER. The following are the important parameters that influence the oceanic heat budget [Stewart, 2005]:

1 Incoming solar Radiation (Q_{SWR}): the flux of sunlight into the sea,

2 Outgoing long wave radiation (Q_{OLR}): net flux of infrared radiation from sea,

3 Sensible heat flux (Q_{SHF}): flux of heat out of the sea due to conduction,

4 Latent heat flux (Q_{LHF}): flux of heat carried by evaporated water,

5 Advection (Q_{ADV}): heat carried away by the ocean currents.

Therefore the total heat budget sums up, algebraically, as follows with its units as Watts/m^2.

$$NetHeatFlux(Q_T) = Q_{SWR} + Q_{OLR} + Q_{SHF} + Q_{LHF} + Q_{ADV} \tag{6.1}$$

6.1.1 Incoming Solar Radiation(Q_{SWR})

Incoming solar radiation is the amount of sunlight received by the earths surface. Insolation (incoming solar radiation) on the earth surface is dependent on latitude, season, time of the day and cloudiness [Ahrens, 2007]. Thus the Polar Regions are heated less than the tropical regions; areas which are prevailed by cool weather during winter are warmer during summer and also cloudy days have less insolation transferred than a warm sunny day. Insolation also depends on the height of the sun above the horizon, length of the day, cross–sectional area of the surface absorbing the sunlight. Attenuation of insolation is due to the presence of clouds in the path, gas molecules which absorb radiation, aerosols which scatter and absorb radiation [Ahrens, 2007]. Reflectivity of the earths surface is dependent on the solar elevation angle and roughness of the sea surface. As observed from the figure (6.1), the net shortwave radiation was always positive in the study region with maximum recorded during February to April and minimum during June and July, along the coast owing to the presence of clouds during the SWM season. During the rest of the year, Q_{SWR} did not show much variation, even

spatially. The climatological net shortwave radiation in the region is observed to be varying between 170 and 280 Wm^{-2}.

6.1.2 Outgoing Longwave Radiation (Q_{OLR})

Ocean surface radiates as a black body at temperature of 290° K at wavelength near 10μm which are strongly absorbed by cloud and water vapour. The long wave radiation also is influenced by cloud thickness, cloud height, atmospheric water vapour content, water temperature and ice / snow cover [Ahrens, 2007]. Water vapour and clouds determine the net loss through infrared radiation. The hotter the water, more the heat that is radiated at a rate proportional to the fourth power of temperature. Tropical regions loose less heat than cold Polar Regions. If we assume that the temperature difference between poles and the equator is approximately 25° K i.e., between 273°K and 298°K, then the ratio of maximum to minimum is 298/273 = 1.092; when raised to the fourth power it is 1.42. This indicates 42% increase in the emitted radiation from poles to equator and over the same distance; water vapour can change the net emitted radiance by 200% [Stewart, 2005].

From the climatological monthly mean (Figure 6.2) of net long wave radiation that is emitted from the earths surface, it was observed that except during the SWM season, rest of the year has greater OLR. This is because of the presence of clouds during monsoon period would trap long wave radiation from getting released into the upper atmosphere. The climatological range of OLR over SEAS was between 15 and 100 Wm^{-2}. From insolation and OLR data, it was observed that the months of June and July have less insolation as well as less OLR. Also, February, March and April are the months when the region receives maximum insolation and also releases maximum OLR.

6.1.3 Sensible Heat Flux (Q_{SHF})

Sensible heat flux is the process where heat energy is transferred from the earths surface to the atmosphere by conduction and convection. Sensible heat flux can be expressed by the amount of heat transmitted per unit of area per unit of time (http://disc.nasa.gov/hydrology). In the oceans, it is primarily influenced

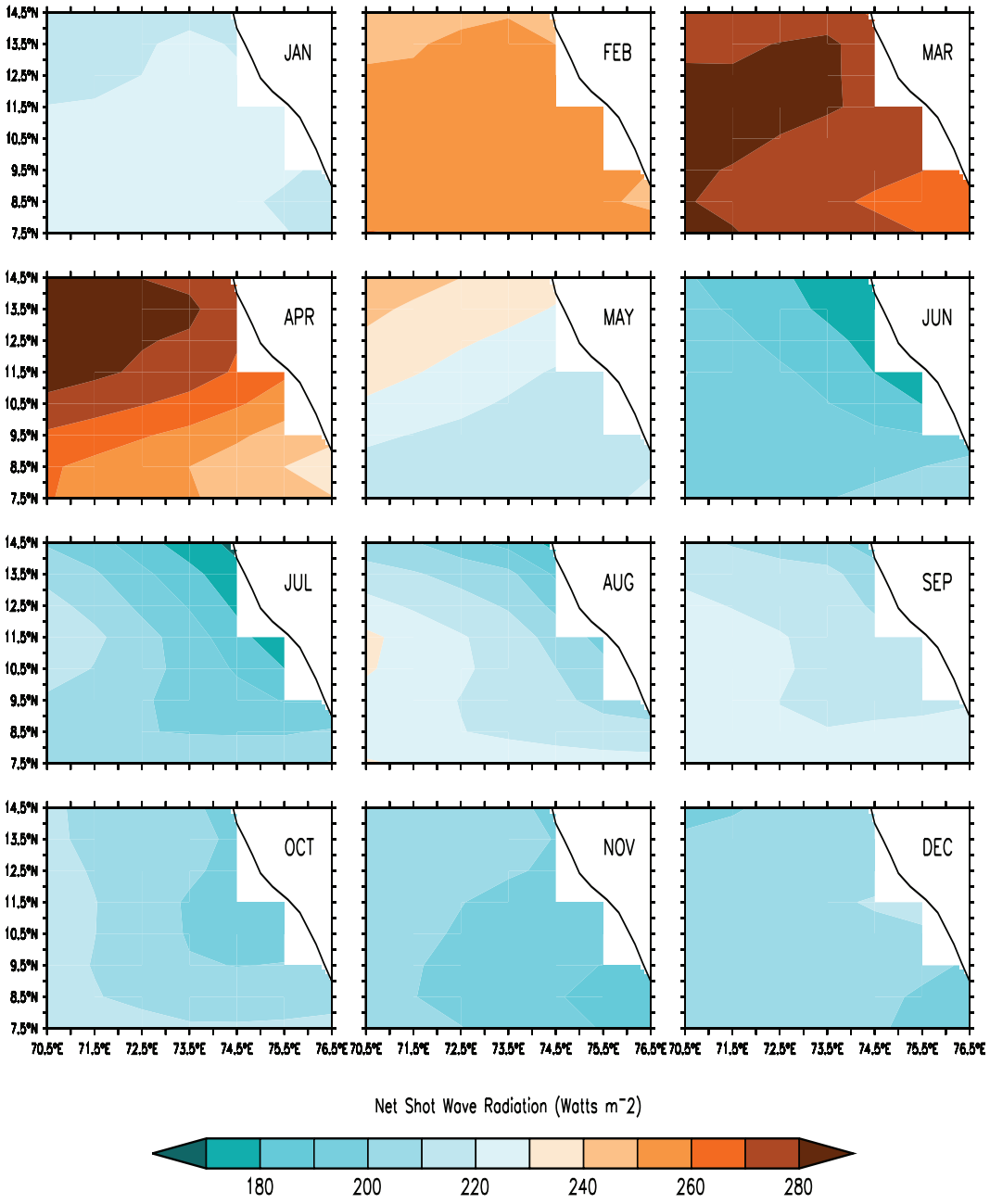

Figure 6.1: Monthly variability of Net Shortwave radiation over SEAS

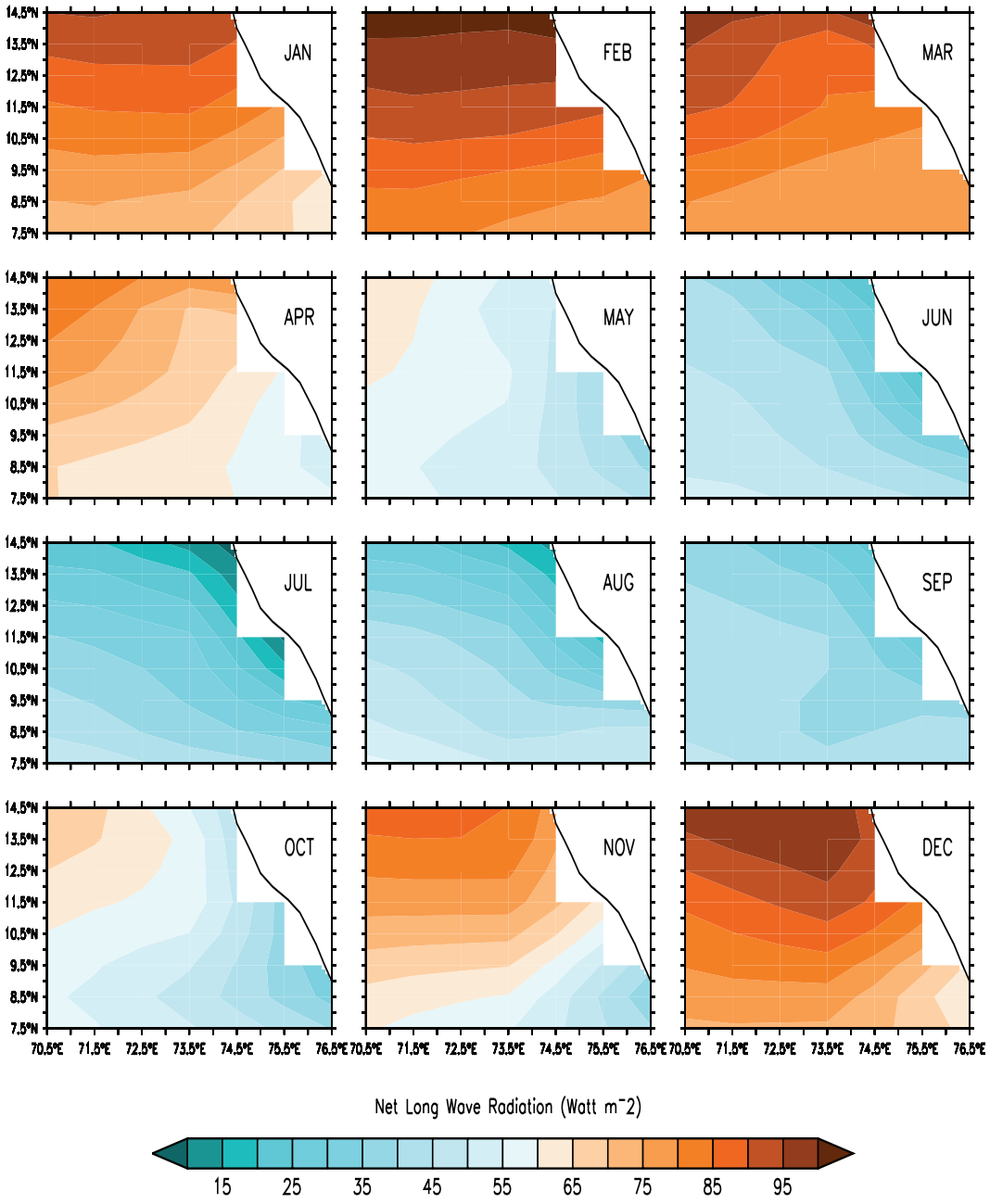

Figure 6.2: Monthly variability of net long wave radiation over SEAS

by wind speed and air-sea temperature difference. Heavy winds and large temperature gradients often cause high outward fluxes. Compared to the other three terms of the surface fluxes, sensible heat flux is very low and non variant over the region all through the year (6.3). Only during June and July months, considerable amount of heat was released into the atmosphere and again in December. This is because of the high SWM winds prevalent during June and July and the NEM winds during December. Also, during strong upwelling periods, the sensible heat flux is directed downwards and this will stabilize the air, trapping the evaporated water vapour in the lowest layer of the atmosphere and thereby reducing the evaporative power of the air with increasing humidity [Hareesh Kumar and Mathew, 1997]. For rest of the year, the region was prevailed by less intense winds and also low air-sea temperature difference. The climatological mean values ranged from -1.0 to $15.5 \mathrm{W}m^{-2}$ in SEAS.

6.1.4 Latent Heat Flux (Q_{LHF})

Latent heat flux is the flux of heat from the earths surface towards the atmosphere which is associated with the evaporation of water at the surface and subsequent condensation of water vapour in the troposphere. It is influenced by wind speed and relative humidity. High winds and dry air evaporate much more water than weak winds with relative humidity near 100% [Stewart, 2005].

Compared to sensible heat flux, the contribution of latent heat flux is greater towards the heat budget of the region. From figure 6.4, it is observed that the latent heat flux was high during May, June and July and for the rest of the year, it was relatively less. This indicates that the ocean looses heat during the above period much more rapidly. The monthly mean values ranged from 60 to $180 \mathrm{W}m^{-2}$.

6.1.5 Net Heat Flux (Q_{net})

The net heat flux over SEAS is shown in figure 6.5. From the figure, it is observed that the region gains heat for most part of the year except during June, November, December and up to some extent during January. Pre-monsoon heating is observed from February and the maximum gain in the heat at the surface

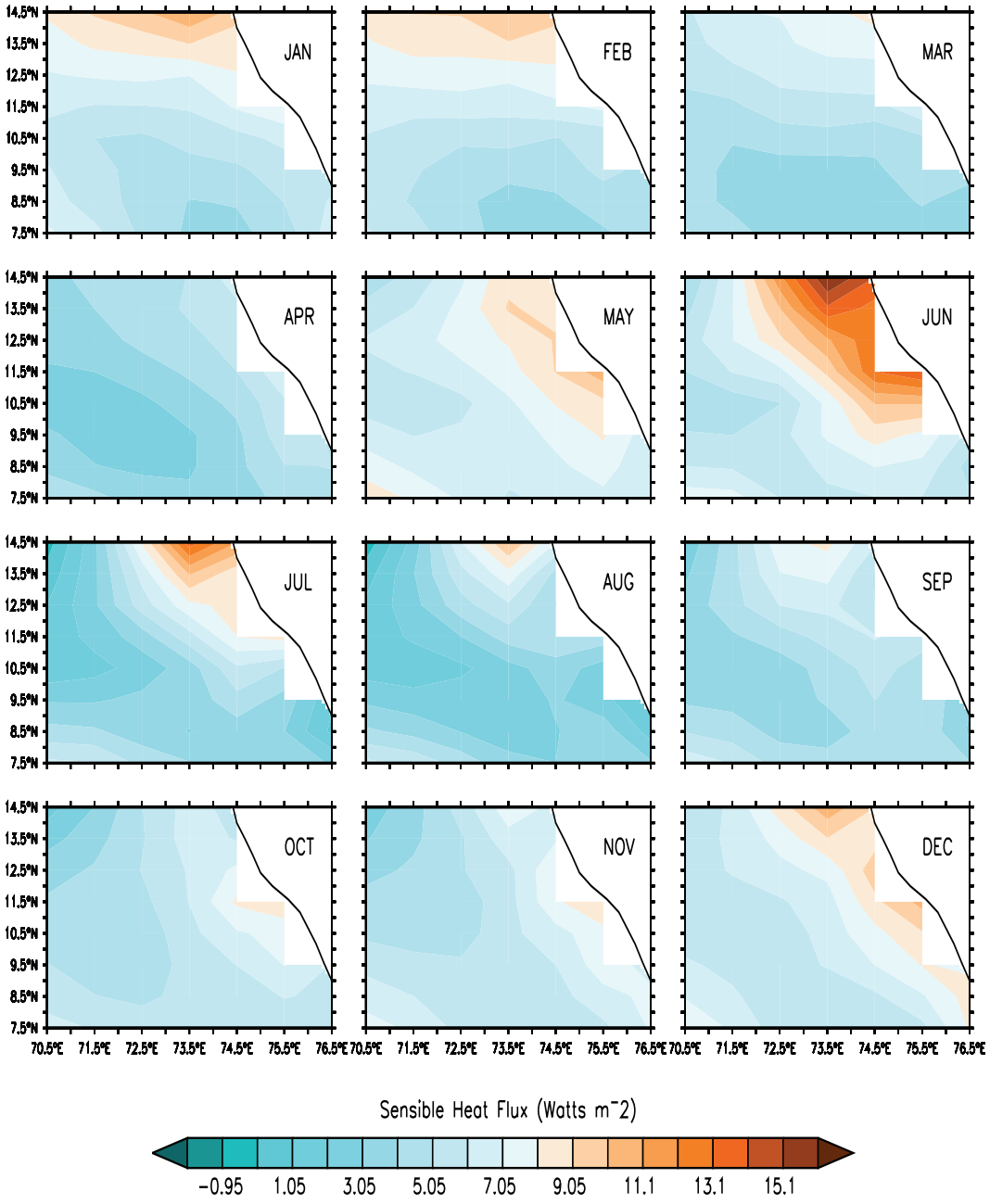

Figure 6.3: Monthly variability of sensible heat flux over SEAS

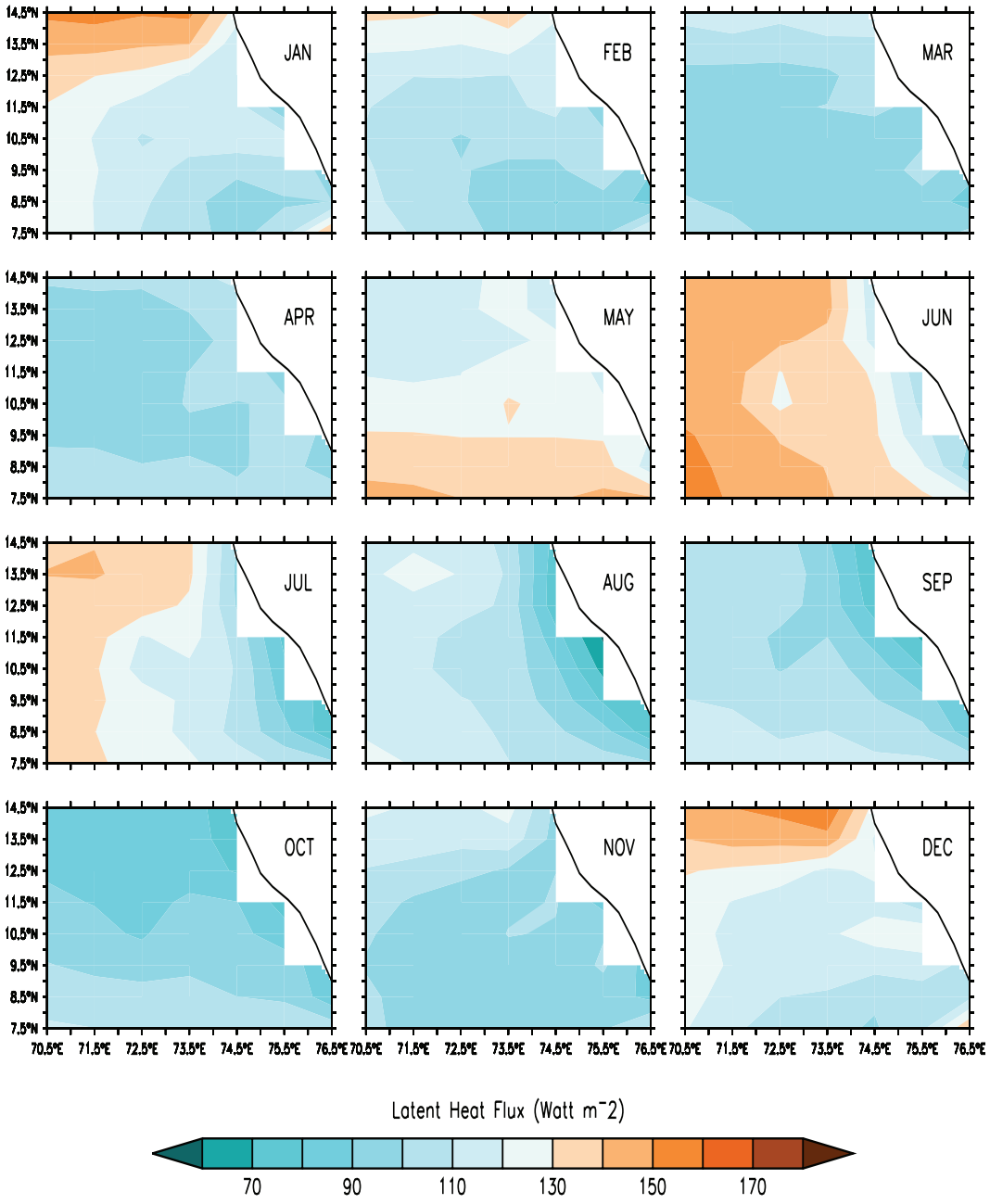

Figure 6.4: Monthly variability of Latent heat flux over SEAS

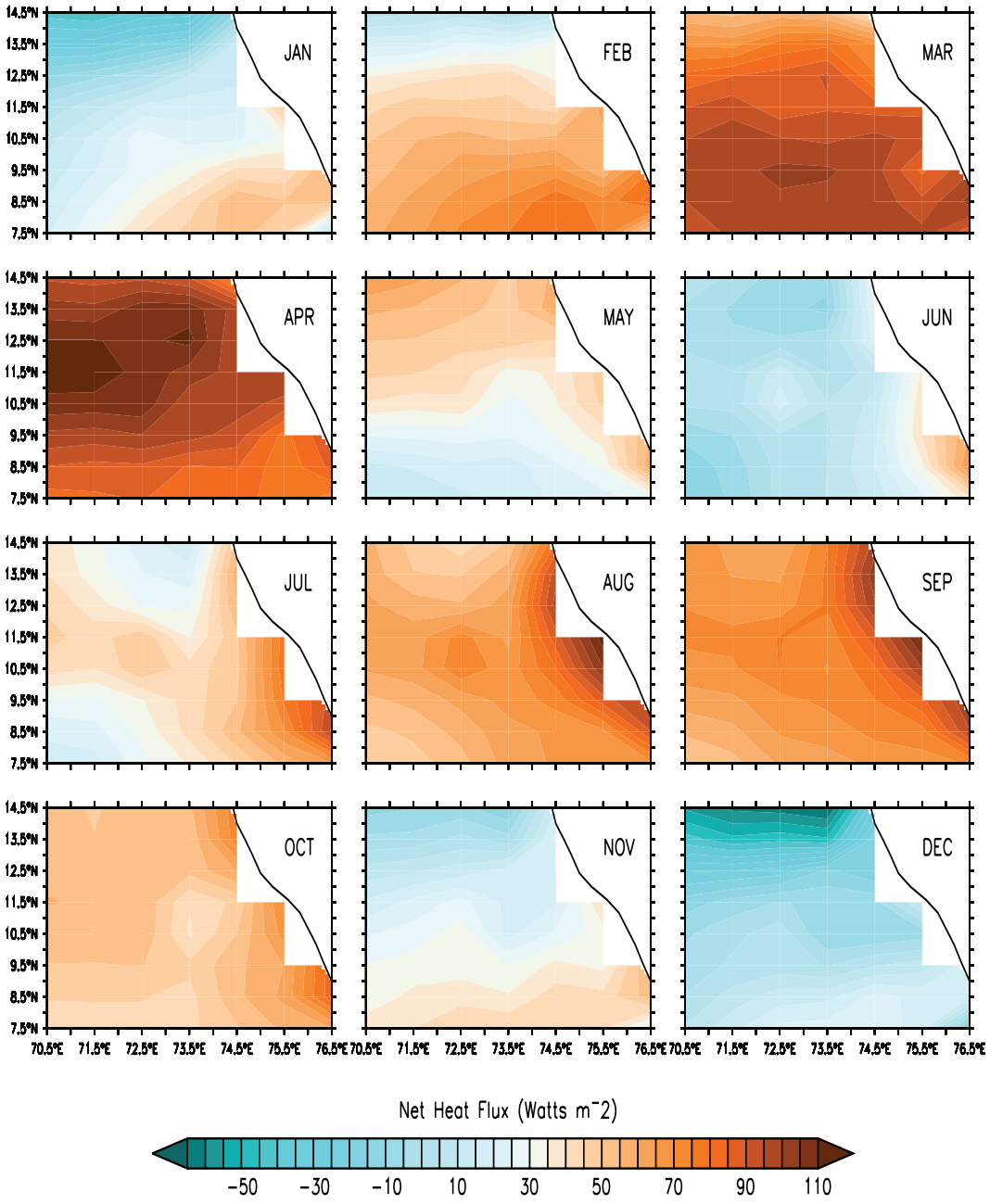

Figure 6.5: Monthly variability of Net heat flux over SEAS

was during March and April. This intense heat during the pre-summer monsoon season was due to the prevailing weak winds and clear skies. With the onset of SWM winds over the region, there is a net loss in the energy ($\sim -20 W m^{-2}$) during that period. Reduced insolation and large latent heat flux are the reasons for this loss of heat during June. In July, the coastal region continues to receive heat though in lesser magnitude. During the season of coastal upwelling, the evaporation drops to less than 3mm/day [Hastenrath and Lamb, 1979]. Also, the flux of sensible heat is directed downward. This will stabilize the air, trapping evaporated water vapour in the lowest layer and reducing the evaporative power of the air with increasing relative humidity [Hareesh Kumar and Mathew, 1997]. Surprisingly, even during the monsoon months of August and September when the region receives heavy rainfall and runoff, the ocean is seen to be gaining more heat than compared to some of the relatively dry months like that of February and November. The reason for such unconventional behaviour could be due to the processes that are intrinsic to the ocean and not much dependent on the atmosphere. This is explored in the following sections.

6.2 Evaluating the Heat Budget Terms

Southeastern Arabian Sea has been little studied especially beyond the monsoon related parameters, Arabian Sea mini warm pool, to some extent seasonal upwelling and the circulation pattern in the region. It is in this context that a detailed heat budget study has been carried out for SEAS in order to gauge the mechanisms in heat budget terms over a year, especially the role of coastal upwelling in modulating the heat budget terms with available high quality data sets. A preliminary heat budget over the Arabian Sea for the first time was computed by Duing and Leetma [1980] and they concluded that the heat loss owing to advection across the equator and due to upwelling exceeding the heat gained from atmosphere during summer monsoon. Coastal upwelling was observed to be having a profound influence on the heat budget during SWM. Later many studies based on both observed and simulated, on the heat budget were carried out by Hareesh Kumar and Mathew [1997], Loschnigg and Webster [2000], Shenoi et al.

[2002], de Boyer Montegut et al. [2007] and Wilson-Diaz et al. [2009] over the Arabian Sea. However, as all these studies were executed taking into consideration the Arabian Sea as a whole, wherein the domination of Somalia coastal upwelling and convective cooling in the Northern Arabian Sea were the dominant factors that influenced the heat budget. Also, it is a region where there are heavy rainfall events, over the ocean and river runoff during the SWM leading to stratification. This brings about positive feedback that result in deep convection in the atmosphere. For this reason and as rightly remarked by Shenoi et al. [2002], eastern Arabian Sea requires a detailed heat budget of its own. Therefore, the aim of this chapter is to develop an understanding on how the air-sea fluxes behave and influence the ocean and up to what extent, especially during the upwelling season.

Thermodynamics of the upper ocean are influenced by the cooler subsurface waters entraining towards the surface during upwelling [by changing the stratification]. In order to estimate and understand the processes that influence the upper ocean heat budget of SEAS, heat budget has been computed between 7° - 15°N and 70° - 78°E up to a depth of 50m as followed by Shenoi et al. [2002]. The depth of the volume is considered as 50m because the mixed layer in this region for all seasons was shallower than 50m. Area average of the flux data is computed and averaged for a climatological year to generalize the phenomena taking place in this region. The period covers the years 2000 to 2008 as it is the common period over which all data was available.

The rate of change of heat in the region is balanced by the flux of heat through its boundaries due to advective and non-advective processes. Assuming that the fluid is incompressible and following Gauss theorem to express the conservation of heat as follows:

$$\frac{1}{A}\frac{\partial}{\partial x}\int(\rho_w C_P T)\,\mathrm{d}v = \frac{-1}{A}\int(\rho_w C_P T)u.n\,\mathrm{d}s - \frac{1}{A}\int F.n\,\mathrm{d}s \tag{6.2}$$

Where T is the temperature, u is the velocity; F is non advective fluxes, n is the unit vector normal to the surfaces bounding the control volume (directed outwards). ρ_w is the density of sea water 1026 kgm^{-3}, Cp is the specific heat capacity of sea water at constant temperature and pressure 4000 J$kg^{-1}K^{-1}$. The temperature T is utilized from the temperature profiles of the region obtained from CORIOLIS gridded product which is of high spatial (0.25° x 0.25°) and

temporal (weekly) resolution than the available climatological datasets. The non-advective term F consists of the surface fluxes and diffusion through the bottom of the control volume; diffusion through the lateral boundaries is negligible as there is an opening on both northern and southern boundaries of the region where one can assume owing to the direction of currents in the region, the energy entering the control volume is balanced by the energy leaving that control volume. All the fluxes are divided by the area at surface A so that all the surface fluxes are represented in Wm^{-2} to bring uniformity in the notation. The terms are classified as the surface fluxes which are resultant of the atmospheric processes and the advective terms which are treated separately as they are intrinsic to the ocean.

6.2.1 Surface Fluxes (Q_{SF})

The net heat flux through the surface is:

$$Q_{SF} = Q_{SWR} + Q_{OLR} + Q_{LHF} + Q_{SHF} \tag{6.3}$$

Where Q_{SWR} is the net shortwave radiation,Q_{OLR} is net long wave radiation, Q_{LHF} is latent heat flux and Q_{SHF} is sensible heat flux through the surface respectively. Climatological monthly mean surface fluxes are shown in figure 6.6. Except Q_{SHR} and Q_{OLR}, rest of the fluxes show bi- modal distribution. Q_{SWR}, increased from January to April and later, decreased later till June. From June, it again showed increase, up to September followed by a drop to November; this was followed by a slight raise towards December to match January values. Overall, the Q_{SWR} was observed to be greater than 200 Wm^{-2} all throughout the year except during June and July when it was hampered by the presence of thick clouds during to the SWM. Q_{OLR} too increased from January to March and later showed a decreasing trend up to July. Q_{OLR} increased from August till December. $Q_{OLR}$was greater than 50 Wm^{-2} during all the year except during the SWM season. Unlike Q_{SWR} and Q_{OLR},Q_{LHF} showed decreasing trend from January to April and later as the summer season approached the region, the latent heat flux increased till June with heightened evaporation. Later from July, the Q_{LHF} term showed a decline till October and again increased towards the end

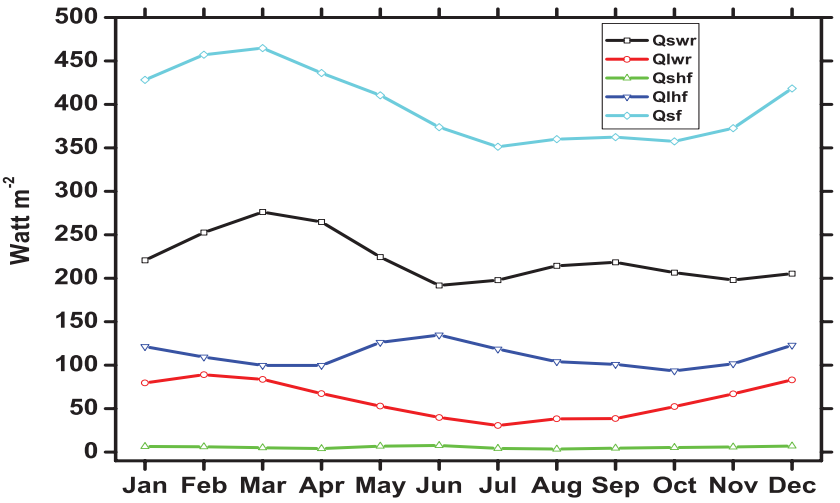

Figure 6.6: Climatological monthly mean fluxes at the surface of the Ocean: Net surface Flux (Q_{SF}), Net shortwave radiation (Q_{SWR}), Net Longwave radiation (Q_{OLR}), Net latent heat flux (Q_{LHF}) and Net sensible heat flux (Q_{SHF})

of the year. The contribution of sensible heat flux is very feeble over the region as it did not show any variation and its magnitude remained near to zero indicating very minute contribution towards the heat budget of this region. As evidenced from the above figure, the net surface flux peaks during NEM season. A fact worth mentioning here are that all the fluxes showed positive values indicating gaining of heat throughout the year from the surface. Therefore this gain in heat from the surface has to be compensated by oceanic processes.

6.2.2 Oceanic Processes

Diffusion through the bottom and advection of heat together can be clubbed as the oceanic processes. The advective processes are classified into two kinds depending on the direction of flux. Firstly, flux on both north and southern boundaries. Here, in this region, depending on the direction of the currents over a year, it is assumed that the amount of flux entering from one end is leaving from the other end thereby making it sufficient to compute the flux at one boundary to know the total flux through the lateral boundaries. Second part of the advective fluxes is the cross shore flow at the eastern boundary resulting in upwelling /

downwelling along the eastern boundary. This vertical mass flux through the bottom of the coastal region is balanced by a vertical mass flux through the bottom of the rest of the control volume which is away from the coastal region. Such a process is called the coastal pumping [Shenoi et al., 2002]. This causes over turning and thereby removes heat from the control volume. Vertical mass flux at the western, northern and southern boundaries are ignored in comparison to the eastern boundary as it the region of coastal upwelling. Thus the net flux due to the oceanic processes is:

$$Q_{OP} = Q_{mo} + Q_{cp} + Q_d \tag{6.4}$$

where Q_{op}, Q_{cp} and Q_d are the heat fluxes due to meridional over turning, coastal pumping and diffusion respectively.

Meridional Overturning The transport along the lateral boundaries in the north - south direction is balanced by a mass flux through the bottom of the control volume. The difference between the vertical average of temperature at the bottom of the control volume results in a net flux of heat due to this process. This heat flux is estimated as:

$$Q_{mo} = \rho_w C_p \frac{1}{A} \int v \Delta T_{mo} \, \mathrm{d}x \tag{6.5}$$

Where v is the transport per unit distance along the southern boundary (here only southern boundary is considered to know the flux that is entering the control volume from southern end and leaving from the northern boundary),

$$\Delta T_{mo} = T_{sb} - < T > \tag{6.6}$$

The integral is evaluated along the southern boundary. T_{sb} is the vertically averaged temperature (over the depth of the control volume) at the southern boundary, and ¡ T ¿ is the basin wide average of the temperature at the bottom of the control volume. Both Ekman and geostrophic flows contribute to v; where $Q_{mo} = Q_{moe} + Q_{mog}$ and $v = v_e + v_g$ and

$$v_e = \frac{\tau^x}{\rho_w f}; v_g = \frac{gD}{f} \frac{\partial \eta}{\partial x} \tag{6.7}$$

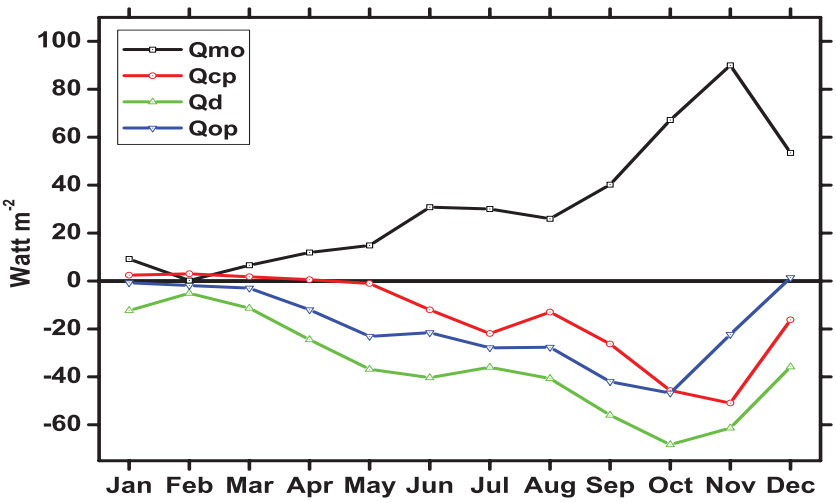

Figure 6.7: Flux of heat (Wm^{-2}) due to Ekman and geostrophic components of meridional overturning and coastal pumping

The subscripts 'e' and 'g' refers to Ekman and geostrophic flows respectively. The geostrophic current is assumed to constant over the depth of the control volume. is the zonal wind stress and is the sea surface height, f is the Coriolis parameter, $g = 9.81ms^{-2}$ is the acceleration due to gravity and D is the depth of the control volume considered to be 50m. Wind stress climatology computed from the QuikScat measured winds was used to estimate the zonal wind stress and the absolute dynamic topography obtained from AVISO was used to compute climatological sea level of the region.

From the figure (6.7), it is observed that none of the fluxes show any variation till the onset of SWM which is coincident with coastal upwelling in the region along the eastern boundary of the ocean. An exception is observed with geostrophic component of meridional overturning (Q_{mog}), showing heat gain ($\sim 10Wm^{-2}$) up to June, which can be attributed to oceanic flow into and out of the control volume. The heat loss due to meridional overturning owing to the geostrophic component is compensated by the heat gained through the Ekman component during the SWM season. Q_{mog} contributed to bulk of the heat gained in the region during October and November which started to decrease by December. From the above, it is be stated that Ekman is a major contributor to

heat ($\sim 40 W m^{-2}$) gain during the SWM season while geostrophy is the major contributor ($\sim 90 W m^{-2}$) during post SWM period. In short, heat gained due to Ekman component is being compensated by the heat lost due to geostrophy during the SWM. Thus it can be firmly stated that meridional overturning is not a significant contributor to heat lost during the upwelling season.

Coastal Pumping Cross shore flux at the eastern boundary has to be compensated by the vertical mass flux through the bottom of the control volume over rest of the region. The difference in average temperature between the coastal region and the rest of the control volume at the bottom results in a flux of heat. This process is known as coastal pumping [Shenoi et al., 2002] and is derived as follows:

$$Q_{C_p} = -\rho_w C_p \Delta T_{C_p} \frac{1}{A} \int_l u.n \, \mathrm{d}l \tag{6.8}$$

Where u is the cross- shore transport per unit distance along the coast, n is the unit vector normal to the eastern boundary (positive out of the coast), l is the coordinate along the coast and the integral is evaluated along the coast. ΔT is the average difference in temperature at the bottom of the control volume between the coast and the rest of the basin, arrived at as:

$$\Delta T_{C_p} = < T_c > - < T_l > \tag{6.9}$$

Where $< T_c >$ is the average temperature along the coast and $< T_l >$ is the average temperature at the coast of the control volume. Like meridional overturning, coastal pumping is also a combination of Ekman pumping and geostrophic components, i.e., $Q_{cp} = Q_{cpe} + Q_{cpg}$ and $u = u_e + u_g$, where

$$u_e = \frac{K x n \tau}{\rho_w f}; u_g = \frac{gD}{f} \Delta \eta \tag{6.10}$$

where τ is the wind stress vector, k is the unit vector normal to the earths surface, D is the depth of the control volume, and is the sea level. The dynamic topography obtained from merged altimetry data has been used for computing geostrophic component (u_g), of coastal pumping.

As suggested by Duing and Leetma [1980] for the entire Arabian Sea basin, herein, the SEAS also, coastal upwelling forced by Ekman pumping along the

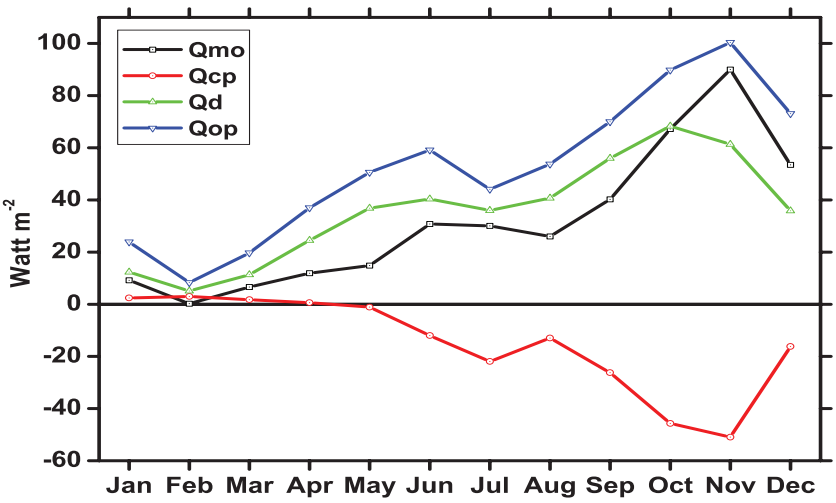

Figure 6.8: Heat Fluxes due to Oceanic Processes Meridional Overturning, Coastal Pumping, Diffusion

eastern boundary of the ocean is the dominant term in the heat budget of the region during SWM. The upwelling triggered by the monsoon winds along the coast brings up the cooler subsurface waters towards the surface and thereby cooling the region by ~ 2.5°C during the SWM (as observed in chapter 5). This results in heat loss due to coastal Ekman pumping ($60Wm^{-2}$) during the SWM. For rest of the year, coastal Ekman pumping is non-existant as seen from figure (6.7). Geostrophic component of coastal pumping resulted in the heat gained over the region up to $30Wm^{-}2$ during the summer monsoon. The region began to lose heat from August and reached its peak by November due to geostrophic component of coastal pumping.

Diffusion The flux of heat through bottom of the control volume due to diffusion process is computed as:

$$Q_d = -\rho_w C_p k \frac{1}{A} \int_s \frac{dT}{dz} \, \mathrm{d}S \tag{6.11}$$

where k = 2 x $10^{-4} m^2 s^{-1}$ is the eddy diffusivity coefficient, $\frac{dT}{dz}$ is evaluated at 50m depth, and the integral is over the surface area of the basins. The choice of k has been considered to be constant over the region as followed by Shenoi

et al. [2002]. Diffusion results in loss of heat from the control volume as seen in figure 6.8. The loss is minimum during February - March ($\sim 15 W m^{-2}$) and is maximum during September - October ($\sim 60 W m^{-2}$).

In SEAS, the dominant oceanic processes are coastal Ekman Pumping, Meridional overturning due to Ekman flow and diffusion during the summer monsoon. Among these, the Ekman components are directly influenced by winds, while the coastal pumping removes the heat, meridional over turning brings in heat to the control volume which is a new finding of this study. The same is the case with geostrophic components of coastal pumping and meridional overturning, when the geostrophic component (Q_{mog}) removes heat, Q_{cpg} introduces heat during the summer monsoon. Hence, we attribute this as the reason for overall weak upwelling in the region when compared to the eastern boundary upwelling regions elsewhere. Diffusion also results in loss of heat from the control volume throughout the year and is the only component that is not influenced by winds. Here, among the overall oceanic processes, meridional overturning results in gain of heat flux into the region, while the coastal pumping and diffusion results in loss of heat.

6.3 Rate of Change of Heat

The resultant heat flux owing to surface fluxes and oceanic processes result in change of heat content in the control volume. The rate of change of heat is obtained using the left hand side of the equation 6.1. Both Q and Q_t show bi-modal distribution in the region (Figure 6.9) with minima during the SWM and the coincident upwelling season of JJAS. From net heat flux curve, it can be understood that all through the year, SEAS gain heat though with varying intensities. Thus for this region, it can be concluded that the heat flux from the surface is far greater than that can be compensated by oceanic process. The sources of heating (primarily the fluxes with considerable contributions from Ekman and geostrophic components of the flow) are found to be compensated by cooling from vertical diffusion and coastal upwelling. However, it is evident that upwelling is the major factor in regulating the heat budget of the region during the SWM. For

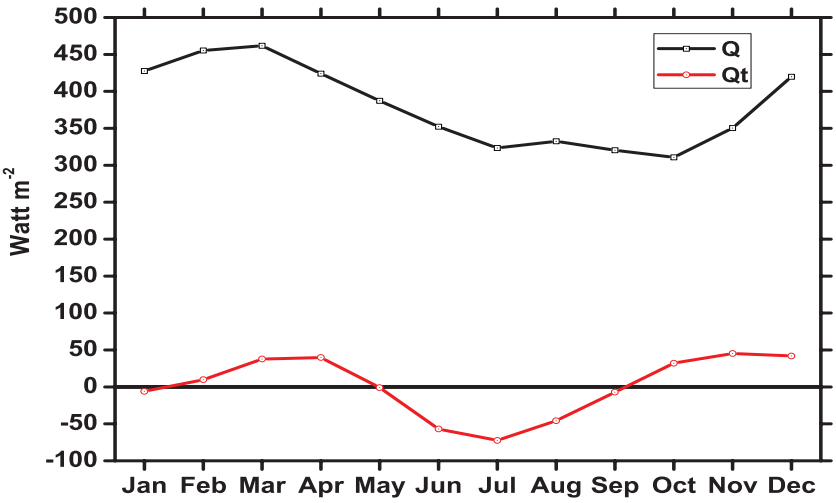

Figure 6.9: The net heat flux $Q = (Q_{sf} + Q_{op})$ into and out of the control volume and the rate of change of heat Q_t

the rest of the year, only the surface fluxes contribute towards the heat budget while the oceanic processes are feeble.

7

Interannual variability and influence of Climate Change on Upwelling

7.1 Introduction and Relevance

The postulation on enhancement in the coastal upwelling with global warming was first put forward by Bakun [1990]. It has been stated that the global green house warming will intensify the alongshore winds thereby increase the intensity of upwelling. To support this concept, the increase of green house gases has resulted in increase of day time heating of the oceans and decrease in night cooling [Bakun, 1990]. This results in building up of pressure gradients between the oceans and the adjacent land, thereby intensifying the alongshore winds. A study applying ecosystem models for estimating coastal upwelling under the global warming scenario, carried out by Mote and Mantua [2002] however, could not bring out considerable inter-decadal changes in the intensity of coastal upwelling. A more recent study on the impact of global warming on the productivity of the Arabian Sea was by Goes et al. [2005], who attributed the increase to the warming of Eurasian land mass. But it was found later that the reported increase in the productivity was limited to western Arabian Sea and not to the eastern portions [Prakash and Ramesh, 2007]. The present study is aimed at investigating the characteristic roles of agencies that bring about variability in upwelling along the

southwest coast of India, of the eastern Arabian Sea through its indices based on SST and the Ekman transport from two decades of satellite measured high resolution data products.

Oceanic heating has been attracting wide spread concern owing to its influence on the bio-diversity of a region and its adjacent land mass. There have been studies by Levitus et al. [2000] and Levitus et al. [2001] and the references therein on the extent of warming of the oceans. It has been stated that there exists a warming of ~ 0.1°C in the upper 1000m of the overall oceans and the rates were different for each ocean basin. This warming, of course, was attributed to the increase in anthropogenic gases in the earths atmosphere. The warming of Indian Ocean was studied in detailed by Bijoy et al. [2008] using model simulations and observational data and they concluded that there is an increase of 0.4°C rise in SST. This warming trend was observed to be more dominant to the north of 12°N in the eastern Arabian Sea but a cooling trend was observed along the Somalia coast. The satellite measured SST (Figure 7.1) over SEAS shows a slight increase over the past two decades, of which the warming was rapid during the period 1992 to 1998 and again from 2004 to 2007. The cooling episodes of 2 -3 years, observed within the 20 years period, confirm the quasi decadal variability of the Arabian Sea Bijoy et al. [2008]. This dynamical behaviour of SST over the study period has its influence on the strength of upwelling which is explained in the following sections.

7.2 SST Variability

The SST upwelling indices (Figure. 7.2), computed and compared between last two decades indicate that the temperature gradients along the coast with respect to their offshore components have increased in the later. It can be attributed to two reasons, one of them, certainly is the increase in offshore temperatures and the other, could be due to greater decrease in the coastal temperatures; of these two reasons, based on figure 7.1, the increase in temperature gradients is related to the rise in offshore temperatures with time in the global warming context [Jayaram et al., 2009]. Next, upwelling signals were predominant from 8° to 12°N for all the study years. Particularly, for the years 1988, positive temperature gradients, up

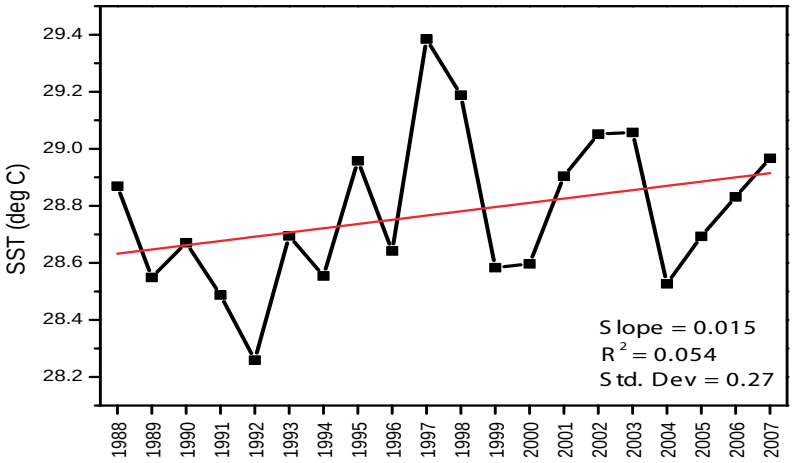

Figure 7.1: Annual mean of SST over SEAS from 1988 to 2007

to 0.5°C were observed all along the coast during summer monsoon, while for the remaining years, the gradients was limited up to 12°N with varying magnitudes. As an exception, during 2002 and 2003, positive gradients were observed up to 15°N. For the later years, a continuous fall in the northward extent of upwelling was observed up to 2007. Further, the temperature gradients were observed to be high during 2003. For all the years, high upwelling index of SST was observed between 8° and 9°N, but for the year 2003, a secondary peak was also observed between 10° and 11°N. This phenomenon was repeated, though very mildly, in 2004 also.

To substantiate and clearly distinguish the positive temperature gradients during all the years, SST upwelling index anomalies were computed by subtracting the monthly climatological mean [computed from AVHRR data] from the actual monthly latitudinal temperature gradient [Nykaer and Camp, 1994]. From the SST upwelling index anomaly (Figure 7.3) it was observed that, the period between 1998 and 2007 had higher upwelling conditions favouring development of temperature gradients along the coast than the previous decade of 1988 - 1997; this is due to greater increase of offshore temperatures in the recent decade. For the year 1988, positive anomalies were observed from north of 11°N which was not intense during the years, 1988 to 1997. Following are strong upwelling years

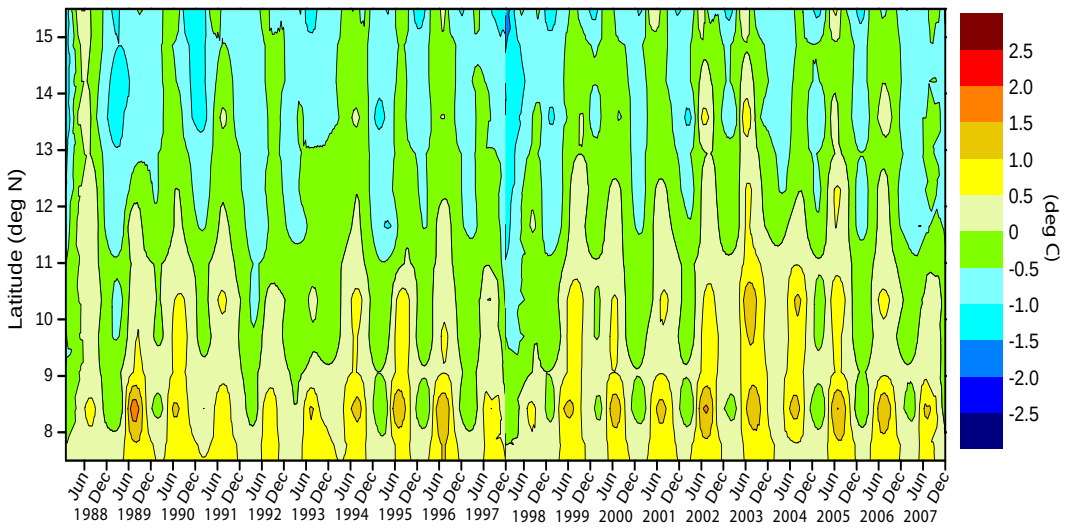

Figure 7.2: Interannual variability of latitudinal temperature gradient from 1988 to 2007

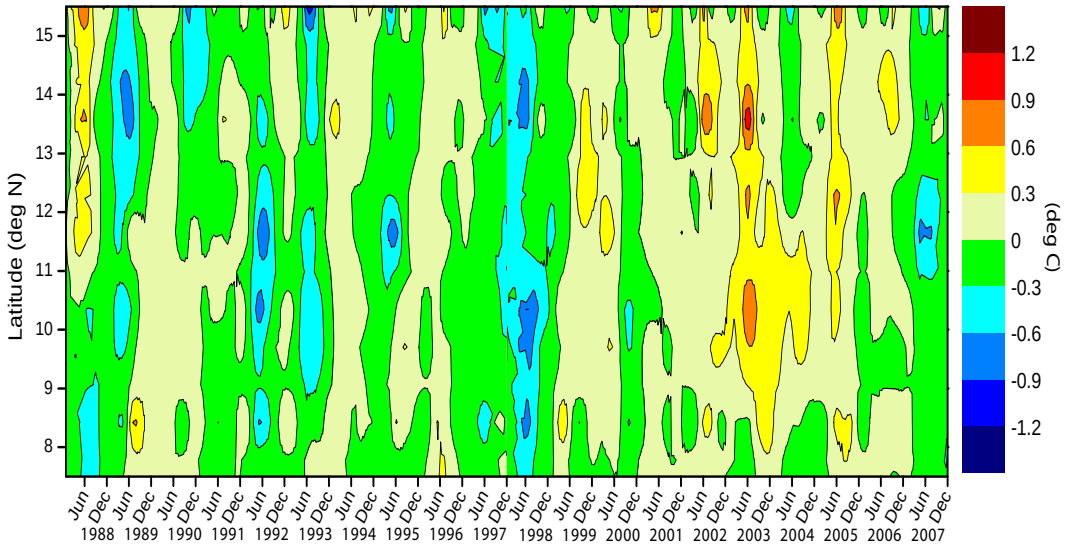

Figure 7.3: Interannual variability of latitudinal temperature gradient anomaly from 1988 to 2007

as evident from the SST upwelling index (LTG and its anomaly): 1989, 1996, 2002, 2003 and 2005 and weak upwelling years are 1988, 1991, 1992, 1993, 1997, 1998 and 2007.

7.3 Wind Stress Variability

Ekman mass transport computed along the southwest coast of India is an indicator for the intensity of upwelling of the region for the years 1992 to 2007 (Figure. 7.4). During the year 1992, intense onshore transport was observed during SWM and also during 1999, though in lesser intensity. High Ekman offshore transports were observed between 8° and 10°N from years 2000 to 2004 during summer monsoon. The mass transport values lies in the range of 500 - 2500 kg/m^2/s. Later from 2005 to 2007, the offshore Ekman transports have decreased. This was due to the weak meridional winds prevailing along the coast during the upwelling seasons of 2005 - 2007 [summer monsoon] (Table 7.1). As the wind direction is always meridional [Shetye, 1984] along the coast, the Ekman transport is offshore even in the non upwelling season; this would be of very less intensity.

To delineate high upwelling regions and periods, anomalies were computed by subtracting the monthly climatological Ekman transport from the corresponding monthly values. The regions where high upwelling was prevalent, these regions would have higher values of Ekman transport [Nykaer and Camp, 1994]. The anomaly (Figure. 7.5) shows a clear picture of the Ekman transport in the study region for years 1992 to 2007. Greater positive anomalies were observed during 1992, 1996, 1997, 1998 and 1999, indicating less offshore Ekman transport. The year 2000 was having higher values among all the years of study. During the year 2004, both the monsoons had equal amount of offshore transport. For the years 2005 to 2007, the picture was completely different from the previous years. During that period, positive anomalies were observed all along the coast.

The year 2005 show positive anomaly during summer monsoon, indicating very feeble offshore transport. A significant observation was the prevalence of upwelling off 8N during October and November of 2005; this coincides with the reported anomalous upwelling in the region during 2005 by Gopalakrishna et al. [2008]. In 2006, the negative anomalies were punctuated by positive anomalies.

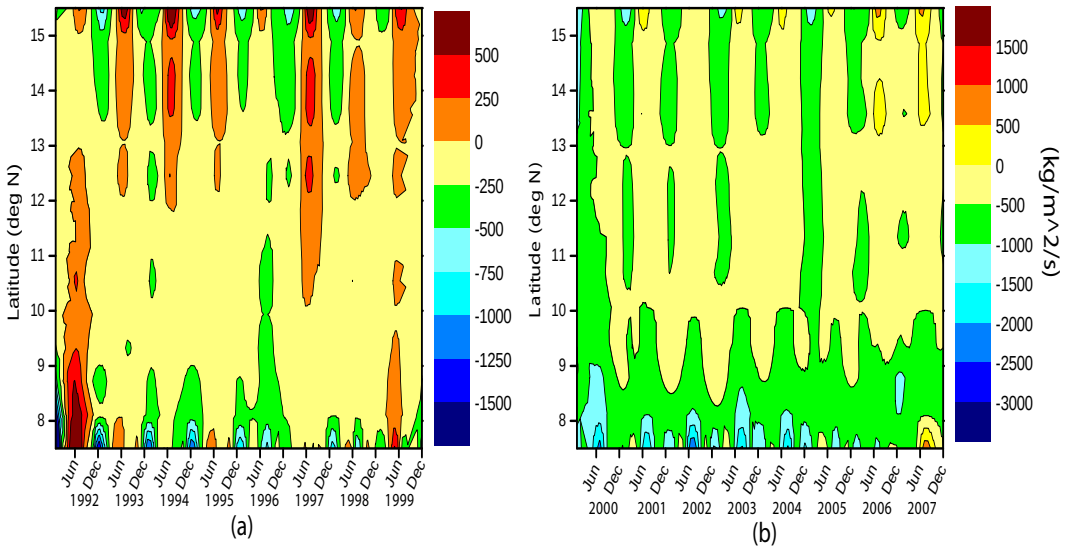

Figure 7.4: Interannual variability of Ekman transport (a) ERS 1 & 2 (b) QuikScat from 1992 to 2007

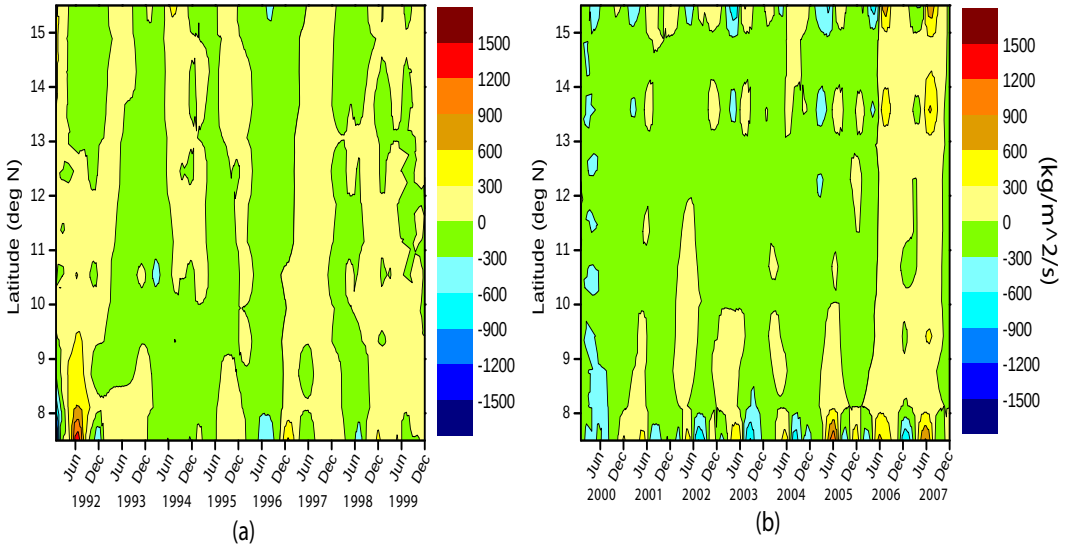

Figure 7.5: Interannual variability of Ekman transport anomaly (a) ERS 1 & 2 (b) QuikScat from 1991 to 2007

Dominant negative anomalies indicating offshore transport were observed during the winter monsoon months. Offshore Ekman transport was found to be very feeble in 2007. This drop in the offshore component of Ekman transport is attributed to a drastic decrease in meridional wind speed in the region during 2005, 2006 and 2007 years. In order to confirm the speeds of the wind during the upwelling season, the regional average wind speed, its zonal and meridional components during the summer monsoon months (JJAS) is given in table 7.1

Table 7.1: Average of wind speed magnitude, zonal and meridional during SW monsoon months of June, July, August and September

Year	Wind Speed (W_{mag}) in m/s	u Wind in m/s	v Wind in m/s
2000	7.384	7.191	-1.319
2001	7.436	7.226	-1.138
2002	7.251	7.014	-1.438
2003	7.278	7.102	-0.9141
2004	7.305	7.139	-0.9393
2005	7.730	7.629	-0.6205
2006	6.918	6.861	-0.2200
2007	7.663	7.597	-0.1984

From table. 7.1, it is observed that, even though the magnitude of total wind and zonal component of the wind have maintained certain uniformity, meridional wind speed during SWM along the coast for the years 2005, 2006 and 2007 has decreased significantly from the previous years. An interesting pattern from wind observations for those three years was that the total wind speed and zonal component were higher than the previous years, while the meridional component showed a decline. This was also observed in LTG where the temperature gradient between the offshore and coastal regions for those years was minimal.

7.4 SLA Variability

From the SLA (Figure 7.6) plotted from 2000 to 2009, the strength of upwelling can be indexed in term of SLA. A consistency in high and low of SLA has been

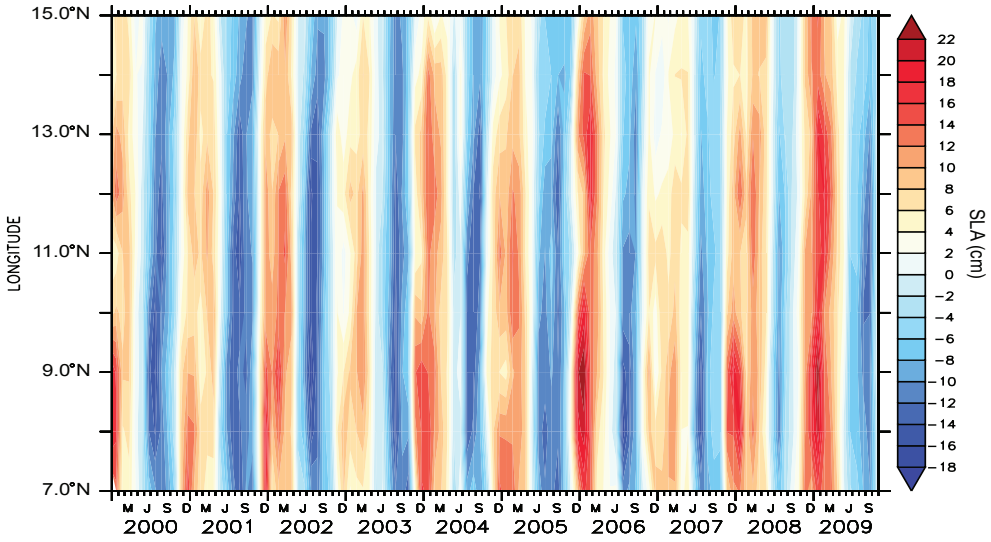

Figure 7.6: Sea Level Anomaly along southwest coast of India from 2000 to 2009

observed between every January and July respectively with distinct interannual variability. The intensity and spread of the coastal Kelvin wave in both its upwelling and downwelling phases of a year can be observed all along the coast. Strong negative anomalies which are the signatures of upwelling could be found up to 13°N for all the years; however, the positive anomalies are observed to be extending up to 15°N. Also a clear biennial oscillation signal in the strength of upwelling / downwelling could also be noticed. Intensity of upwelling was observed to be less for 2005, 2007, 2008 and 2009. This drop in upwelling intensity corroborates with the decrease in upwelling intensity observed from QuikScat derived Ekman transport and SST based upwelling index [Jayaram et al., 2010a].

7.5 CHLA Variability

The decrease in the intensity of upwelling and the resultant drop in productivity of the region are evident from the results on chlorophyll-a concentration of the study region (Figure. 7.7). This figure shows the mean chlorophyll-a concentration during the summer monsoon period from 1998 to 2007. The decrease in productivity for 2005 to 2007 is attributed to the lack of sufficient amount of off-

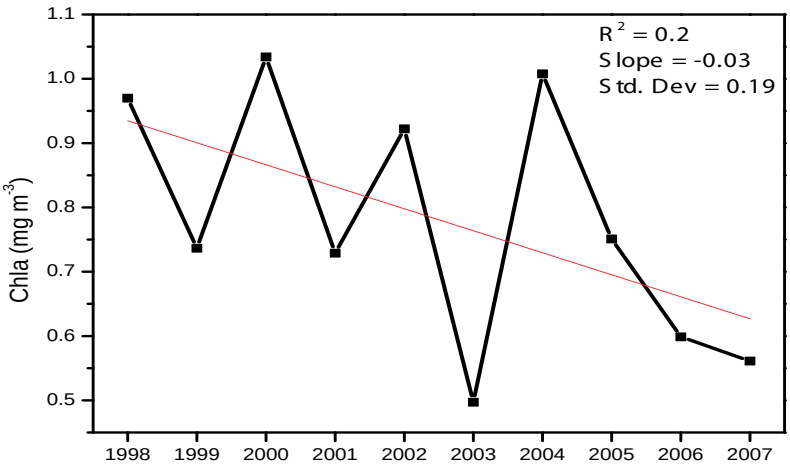

Figure 7.7: Inter-annual variability of mean chlorophyll-a for summer monsoon months (JJAS) from 1998 to 2007

shore transport of nutrient rich coastal waters due to weak meridional winds and thence cooler, nutrient rich subsurface waters remained trapped below, inhibiting the chlorophyll-a production in the surface waters. This also resulted in greater coastal SSTs for those years.

7.6 Upwelling during extreme climatic events

The satellite derived proxies of upwelling like SST, SLA and Chlorophyll were examined for their behaviour during the events of ENSO, IOD and precipitation anomalies in SEAS. Figure 7.8 shows the time series of the climatic indices considered for the present study obtained from various agencies. During the past two decades considered for this study, in reference to the NOAA - Climate Prediction Center, a total of six *El-Nino* events occurred out of which two were designated as strong (1991 - 92 and 1997 - 98); four *La - Nina*s, where one was strong (1988 - 89).

Influence of ENSO on upwelling along the southwest coast of India had been studied by Munikrishna [2008] and the references therein. The modulation of upwelling in the region has been attributed to the atmospheric tele-connection

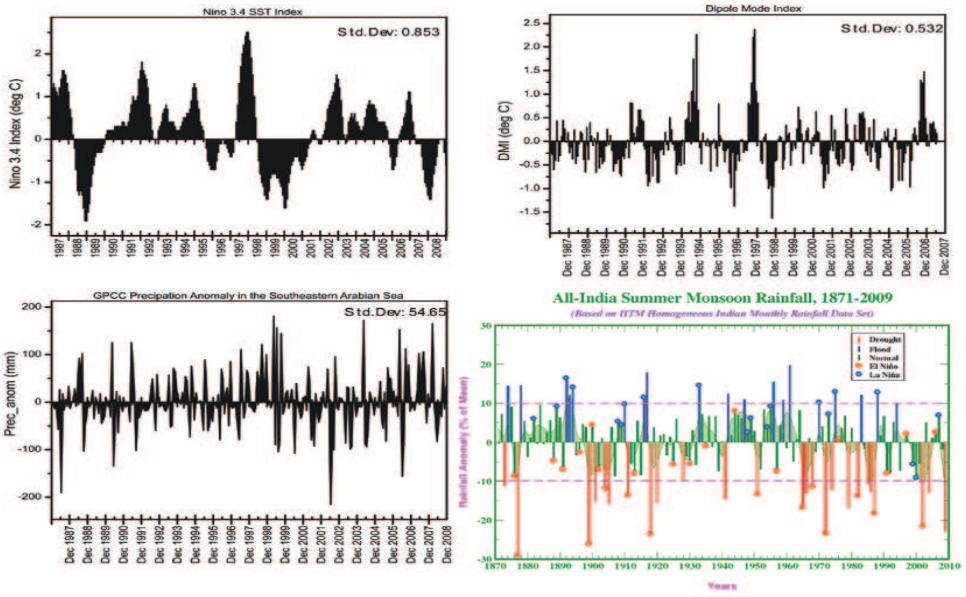

Figure 7.8: Climatic indices considered for the study a. *Nino* 3.4 SST, b. Dipole Mode Index, c. GPCP rainfall anomaly in the study region, d. IITM homogeneous Indian monthly rainfall data

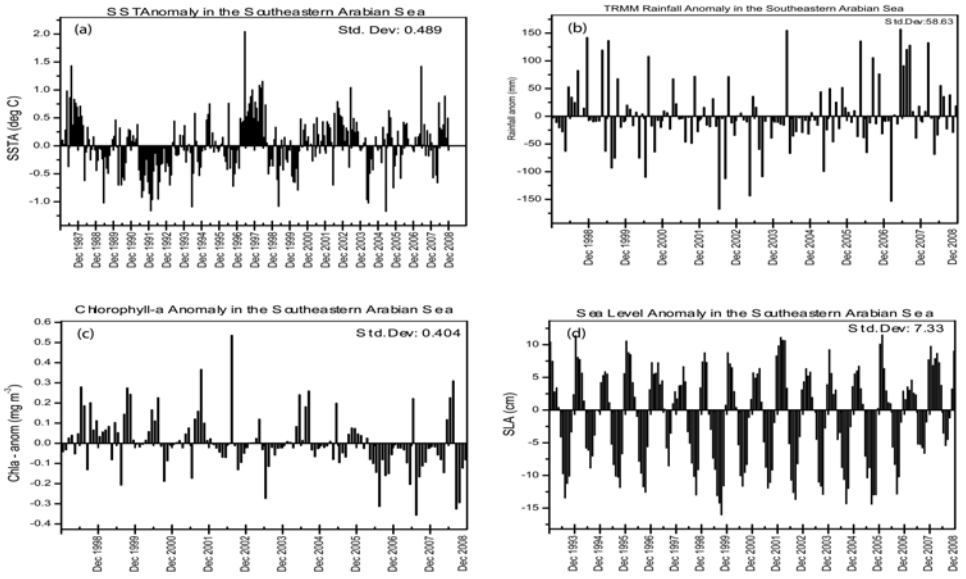

Figure 7.9: Anomalies of a. SST, b. TRMM Rainfall, c. Chlorophyll-a, d. Sea Level; in SEAS

between the Pacific and the Indian Oceans. The gradient of SST along the latitudes and the offshore Ekman transport in the region had shown the influence of ENSO on the coastal upwelling [Jayaram et al., 2010a]. From figures. 7.8 and 7.9 it is observed that except during 1991 - 92 *El-Nino*, the SST anomalies were in tune with the *Nino* 3.4 SST for 1987 - 88, 1997 - 98, 2002 - 03, 2006 - 07. Chlorophyll anomaly was positive for 1998 - 99 *La - Nina* and was negative for 2002- 03 mild *El- Nino*. Since SeaWiFS data is available from 1997 September onwards the impact of 1997- 98 strong *El-Nino* could not be captured but the chlorophyll data for September 1997 can be perceived in figure. 7.8 where negative anomalies were observed all over the region. During 1998 - 99 *La - Nina*, positive chlorophyll anomalies were noticed for September 1998. Chlorophyll for September were considered in figure 7.10 due to the relatively cloud free images when compared to the other months of SWM season. The SLA did not show much variation except during the 1997 - 98 *El - Nino* when average anomalies were found to be hovering around -7cm. Comparatively weak upwelling signatures that were observed for the year 2005 and later, are attributed to abnormal decrease in the alongshore winds as discussed by Jayaram et al. [2010a]. From figure 7.11, SST anomaly during 1997 *El - Nino* showed higher positive anomalies of the magnitude greater than 1°C during the upwelling period. Similarly for *La - Nina* year of 1998 - 99, the region showed relatively cooler SSTs as indicated by negative anomalies very near to the coast. But considerable cooling was not observed because of the intense warming from previous years *El-Nino*. SLA (Figure 7.12) showed paltry negative anomaly during the *El - Nino* of 1997 than during normal years and for mild events, there was no marked depreciation in the magnitude of negative SLA which is a signature of upwelling. Thus it can be inferred that the ENSOs impacts can be experienced in the upwelling regime of SEAS as observed from the anomalies of SST, CHLA and SLA.

Indian Ocean Dipole (IOD) is the pattern with anomalously low sea surface temperatures off Sumatra and high sea surface temperatures in the western Indian Ocean, with accompanying wind and precipitation anomalies [Saji et al., 1999]. This causes severe rainfall events in east Africa and droughts in Indonesia. This type of an IOD is called positive IOD and vice- versa. In the recent years, Indian Ocean Dipole has captured the attention of many researchers around the

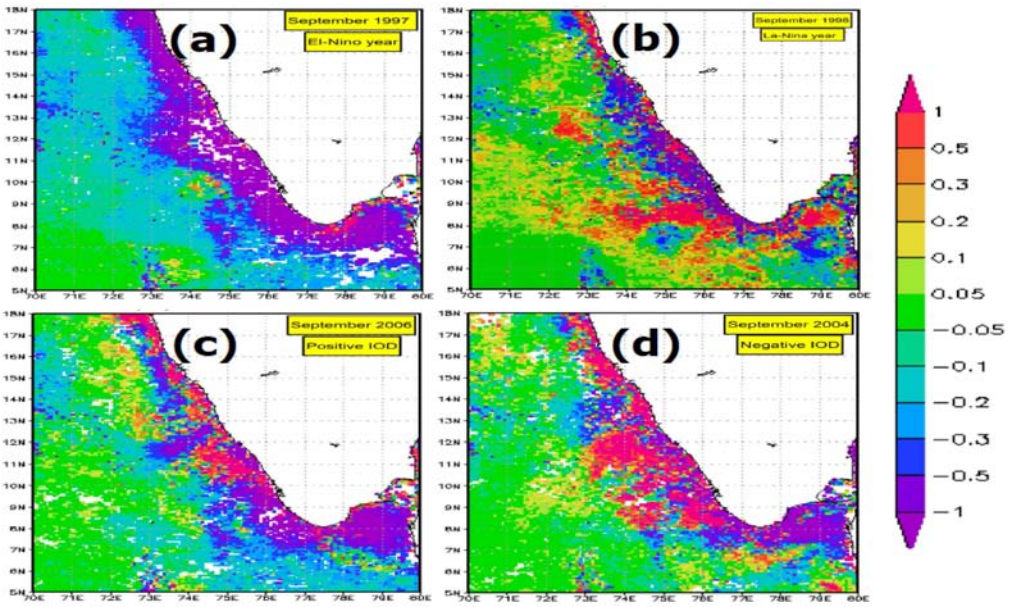

Figure 7.10: Chlorophyll anomalies during a. *El- Nino*, b. *La- Nina*, c. Positive IOD, d. Negative IOD. in SEAS, these figures were plotted online using GIOVANNI

world starting from Saji et al. [1999] till the recent study on the IODs of 2003, 2006 and 2007 by Rao et al. [2009] and the references therein. Table 7.2 show the positive and negative IOD events that occurred during the study period [Yuan et al., 2008]. Major positive IOD events observed from figure 7.8 are 1990, 1993, 1997, 2003 and 2006. On inspection of SST anomalies from figure 7.9 it was observed that the SST was warmer during all these years indicating weak upwelling. The chlorophyll anomalies showed negative during positive IOD of 2003 and 2006. Positive anomalies of SST (Figure. 7.11) were observed during the positive phase of IOD of 2006 indicating weak upwelling in the region. Similarly, negative anomalies were observed during the negative phase of IOD of 2001. Weak upwelling signatures were also observed from SLA (Figure. 7.12) during positive IOD of 2006 and opposite during the negative IOD of 2001. This confirms that the upwelling in the SEAS is indeed influenced by these large scale climatic events.

Rainfall is a complex phenomenon which is influenced by both *El-Nino* and IOD as opined by Ashok et al. [2001] and Ashok et al. [2004] and Ashok and Saji

Table 7.2: Years of *El-Nino* and *La-Nina* during the period of study

El-Nino	*La-Nina*
1987 - 88	1988 - 89(strong)
1991 - 92 (strong)	1998- 99
1994 - 95	2000 - 01
1997 - 98 (strong)	2007- 08
2002 - 03	–
2004 - 05	–

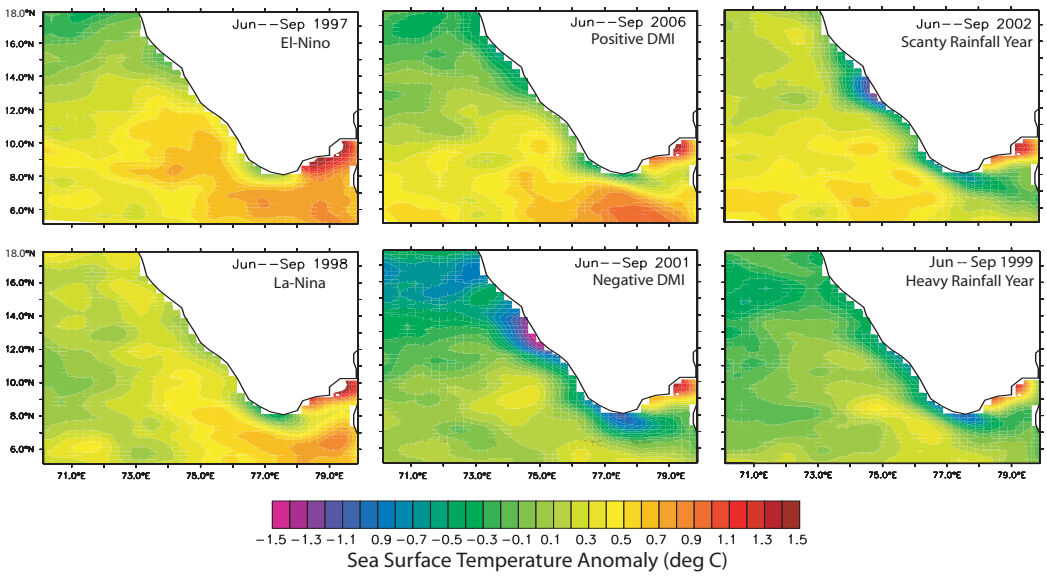

Figure 7.11: SST anomalies in the SEAS during the extreme climatic events

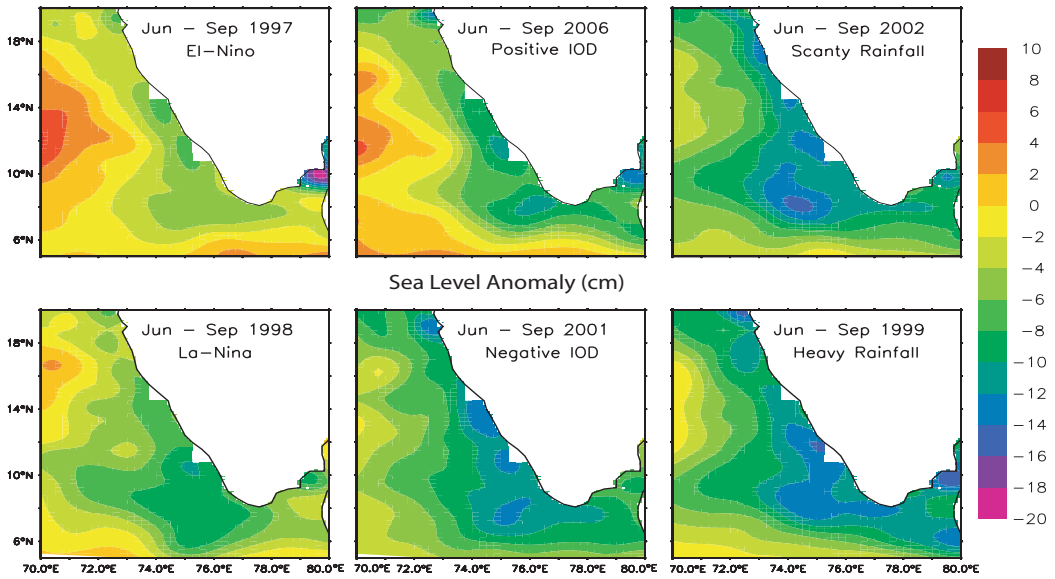

Figure 7.12: SLA in the SEAS during the extreme climatic events

[2007]. Apart from these large scale global climatic phenomena, local forces also do influence the rainfall in SEAS; so does rainfall influence SST by the amount of fresh water introduced into the ocean. These signatures can be surmised on a broad scale through SST maps of the region. From figures 7.8 and 7.11 it was observed that during the years when rainfall was scanty, SST was warmer and vice versa. SLA did not show any variation with respect to rainfall; chlorophyll is not considered for rainfall influence though it can serve as an indicator of clouds over the region of interest.

The impact of global warming and climate change vis-a-vis coastal upwelling along the southwest coast of India was studied for the period 1988 to 2007. The term upwelling is frequently applied to illustrate a variety of conditions involving upward transport of waters in the ocean and often there arises a confusion in describing the effect of process rather than the actual process itself [Sharma, 1973]. To circumvent this mystification, a driving force (alongshore winds) and its influence as an after effect (low sea surface temperature) has been emphasized. Ekman transport for the past two decades has shown hitherto unknown features like the intra - regional variability along the coast on an annual time scale.

The upwelling indices show an increase in temperature gradients with time, which is an indication of rise in the open ocean temperatures than the corresponding coastal region. The investigation has covered two decades of events which reveal that during the later decade, especially upto 2004, a consistent enhancement in the strength of upwelling now stands reversed, notably for the last three years. The Ekman transport for the years 1992 and 1997, which happens to be ENSO years, evidenced strong onshore transports. Even though 2007 is not an ENSO year, onshore transport was observed between 13° and 15°N. Offshore transport was greater off 8° and 15°N during winter monsoon. Though wind direction was considered as the driving factor for the occurrence of coastal upwelling, wind speed is also an important factor in determining the strength of upwelling. This is evident from the indices of 2005, 2006 and 2007 when the meridional component of wind speed was very less and thereby feeble upwelling transpired. This decrease was also observed from the chlorophyll data for the same region. Therefore it should be understood that the nutrients present in the sub surface layers were not being transported to the surface owing to mild Ekman transport. Further, even in a global warming scenario, for coastal upwelling to increase or decrease, more conducive wind pattern is a necessary pre-condition. A marked decrease in upwelling was also observed during ENSO years. During the years where ENSO and IOD appeared together, the decrease in upwelling was more evident. This can be further inferred for 1991 - 92 and also, 1997 - 1998. Thus we conclude that the global warming does play a role in determining the strength of coastal upwelling and so are the conditions in wind speed and direction prevailing in this region.

8

Conclusions

Satellite remote sensing is being effectively used in monitoring the oceans and their variability hitherto unknown, augmenting the *in-situ* measurement techniques. Advancements in sensor physics as well as in retrieval algorithms have made satellite oceanography an indispensible tool in oceanic research, today [Saitoh et al., 2011]. The principal ocean components that could be measured with reasonable accuracy are sea surface temperature, surface chlorophyll-a concentration, sea level anomaly, sea surface winds, significant wave height and geostrophic currents; very recently, satellites have been launched on an experimental basis even to measure gravity and sea surface salinity. Though remote sensing quantifies mainly in the surface parameters, it can well depict the processes that are occurring within the upper ocean too. One such oceanic phenomenon which has both physical and biological implications with respect to a given region is in the occurrence of Upwelling.

Upwelling is a physical process involving the entrainment of cool, nutrient rich subsurface waters to the surface, as a result of concurrent movement of surface waters to offshore regions. This process is mostly governed by the wind and current pattern prevalent in the region and it is often a region of divergence. Of greater importance is its profound impact on the local fisheries as well as regional climate. Along the Indian coast, upwelling is observed along the southwest [Kerala - Kanara] coast, Gujarat coast and central east coast. These regions contribute immensely to the fisheries of India, as discussed earlier and thus it is imperative to study and understand the process of upwelling, fully utilising the

knowledge from satellite remote sensing. While the west coast of India accounts for 70% fish yield of the total Arabian Sea production, the southwest coast alone accounts for 53%; hence this region is of considerable importance in the Indian context.

The signatures of upwelling facilitated through remote sensing are cooler sea surface temperatures, high chlorophyll-a concentration, lower sea level and along shore wind stress. The data products that were used for this study (mostly from 2000 to 2009; in specific cases, the period considered are more than that stated above, depending on data availability) were obtained from the measurements by Advanced Very High Resolution Radiometer (AVHRR) and Tropical Rainfall Measuring Mission Microwave Imager (TMI) for SST and Sea viewing Wide Field of View Sensor (SeaWiFS) and MODerate resolution Imaging Spectro-radiometer (MODIS) on board Aqua for chlorophyll-a concentration. Merged altimeter product of Topex / Poseidon, Jason 1 & 2, Envisat, GFO, ERS 1 & 2 obtained from AVISO provides sea level anomaly and geostrophic currents. Additionally, QuikScat measured winds were made use of for deriving along shore wind stress and the curl of wind stress.

Upwelling along the southwest coast of India is an annually recurring phenomenon that occurs during the southwest monsoon (June to September). The net heat change accounts for more than 65%, greater than the combined effects of net radiation gain, heat loss through evaporation and sensible heat loss. Though intensity wise, this upwelling, less when compared to the other thoroughly studied upwelling regimes of the Arabian Sea [like those off Somalia and Oman], it has profound impacts on the coastal fisheries of India. Upwelling in south eastern Arabian Sea commences around May from near the southern tip of India. This extends northward with time and by July, the whole of southwest coast of India from 8oN to 15oN is an upwelled region. A fall of 4°C in sea surface temperature is often observed in this region. Factually, the average chlorophyll-a concentration in the region is approximately 4 - 5mgm^{-3} during the upwelling season (compared to less than 0.5mgm^{-3} during other seasons). Another peculiarity of this region is that: though the signatures of upwelling from the altimeter data are observed by late April, the biological productivity signatures like increase in the surface

chlorophyll-a concentration(s) are observed only by the arrival of southwest monsoon winds into the region by June. This could be attributed to the fact that the subsurface nutrients are churned by the heavy monsoon winds, thereby breaking up the prevailing stratification; this paves way for nutrients to entrain to surface. In order to understand this process in a better way, a relationship study between chlorophyll-a concentration and the mixed layer depth was conducted and results are presented in this thesis.

Generally, any study on upwelling is incomplete without ascertaining the forcing factors and the resultant processes. To this extent, the atmospheric forcing in terms of sea surface winds, their frequency of variability, climatological pattern in the region are also evaluated and discussed in detail. An index was computed based on the offshore Ekman transport derived from sea surface winds for understanding the strength of upwelling for this region. Another factor that is responsible for upwelling is the remote forcing and the divergent current pattern, which was also discussed and dealt in detail.

The inter relationship between the forcing factors and responses were deduced on different time and space scales. The inter-annual variability of these signatures has also been studied, based on upwelling indices computed from sea surface winds and sea surface temperature. It has come to our notice that there is a noteworthy decrease in the strength of upwelling, post 2004, due to decrease in the strength of meridional winds. The resultant picture points out to a decline in surface chlorophyll content. Also an index was computed based on surface chlorophyll extension along the southwest coast of India, by comparing the data of upwelling and non upwelling months. It was observed and reported herein that the maximum extent of upwelling in the south eastern Arabian Sea along the southwest coast of India is approximately up to 300kms from the coast.

The signatures of upwelling such as low SST, equator ward wind stress, positive wind stress curl, negative SLA and high chlorophyll clearly demonstrate the spatial and temporal evolution of upwelling in SEAS. The long term averages of these analysed signatures show different spatial and temporal variability within SEAS. SST and wind stress showed semi annual variability while the SLA and chlorophyll showed annual variability.

The term upwelling is frequently applied to illustrate a variety of conditions involving upward transport of waters in the ocean and often there arises a gap in understanding the effect of such process rather than the actual process itself. Thus to further delve into the process of upwelling in SEAS, the signatures of upwelling have been classified into its forcing factors and their resultant affects. It has been suggested in literature and also observed through our results that wind and remote forcing of planetary waves are the forces that trigger upwelling while cooling of SST and increase in chlorophyll are the responses of upwelling.

Significant findings of this study are presented in bold in the following paragraphs, apart from numerous other observations / results that are stated within individual chapters, presented earlier.

To sum up on the forcing factors of upwelling in SEAS, it is discerned that the main contributing factors for the **generation of upwelling are the along shore wind stress and remote forcing**. The study was also aimed at understanding the modulation of upwelling with respect to these forces. The intra - seasonal and other minor frequencies of variability in the wind stresses and the strength of coastal Kelvin wave will modulate upwelling and also its after affect(s). From the wavelet transforms of both the components of wind stress, it was observed that the **meridional (along shore) component of the wind stress** showed variability within the basin and **had both significant semi-annual and annual modes of variability** along with other frequencies like the Madden - Julian Oscillations. **The zonal component of wind stress** had only annual mode of variability and the **Madden - Julian Oscillations were absent**. **Wind stress curl was positive near to the coast** during the summer monsoon season **indicating the presence of upwelling**. Wavelet analysis of SLA along the coast showed significant annual mode of variability. To discern the region of variability, the SLA data was subjected to Empirical Orthogonal Function on spatial scale. The resultant first mode was having 67% variance and was located between 74° and 75°E and 7° and 9°N. This region is where the sea level showed alternate high and low during winter and summer monsoon seasons, respectively and is named [Shankar and Shetye, 1997] as Lakshadweep High and Low. Since these offer maximum variability in the region they are reflected in the first mode of EOF of SLA. Hovmuller diagram of SLA along the coast showed the northward limit of

the effect of remote forcing and also the strength of upwelling, as obtained from SLA.

The detailed analysis to **deduce cause-effects between wind forces, remote forcing (SLA) and SST** resulted in finding that the southernmost and central regions of the south west coast of India, clearly defines the **impacts due to wind forces in the order of 4 - 7 days** leading due to reduction in SST coincident with the upwelling season. Such impacts are not prominent towards the northern sector. **SST reduction** occurred during the south west monsoon season or otherwise during the upwelling regime wherein the remote forcing of planetary waves **often fall in the period of 20 days which stands out most distinct in the southern region**.

Upwelling associated surface features indicated a cooling in SST, wherein the wind stresses can play a role in reducing SST and such wind impacts do occur in a 4-7 day cycle. Thereafter, in the absence of such periodicities, except for seasonal signatures, the resultant **SLA had a peak around 20days**, which is linked **to the influence of planetary waves** (remote forcing) mainly prevalent in the southernmost regions. To the contrary, the northern sector, evidenced a composite impact on SST brought about by the identical combination of wind stresses and SLA of varying orders falling within 20-60 days (multiple peaks). Further, based on magnitude of coherence, the impact of planetary waves does not bring about good influence on upwelling inferred through SST. Likewise, for the central coastal regions, though remote forcing of variable periods less than 40days were inferred through SLA variation, the lower order 4-7days period wind stress often dominated SST variability. Another important conclusion that could be drawn from this analysis is that the **peak in SLA in 40 day band was due to the remote forcing of planetary waves generated elsewhere and that in 20day band were due to the locally generated Kelvin and Rossby waves**.

A detailed analysis on available remote sensing data has paved the way to establish the linkages between wind stress, SLA and SST on one hand whereas, the sub regional productivity in the upwelling zone was explored by understanding the relation between wind and chlorophyll. The above analysis was partially supported by data on mixed layer depth. By adopting this approach, selectively

locating three representative areas, it has been possible to deduce the impact of wind stresses on SST followed by extracting time bands too. In continuation of the above, the upwelling index based on latitudinal temperature gradient divulges the intensity of upwelling along the coast at more number of transects. An exercise on correlating the two upwelling indices also proved beneficial to unmask the memory of the ocean with respect to SST, followed by a well quantified exercise to understand the relationship between wind and chlorophyll. The work in this area provides information on time lags in occurrence of peak events and so also provides insight into the stabilization features of the ocean responding to the drop in wind stress and consequently influences chlorophyll concentration for SEAS, as discussed in chapter 5. **This enhanced knowledge has prompted to prepare monthly maps on chlorophyll extension index** which should support ocean operations in the field of fishery activities and aid the demarcation of potential fishery zones.

A comprehensive heat budget for the region involving the solar fluxes, ocean processes such as advection was computed to understand the modulation of heat budget terms with during upwelling. It was found from the study that **the heat gain at surface is far greater than that can be lost or compensated by oceanic process**. The sources of heating, (primarily the fluxes with considerable contributions from Ekman and geostrophic components of the flow) exceeds the cooling from vertical diffusion and coastal upwelling. However, it is evident that **upwelling is the major factor in regulating the heat budget of the region during the SWM**. For the rest of the year, only the surface fluxes contributed towards the heat budget while the oceanic processes were feeble.

As the basic mechanism behind the coastal upwelling region has been deduced, it is thus essential to find out the interannual variability using the indices of upwelling; next, the strength of upwelling during extreme climatic events such as IODs and ENSOs also becomes of considerable interest. Such an exercise will immensely help in monsoon and ecosystem studies. Based on the interannual variability of upwelling indices from 1988 to 2007, applying both SST and wind, it has been observed that there is **a drop in the strength of upwelling after 2004**. This decrease in the intensity of upwelling is attributed to **the decrease in the meridional component of wind speed which is one of the driving**

forces of upwelling in this region. The dwindling of Ekman transport, post 2004, could not transport enough nutrients towards the surface and therefore the decline in surface chlorophyll concentration too for those years is noted. **Interannual variability of SLA** also confirmed the **reduction in upwelling intensity post 2004**. This is one of the significant findings of the study. Another result that was observed is the presence of biennial oscillations, is in the strength of upwelling Kelvin-Rossby waves of the region. **A marked decrease in upwelling was also observed during ENSO years**. During the years where **ENSO and IOD appeared together, the decrease in upwelling was more evident**. This can be further inferred for 1991 - 92 and also for 1997 - 1998. Thus we conclude that the **global warming does play a role in determining the strength of coastal upwelling** and so are the conditions in wind speed and direction prevailing in this region.

The work carried out for thesis is an attempt to present an understanding of upwelling in southeastern Arabian Sea as observed from various remote sensing platforms. This analysis has brought out vital information on spatial and temporal variability and relationship between the driving forces and resultant phenomenon of upwelling. The study could also bring out the role of atmospheric forcing such as heat in controlling the heat budget of the region. Additionally, in future, very recent satellite data products can further augment the studies under this topic. There is still scope for improvement in the form of incorporating continuous and systematic *in-situ* measurements, especially with regard to chlorophyll and temperature profiles (Note: The forth coming publication by Ravichandran et al. [2011]) which as of now are partially incoherent. Also, to determine the contribution of wind forcing and remote forcing towards driving and modulation of upwelling and the resultant productivity in this vital region along the Indian coast, it is important to have a robust ecosystem model.

References

Ahrens.C.D. *Meteorology Today: An Introduction to Weather, Climate and the Environment*, Chapter 2, pages 26 – 46. Thomson / Brooks, 2007. 105, 106

Antony. M.K. , S.G. Narayana, and Y.K. Somayajulu. Offshore limit of coastal ocean variability identified from hydrography and altimeter data in eastern Arabian Sea. *Continental Shelf Research*, 22:2525 – 2536, 2002. 89, 90

Apel.J.R. *Principles of Ocean Physics*. Academic Press, 1987. 2

Ashok.K, Z. Gaun, and T. Yamagata. Impact of the Indian Ocean Dipole and the relationship between the Indian monsoon rainfall and ENSO. *Geophysical Research Letters*, 28:4459 – 4462, 2001. 134

Ashok.K, Z. Guan, N.H. Saji, and T. Yamagata. Individual and combined influences of enso and the Indian Ocean dipole on the summer monsoon. *Journal of Climate*, 17:3141 – 3155, 2004. 134

Ashok.K and N.H. Saji. On the impacts of ENSO and Indian Ocean Dipole events on the sub-regional Indian Summer monsoon rainfall. *Natural Hazards*, 42:273 – 285, 2007. 134

Bakun. A. Global climate change and intensification of coastal ocean upwelling. *Science*, 247:198 – 201, 1990. 8, 123

Bakun. A and V. Agostini. Seasonal patterns of the wind induced upwelling / downwelling in the Mediterranean Sea. *Scientia Marina*, 65:243 – 257, 2001. 11

Banse. K. On upwelling and bottom - trawling off the southwest coast of India. *Journal of Marine Biological Association of India*, 1:33 – 49, 1959. 18

Banse. K. Hydrography of the Arabian Sea shelf of India and Pakistan and effects on demersal fishes. *Deep Sea Research*, 15:45 – 79, 1968. 18

Bhat. G.S., S. Gadgil, P.V. Hareesh Kumar, S.R. Kalsi, P. Madhusoodanan, V.S.N. Murty, C.V.K. Prasada Rao, V. Ramesh Babu, L.V.G. Rao, R.R. Rao, M.Ravichandran, K.G. Reddy, P. Sanjeeva Rao, D. Sengupta, D.R. Sikka, J. Swain, and P.N. Vinayachandran. Bobmex: The Bay of Bengal Monsoon Experiment. *Bulletin of American Meteorological Society*, 82:2217 – 2243, 2001. 3

Bijoy. T, C. Gnanaseelan, P. Ananth, and P.S. Salvekar. North Indian Ocean warming and sea level rise in an OGCM. *Journal of Earth System Science*, 117:169 – 178, 2008. 124

Boe. J, A. Hall,F. Colas, J.C. McWilliams,X. Qu, J. Kurian and S. B. Kapnick. What shapes mesoscale wind anomalies in coastal upwelling zones? *Climate Dynamics*, 117:doi: 10.1007/s382-011-1058-5, 2011. 60

Boyer. T, S. Levitus, H. Garcia, R.A. Locarnini, C. Stephens and J. Antonov. Objective analysis of annual, seasonal and monthly temperature and salinity for the world ocean on 0.25 degree grid. *International Journal of Climatology*, 25:931 — 945, 2005. 39

Brown. C.W, L.N. Connor, J.L. Lillibridge, N.R. Nalli, and R.V. Legeckis. *An Introduction to Satellite Sensors, Observations and Techniques*, Chapter2, pages 21 – 50. Springer, 2005. 4

Bruce. J.G, D.R. Johnson, and J.C. Kindle. Evidense for eddy formation in the eastern Arabian Sea during the Northeast Monsoon. *Journal of Geophysical Research*, 99:7651 – 7664, 1994. 18, 61, 75, 86

Bruce. J.G, J.C. Kindle, L.H. Kantha, J.L. Kerling, and J.F. Bailey. Recent observations and modeling in the Arabian Sea Laccadive High region. *Journal of Geophysical Research*, 103:7593 – 7600, 1998. 18

Chauhan. P, M. Mohan, B. Kumari, S. Nayak, and P. Matondkar. Surface chlorophyll-a estimation using IRS-P4 ocm data in the Arabian Sea. *International Journal of Remote Sensing*, 23:1663–1676, 2002. 7

Chauhan. P, A. Sahay, A.S. Rajawat, and S. Nayak. Remote sensing of diffuse attenuation coefficient (k490) using IRS-P4 ocean color monitor (ocm) sensor. *Indian Journal of Marine Science*, 32:279–284, 2003. 7

Chavez. F.P and Monique Messie. A comparison of eastern boundary upwelling ecosystems. *Progress in Oceanography*, 83:8096, 2009. 7, 60

Cushing. D.H. *Marine Ecology and Fisheries*. Cambridge University Press, 1975. 94

Cutler. A.N and J.C. Swallow. Surf currents of the Indian Ocean (to 25°S, 100°SE): Compiled from historical data. Technical report, Meteorological Office, Bracknell, U.K., 1984. 16, 17

Darbyshire. M. The surface waters off the coast of Kerala, southwest India. *Deep Sea Research*, 14:295 – 320, 1967. 19

de Boyer Montegut. C, J. Vailard, S.S.C. Shenoi, D. Shankar, F. Durand, C. Ethe, and G. Madec. Simulated seasonal and interannual variability of the mixed layer heat budget in the northern Indian Ocean. *Journal of Climate*, 20:3249–3268, 2007. 114

Dimarco. S.F., P. Chapman, and J.W.D.Nowlin. Satellite observations of upwelling on the continental shelf south of Madagaskar. *Geophysical Research Letters*, 27:3965 – 3968, 2000. 15

Donlon. C.J, P.J. Minnett, C.Gentemann, T.J. Nightingale, I.J. Barton, B. Ward, and M.J.Murray. Towards improved validation of satellite sea surface skin temperature measurements for climate research. *Journal of Climate*, 15:353 – 369, 2002. xiii, 32

Duing. W and A. Leetma. Arabian sea cooling: A preliminary heat budget. *Journal of Physical Oceanography*, 10:307 – 312, 1980. 113, 119

Falkowski. P. et al. The global carbon cycle: A test of our knowledge of earth as a system. *Science*, 290:291 – 296, 2000. 94

Findlater. J. Observational aspects of the low-level cross equatorial jet stream on the western Indian Ocean. *Pure and Applied Geophysics*, 115:1251 – 1262, 1977. 16, 60

Florenchie. P., C. Reason, J. Lutjeharms, M. Rouault, and S. Masson. Evolution of interannual warm and cold events in the southeast Atlantic Ocean. *Journal of Climate*, 17:2318 – 2334, 2004. 76

Fu. F.F, M. Lefebure, and W. Patzert. Topex / Poseidon science plan overview. Technical report, AGU, 1992. 27, 75

Goes. J.I, T.G. Prasad, H.R. Gomes, and J.T. Fasullo. Warming of eurasian land mass is making the Arabian Sea more productive. *Science*, 308:545 – 547, 2005. 123

Gopalakrishna. V.V., R.R. Rao, K. Nisha, M.S.Girish Kumar, T. Pankajakshan, M. Ravichandran, Z. Johnson, K. Girish, N. Aneesh Kumar, M. Srinath, S. Rajesh, and C.K. Rajan. Observed anomolous upwelling in the Lakshadweep Sea during the summer monsoon of 2005. *Journal of Geophysical Research*, 113: C05001 – 12, 2008. 127

Gopalakrishna. V.V, F. Durand, K. Nisha, M. Lengaigne, T.P. Boyer, J. Costa, R.R. Rao, M. Ravichandran, S. Amrithash, L. John, K. Girish, C. Revichandran and V. Suneel. Observed intra - seasonal to interannual variability of the upper ocean thremal structure in the southeastern Arabian Sea during 2002 - 2008. *Deep Sea Research - I*, 57:739 - 754, 2010. 19

Goswami. B.N and E.N. Rajagopal. Indian ocean surface winds from NCMRWF analysis as compared to quikscat and moored buoy winds. Technical report, Indian Institute of Science, 2003. 25

HareeshKumar. P.V and B. Mathew. On the heat budget of the Arabian Sea. *Meteorology and Atmospheric Physics*, 62:215 – 224, 1997. 109, 113

Hastenrath. S and P.J. Lamb. Climatic atlas of Indian Ocean. part 1: Surface climate and atmospheric circulation. Technical report, Wiscosin University press, 1979. 16, 17, 113

Hastenrath. S and L.Greischer. The monsoonal current regimes of the tropical Indian Ocean: Observed surface flow fields and their geostrophic and wind-driven components. *Journal of Geophysical Research*, 96:619 – 633, 1991. 16, 19

Haugen. V.E, O.M. Johannessen, and G. Evensen. Indian ocean circulation. part 1: Validation of the miami isopycnal coordinate model and part 2: Enso events during 1958 - 1998. *Journal of Geophysical Research*, 107:101029 – 101057, 2002. 19, 91

Hormazabal. S, G. Shaffer, J. Letelier, and O. Ulloa. Local and remote forcing of sea surface temperature in the coastal upwelling system of Chile. *Journal of Geophysical Research*, 106:16657 – 16671, 2001. 84

Jayaram. C, K. A. Joseph, and A.N. Balchand. Decreasing trend in the chlorophyll-a concentration in the southeastern Arabian Sea - observed from satellite data. In *Proceedings of National conference of Ocean Society of India on recent developments in Ocean Science, Engineering and Technology*, 2009. 124

Jayaram. C, N. Chacko, K.A. Joseph, and A.N. Balchand. Interannual variability of upwelling indices in the southeastern Arabian Sea: A satellite based study. *Ocean Science Journal*, 45:27 – 40, 2010a. 71, 92, 97, 130, 133

Jayaram. C, N. N. Menon, K.A. Joseph, and A.N. Balchand. Monitoring of trichodesmium spp. in the Arabian Sea from in-situ and satellite data products. In *Safari International Symposium on " Remote Sensing and Fisheries", held at Kochi*, 2010b. 15

Johannessen. O.M, G. Subbaraju, and J. Blindheim. Seasonal variation of oceanographic conditions off the southwest coast of India during 1971 1975. *FiskDir. Skr. Ser. HavUnders*, 18:247 – 261, 1987. 19, 91

Joseph. P.V. Warm pool over the Indian ocean and monsoon onset. *Tropical Ocean and Atmosphere Newletter*, 53:1 – 5, 1990. 7

Kilpatrick. K.G, G.P. Podesta, and R. Evans. Overview of NOAA/NASA Advanced Very High Resolution Radiometer pathfinder algorithm for sea surface temperature and associated matchup data base. *Journal of Geophysical Research*, 106:9179 – 9197, 2001. 30

Kim. H.J, S.J. Yoo, and I.S. oh. Relationship between phytoplankton bloom and wind stress in the sub-polar frontal area of Japan / East Sea. *Journal of Marine Systems*, 67:205 – 216, 2007. 94, 95

Koracin. D, C.E. Dorman, and E.P. Dever. Coastal perturbations of marine-layer winds, wind stress and wind stress curl along California and Baja California in June 1999. *Journal of Physical Oceanography*, 32:1152 – 1173, 2004. 67

Kurian. J and P.N. Vinayachandran. Mechanisms of formation of the Arabian Sea mini warm pool in the high resolution ocean general circulation model. *Journal of Geophysical Research*, 112:C05009, 1 – 14, 2007. 45

Laing. A and J.L. Evans. *Introduction to Tropical Meteorology: A Comprehensive online and Print Text book*. University Corporation of Atmospheric Research, 2010. 104

Lathuiliere. C, V. Echevin, and M. Lvy. easonal and intraseasonal surface chlorophyll-a variability along the northwest African coast. *Journal of Geophysical Research*, 113:C05007, doi:10.1029/2007JC004433,2008. 100

LeTraon. P.T and G. Dibarboure. Mesoscale mapping capabilities of multiple-satellite altimeter missions. *Journal of Atmospheric and Oceanic Technology*, 16:1208 – 1223, 1999. 27

Levitus. S, J. Antonov, and T.P. Boyer. Warming of the world ocean. *Science*, 287:2225 – 2229, 2000. 124

Levitus. S, J. Antonov, J. Wang, T.L. Delworth, K.W. Dixon, and A.J. Roccoli. Anthropogenic warming of earth's climate system. *Science*, 292:267 – 270, 2001. 124

Levy. M, D. Shankar, J.M. Andre, S.S.C. Shenoi, F. Durand, and C de Boyer Montegut. Basin wide seasonal evolution of the Indian Ocean's phytoplankton blooms. *Journal of Geophysical Research*, 112:C12014, 2007. 93

Loschnigg. J and P.J. Webster. A coupled ocean-atmosphere system of SST modulation for the Indian Ocean. *Journal of Climate*, 13:3342 – 3360, 2000. 113

Luis. A.J and H. Kawamura. Winter time wind forcing and sea surface cooling near the south India tip observed using NSCAT and AVHRR. *Remote Sensing Environment*, 73:55 – 64, 2000. 69

Luis. A.J and H. Kawamura. Characteristics of atmospheric forcing and SST cooling events in the Gulf of Mannar during winter monsoon. *Remote Sensing Environment*, 77:139 – 148, 2001. 69

Luis. A.J and H. Kawamura. Air-sea interaction, coastal circulation and biological production in the eastern Arabian Sea: A Review. *Journal of Oceanography*, 60:205 – 218, 2004. xiii, 17, 18, 19

Lutjeharms. L and E. Machu. An upwelling cell inshore of the east Madagaskar current. *Deep Sea Research-I*, 47:2405 – 2411, 2000. 12, 15

Madhupratap. M, K.N.V. Nair, T.C. Gopalakrishnan, P. Haridas, K.K.C. Nair, P. Venugopal, and M. Gauns. Arabian sea oceanography and fisheries of the west coast of India. *Current Science*, 81:355 – 361, 2001. 12, 13, 19

Masuda. K, T. Takashima, and Y. Takayama. Emissivity of the pure and sea waters in the model sea surface in the infrared window regions. *Remote Sensing Environment*, 24:313 – 329, 1988. 29

Mathew. B. *Studies on upwelling and sinking in the seas around India*. PhD thesis, Cochin University of Science and Technology, 1983. 19

Maull. G. *Introduction to Satellite Oceanography*. Dordrecht, The Netherlands, 1985. 4, 29

McCreary. J.P, P.K. Kundu, and R.L Molinari. A numerical investigation of dynamics, thermodynamics and mixed layer processes in the Indian Ocean. *Progress in Oceanography*, 31:181 – 224, 1993. 61, 75

McCreary. J.P, W. Han, D. Shankar, and S.R. Shetye. Dynamics of East India Coastal Current, 2, numerical solutions. *Journal of Geophysical Research*, 101: 13993 – 14010, 1996. 75

McKeown. W and W. Asher. A radiometric method to measure the concentration boundary layer thickness at an airwater interface. *Journal of Atmospheric and Oceanic Technology*, 14:1494 - 1501, 1997. 33

Milutinovic. S, M.J. Behrenfeld, J.A. Johannessen, and T. Johannessen. Sensitivity of remote sensing derived phytoplankton productivity to mixed layer depth: Lessons from the carbon based productivity model. *Global Biogeochemical Cycles*, 23:GB4005, doi: 10.1029/2008GB003431, 2009. 94

Morel. A and L. Prieur. Analysis of variations in ocean color. *Limnology and Oceanography*, 22:709 – 722, 1977. 34

Mote. P.W and N.J. Mantua. Coastal upwelling in the warmer future. *Geophysical Research Letters*, 29:2138, 2002. 123

Munikrishna. K. Coastal upwelling along the southwest coast of India - ENSO modulation. *Annals Geophysicae*, 26:1331 – 1334, 2008. 131

Munikrishna. K. Study of 19 year satellite sea surface temperature variability along the west coast of India. *Marine Geodesy*, 32:77 – 88, 2009. 89

Muraleedharan. P.M and S. Prasanna Kumar. Arabian Sea upwelling - a comparison between coastal and open ocean regions. *Current Science*, 71:842 – 846, 1996. 3, 12, 90

Muraleedharan. P.M, M.R. Ramesh Kumar, and L.V.G. Rao. A note of poleward undercurrent along the southwest coast of India. *Continental Shelf Research*, 15:165 – 184, 1995. 67, 92

Naidu. P.D, M.R. Ramesh Kumar, and V. Ramesh Babu. Time and space variations of monsoonal upwelling along the west and east coasts of India. *Continental Shelf Research*, 19:559 – 572, 1999. 12, 89

Naqvi. S, D. Jayakumar, P. Narvekar, H. Naik, V. Sarma, W. D'Souza, S. Joseph, and M. George. Increased marine production of n2o due to intensifying anoxia on the Indian continental shelf. *Nature*, 406:346 – 349, 2000. 11

Nisha. K, V.V. Gopalakrishna, T. Pankajakshan, M. Anuradha, S.S.M. Gavaskar, V. Suneel, S.A. Rao, R.R. Rao, M.S. Girish Kumar, M. Ravichandran, M. Krishna, S. Rajesh, K. Girish and Z. Johnson. Reduced near surface thermal inversions in 2005 - 2006 in the souheastern Arabian Sea (Lakshadweep Sea). *Journal of Physical Oceanography*, 39:1184 - 1199, 2009. 58

Nykaer. L and L.V. Camp. Seasonal and interannual variability of coastal upwelling along northwest Africa and Portugal from 1981 - 1991. *Journal of Geophysical Research*, 99:14197 – 14207, 1994. 89, 125, 127

O'Reilly. J.E, S. Maritorena, B.G. Mitchell, D.A. Siegel, K.L. Carder, S.A. Garver, M. Kahru, and C. McCain. Ocean color chlorophyll algorithms for SeaWiFS. *Journal of Geophysical Research*, 103:24937 – 24953, 1998. 34

Panikkar. N.K. The Indian Ocean Expedition. *Current Science*, 2:49 – 53, 1963. 2

Petit. M, A.G. Ramos, F. Lahet, and J. Copa. Satellite derived ers scatterometer - sea surface wind stress curl in the southwestern Indian Ocean. *Geoscience*, 338:206 – 213, 2006. 67

Pickard. G and W. Emery. *Descriptive Physical Oceanography.* Pergamon Press, 1982. 24

Podesta. G.P, S.S.C. Shenoi, J.W. Brown, and R.H. Evans. Advanced Very High Resolution Radiometer Pathfinder oceans matchup database 1985 - 1993 version 18. Technical report, University of Miami, Rosenstial School of Marine and Atmospheric Science, 1995. 30

Pond. S and G.L. Pickard. *Introductory Dynamical Oceanography*. Pergamon Press, 1983. 8, 9, 10, 27

Prakash. S and R. Ramesh. In Arabian Sea getting more productive? *Current Science*, 92:667 – 671, 2007. 123

Prasanna Kumar. S, P.M. Muraleedharan, T.G. Prasad, M. Gauns, N. Ramaiah, S.N. de Souza, S. Sardesai, and M Madhupratap. Why is the Bay of Bengal less productive during summer monsoon compared to the Arabian Sea? *Geophysical Research Letters*, 29:doi: 10.1029/2002GL016013, 2002. 15

Raghu. M, S. Sergio, R. Signorini, J. Chirstian, A. Busalacchi, C. McCain, and J. Picaut. Ocean color variability of the tropical Indo - Pacific baisn observed from SeaWiFS during 1997 - 1998. *Journal of Geophysical Research*, 104:18315 – 18336, 1999. 12, 14

Rao. A.D, M. Joshi, and M. Ravichandran. Oceanic upwelling and downwelling in the waters off the west coast of India. *Ocean Dynamics*, 58:213–226, 2008. 19, 63, 67

Rao. A.S, J.J.Luo, S.K. Brehera, and T. Yamagata. Generation and termination of Indian Ocean Dipole events in 2003, 2006 and 2007. *Climate Dynamics*, 33: 751 – 767, 2009. 134

Rao. L.V.G and R. Jayaraman. Upwelling in the Minicoy region of Arabian Sea. *Current Science*, 35:378 – 380, 1966. 13, 18

Rao. L.V.G and P. Sree Ram. Upper ocean physical processes in the tropical Indian Ocean. Technical report, National Institute of Oceanography, 2005. 9, 10

Rao. R.R, M.S. Girish Kumar, M. Ravichandran, A. R. Rao, V.V. Gopalakrishna, and P. Tadathil. Interannual variability of Kelvin wave propagation in the wave guides of the equatorial Indian Ocean, coastal Bay of Bengal and the southeastern Arabian Sea during 1993 - 2006. *Deep Sea Research - I*, 57:1 – 13, 2010. 61, 75

Ravichandran. M, M.S. Girish Kumar and Stephen Riser. Observed variability of chlorophyll-a using Argo profiling floats in southeastern Arabian Sea. *Journal of Marine Systems*, In-press, 2011. 144

Robinson. I.S *Measuring the Oceans from Space: The principles and methods of satellite oceanography.* Springer - Praxis, 2004. xii, xiii, 4, 5, 6, 23, 25, 26, 28, 29, 37

Saha. K. Some aspects of air - sea interaction in the Indian Ocean deduced from satellite cloud photographs. *Journal of Marine Biological Association of India*, 14:827 – 835, 1972. 7

Saitoh. S, R. Mugo, I.N. Radiarta, S. Asaga, F. Takahashi, T. Hirawake, Y. Ishikawa, T. Awaji, T. In, and S. Shima. Some operational uses of satellite remote sensing and marine gis for sustainable fisheries adnd aquaculture. *ICES Journal of Marine Science*, 68:687 – 695, 2011. 7, 138

Saji. N.H, B.N. Goswami, P.N. Vinayachandran, and T. Yamagata. A dipole mode in the tropical Indian Ocean. *Nature*, 401:360 – 363, 1999. 7, 133, 134

SanilKumar. V, K.C. Pathak, P. Pednekar, N.S.N. Raju, and R. Gowthaman. Coastal processes along the Indian coastline. *Current Science*, 91:530 – 536, 2006. 3

Sanjeevan. V.N, P. Jasmine, B.R. Smitha, P T. Ganesh, Sabu, and T. Shanmugaraj. Eastern Arabian Sea Marine Ecosystems. In *International symposium on Marine Ecosystems Challenges and Oppertunities*, 2009. 18, 93

Sastry. R and P. Myrland. Distribution of temperature, salinity and density in the Arabian Sea along the south Malabar coast (south India) during the post monsoon season. *Indian Journal of Fisheries*, 6:223 – 255, 1959. 18

Satheesan. K, A.Sarkar, A. Parekh, M.R.Ramesh Kumar, and Y. Kuroda. Comparison of wind data from Quikscat and buoys in the Indian Ocean. *International Journal of Remote Sensing*, 28:2375–2382, 2007. 25

Schott. F. Monsoon response of the Somali current and associated upwelling. *Progress in Oceanography*, 12:357 – 382, 1983. 16

Schott. F and J.P. McCreary. Monsoon circulation of the Indian Ocean. *Progress in Oceanography*, 51:1 – 123, 2001. 75

Schott. F.A, S.P. Xie, and J.P. McCreary. Indian ocean circulation and climate variability. *Reviews of Geophysics*, 47:RG1002, 2009. 75

Sears. F.W and M.W. Zemansky. *University Physics*. Addison - Wiley, 1970. 104

Sengupta. D, S.R. Parampil, G.S. Bhatt, V.S.N. Murty, V. Ramesh Babu, T. Sudhakar, K. Premkumar, and Y. Pradhan. Warm pool thermodynamics from the Arabian Sea Monsoon Experiment (ARMEX). *Journal of Geophysical Research*, 113:C10008, doi: 10.1029/2007/JC004623, 2008. 3

Shankar. D and S.R. Shetye. On the dynamics of Lakshadweep high and low in the southeastern Arabian Sea. *Journal of Geophysical Research*, 102:12551 – 12562, 1997. 18, 19, 58, 61, 86, 141

Shankar. D, P.N. Vinayachandran, and A.S. Unnikrishnan. Monsoon currents in the north Indian Ocean. *Progress in Oceanography*, 52:63 – 120, 2002. 13

Shankar. D, V.V. Gopalakrishna, S.S.C. Shenoi, F. Durand, S.R. Shetye, C.K. Rajan, Z. Johnson, N. Araligidad, and G.S. Micheal. Obeservational evidence for westward propagation of temperature inversions in the southeastern Arabian Sea. *Geophysical Research Letters*, 31:L08305, doi: 10.1029/2004GL01952, 2004. 76

Sharma. G.S. Thermocline as an indicator of upwelling. *Journal of Marine Biological Association of India*, 8:8 – 19, 1966. 18

Sharma. G.S. Seasonal variation of some hydrographic properties of the shelf waters off the west coast of India. *Bulletin of National Institute of Science, India*, 38:263 – 276, 1968. 19

Sharma. G.S Upwelling off the southwest coast of India. *Indian Journal of Marine Science*, 7:209 – 218, 1973. 136

Shenoi. S.S.C, D. Shankar, and S.R. Shetye. On the sea surface temperature high in the Lakshadweep Sea before the onset of the summer monsoon. *Journal of Geophysical Research*, 104:703–712, 1999. 13

Shenoi. S.S.C, D. Shankar, and S.R. Shetye. Differences in heat budgets of the near-surface Arabian Sea and Bay of Bengal: Implications for summer monsoon. *Journal of Geophysical Research*, 107:C6:1–14, 2002. 113, 114, 117, 119, 120

Shenoi. S.S.C, D. Shankar, V.V. Gopalakrishna, and F. Durand. Role of ocean in the genesis and annihilation of the core of the warm pool in the southeastern Arabian Sea. *Mausam*, 56:147 – 160, 2005. 19, 91

Shetye. S.R. Seasonal variability of the temperature field off the southwest coast of India. *Proceedings of Indian Academy of Sciences (Earth and Planetary Sciences)*, 93:399 – 411, 1984. 19, 127

Shetye. S.R and S.S.C. Shenoi. Seasonal cycle of surface circulation in the coastal northern Indian Ocean. *Proceedings of Indian Academy of Sciences (Earth and Planetary Sciences)*, 97:53 – 62, 1988. 16, 17

Shetye. S.R, S.S.C. Shenoi, M.K. Antony, and V. Krishna Kumar. Monthly mean wind stress along the coasts of the Indian Ocean. *Proceedings of Indian Academy of Sciences (Earth and Planetary Sciences)*, 97:53 – 62, 1985. 19, 67, 90

Shetye. S.R, S.S.C. Shenoi, A. Gouveia, G. Micheal, D. Sundar, and G. Nampoothiri. Wind driven coastal upwelling along the western boundary of the Bay of Bengal during the southwest monsoon. *Continental Shelf Research*, 11: 1397 – 1408, 1991. 12, 14, 17

Smith. R. *Upwelling*, volume 6, chapter 1, pages 11 – 46. University College London Press, 1968. 8

Smith. S.D. Coefficients for sea surface wind stress, heat flux, and wind profiles as a function of wind speed and temperature. *Journal of Geophysical Research*, 93:15467 – 15472, 1988. 25, 67

Smitha. B.R, V.N. Sanjeevan, K.G. Vimalkumar, and C.Revichandran. On the upwelling off the southern tip and along the west coast of India. *Journal of Coastal Research*, 24:359 – 378, 2008. 19, 63, 89, 93

Stewart. R.H. *Methods of Satellite Oceanography*. University of California Press, 1985. 4, 5, 25

Stewart. R.H. *Introduction to Physical Oceanography*. Dept. of Oceanography, Texas A & M University, 2005. 8, 9, 10, 60, 104, 105, 106, 109

Su. J, J. Wang, T. Pohlmann, D. Xu. The influence of meteorological variation on the upwelling system off eastern Hainan during summer 2007 - 2008. *Ocean Dynamics*, :doi: 10.1007/s10236-011-0404-9, 2011. 10

Subramanyam. R. Ecological studies on the marine phytoplankton on the west coast of India. *Memoirs of Indian Botanical Society*, 1:145 – 151, 1958. 19

Susanto. D, A. Gordon, and Q. Zheng. Upwelling along the coasts of Java and Sumatra and its relation to enso. *Geophysical Research Letters*, 28:1599 – 1602, 2001. 12, 14

Sverdrup. H.U, M.W. Johnson, and R.H. Fleming. *The Oceans Their Physics, Chemistry and General Biology*. Prentice Hall, 1942. 1

Torrence. C and G.P. Compo. A practical guide to wavelet analysis. *Bulletin of American Meteorological Society*, 79:61 – 78, 1998. 70

Vimalkumar. K.G, P.K. Dinesh Kumar, B.R. Smitha, H. Habeeb Rahman, Jacob Josia, K.R. Muraleedharan, V. N. Sanjeevan, and C.T. Achuthankutty. Hydrographic characterization of southeast Arabian Sea during the wane of southwest monsoon and spring intermonsoon. *Environmental Monitoring and Assessment*, 140:231 – 247, 2008. 93

Vinayachandran. P.N and S. Mathew. Phytoplankton bloom in the Bay of Bengal during the northeast monsoon and its intensification by cyclones. *Geophysical Research Letters*, 30:1 – 4, 2003. 12, 14

Vinayachandran. P.N, P. Chauhan, M. Mohan, and S. Nayak. Biological response of the sea around Sri Lanka to summer monsoon. *Geophysical Research Letters*, 31:1 – 4, 2003. 14

Watts. P, M. Allen, and T. Nightingale. Sea surface emission and reflection for radiometric measurements made with the along-track scanning radiometer. *Journal of Atmospheric and Oceanic Technology*, 13:126 – 141, 1996. 29

Wentz. F.J, C. Gentamann, D.K. Smith, and D. Chelton. Satellite measurements of sea surface temperature through clouds. *Science*, 288:847–850, 2000. 24, 31, 32

Wentz. F.J, D.K. Smith, C.A. Maers, and C. Gentamann. Advanced algorithms for Quikscat and SeaWinds/AMSR In *IGRASS 01 Proceedings 2001*, 2001. 23, 24

Wilson-Diaz. D, A.J. Mariano, and R.H. Evans. On the heat budget of the Arabian Sea. *Deep Sea Research - I*, 56:141 – 165, 2009. 114

Wooster. W.S, A.J. Lee, and G. Dietrich. Redefinition of salinity. *Limnology and Oceanography*, 14:437 – 438, 1969. 19

Wyrtki. K. Physical oceanography of the Indian Ocean. Technical report, National Science Foundation, Washington, 1971. 16

Wyrtki. K. An equatorial jet in the Indian Ocean. *Science*, 181:262 – 264, 1973. 12, 13, 14, 16, 19

Yentsch. C.S. Influence of phytoplankton pigments on the color of the sea water. *Deep Sea Research*, 7:1–9, 1960. 33

Yu. J.J, J.J. O'Brien, and J. Yang. On the remote forcing of the circulation in the Bay of Bengal. *Journal of Geophysical Research*, 96:20449 – 20454, 1991. 18

Yuan. Y, C.L. Johnny Chan, Z. Wen, and Li Chongyin. Decadal and interannual variability of the Indian Ocean Dipole. *Advances in Atmospheric Sciences*, 25: 856 – 866, 2008. 134

Appendix-1

This appendix consists of the figures showing weekly evolution of SLA which can be used to infer the propagation of planetary waves in the Northern Indian Ocean as discussed in Chapter 4.

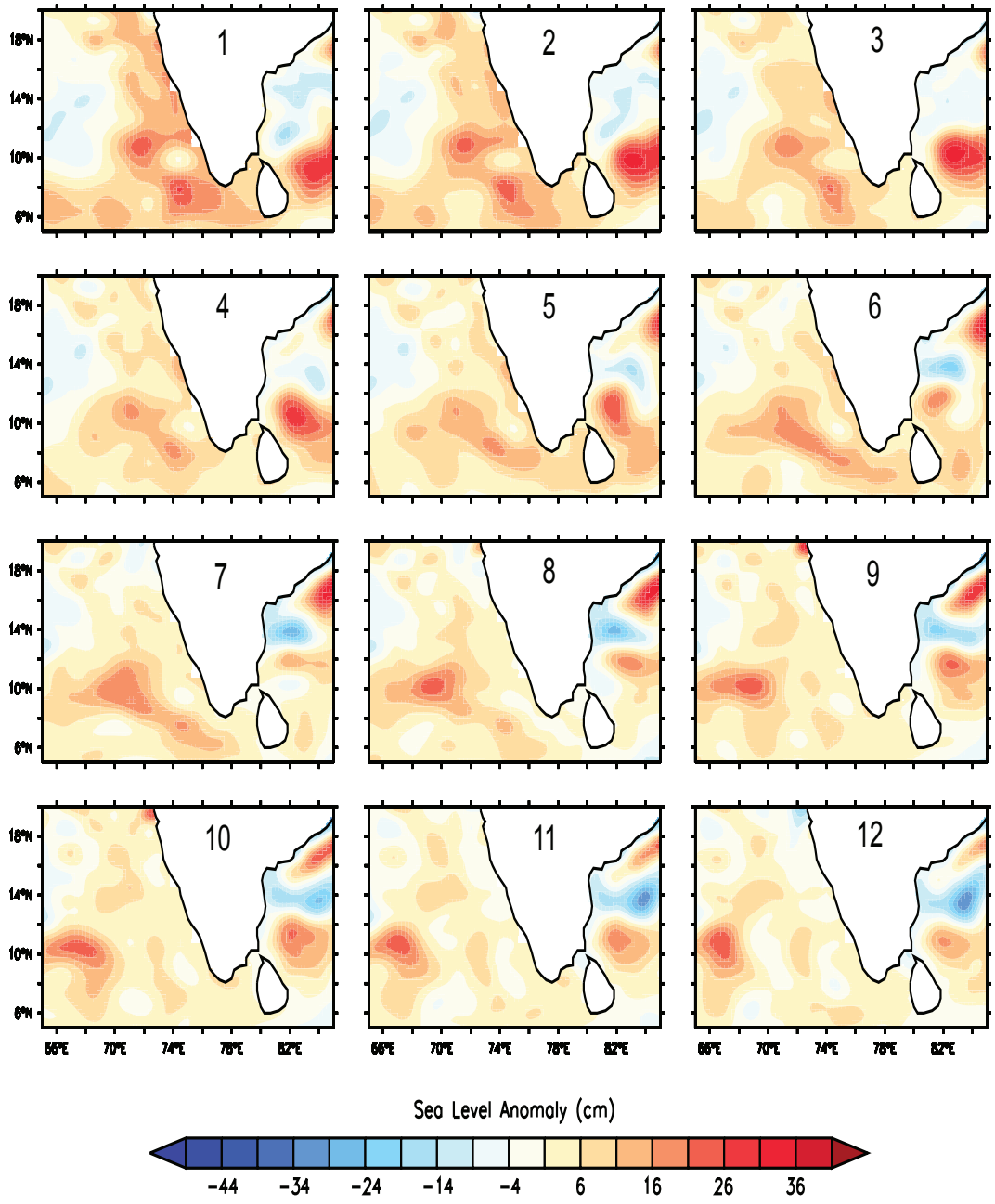

Figure 8.1: SLA in the Northern Indian Ocean during 1 to 12 weeks

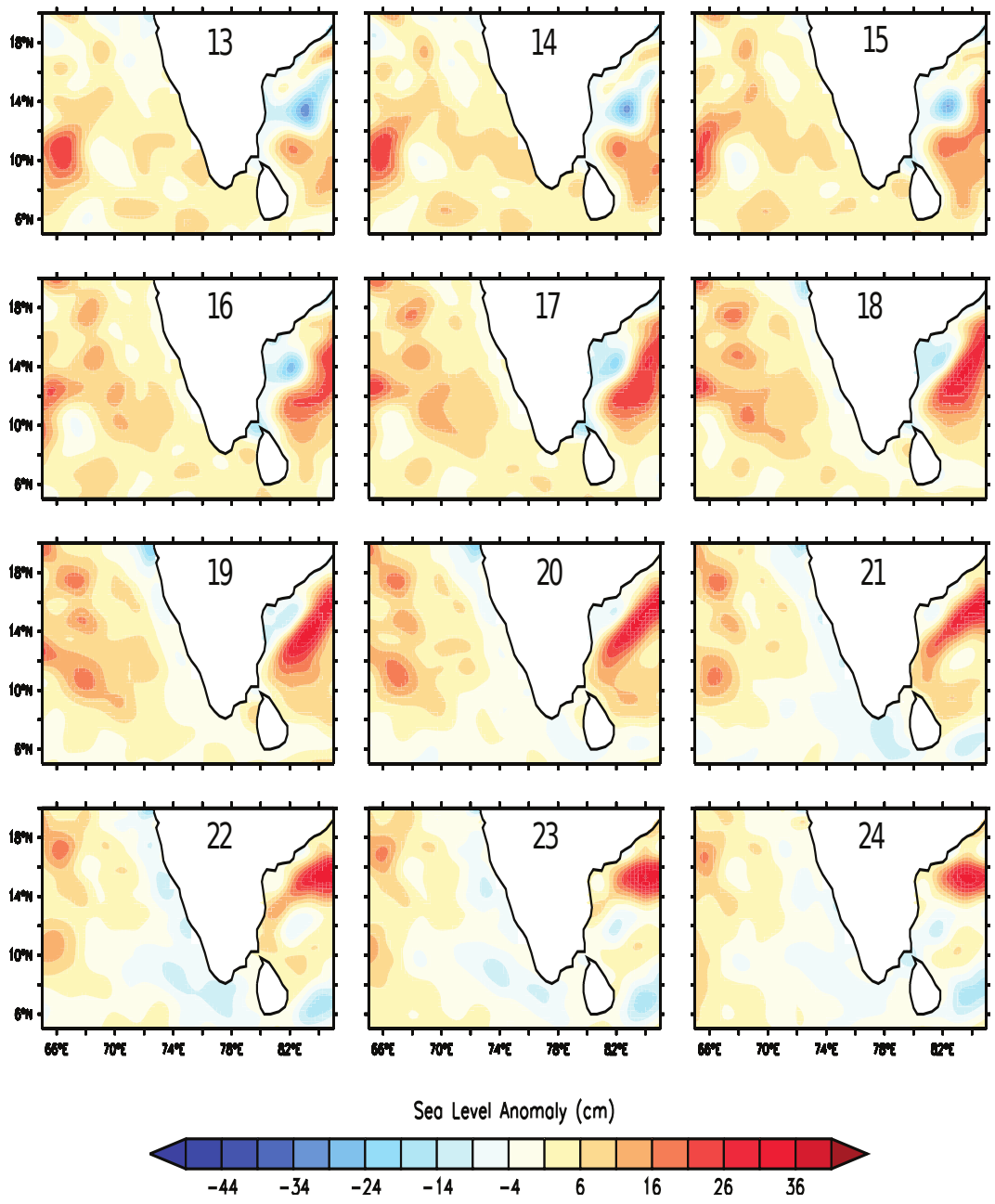

Figure 8.2: SLA in the Northern Indian Ocean during 13 to 24 weeks

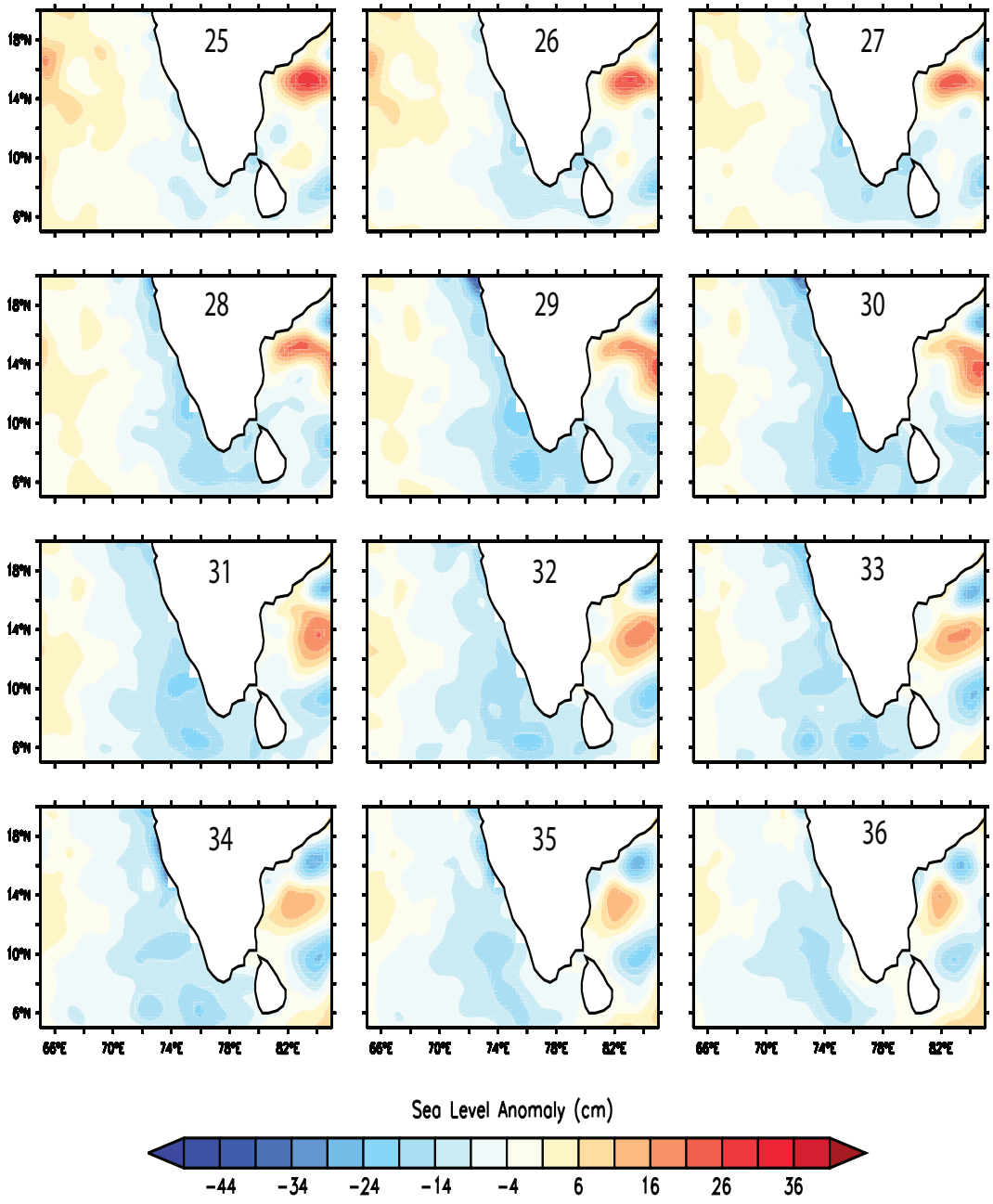

Figure 8.3: SLA in the Northern Indian Ocean during 25 to 36 weeks

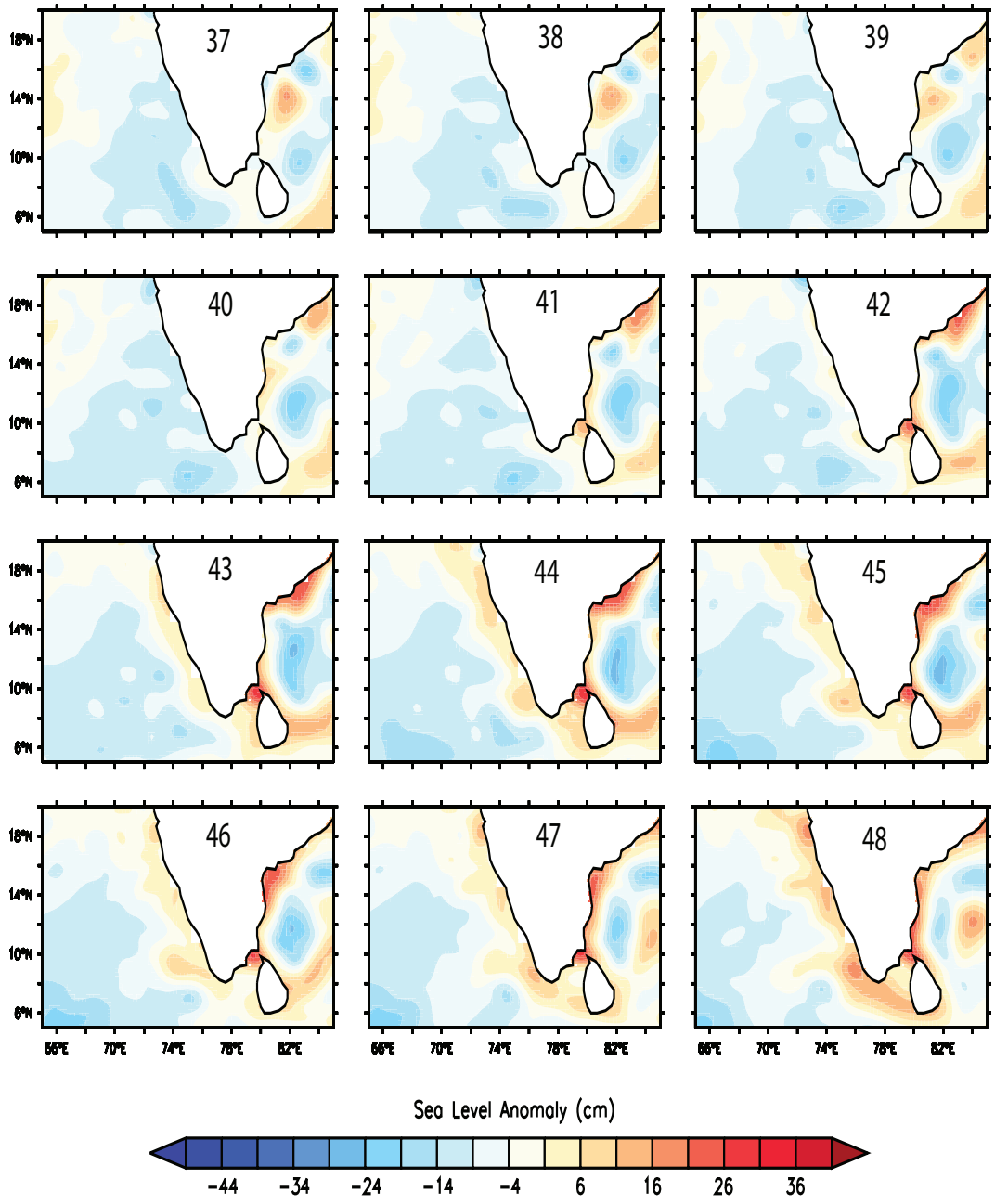

Figure 8.4: SLA in the Northern Indian Ocean during 37 to 48 weeks

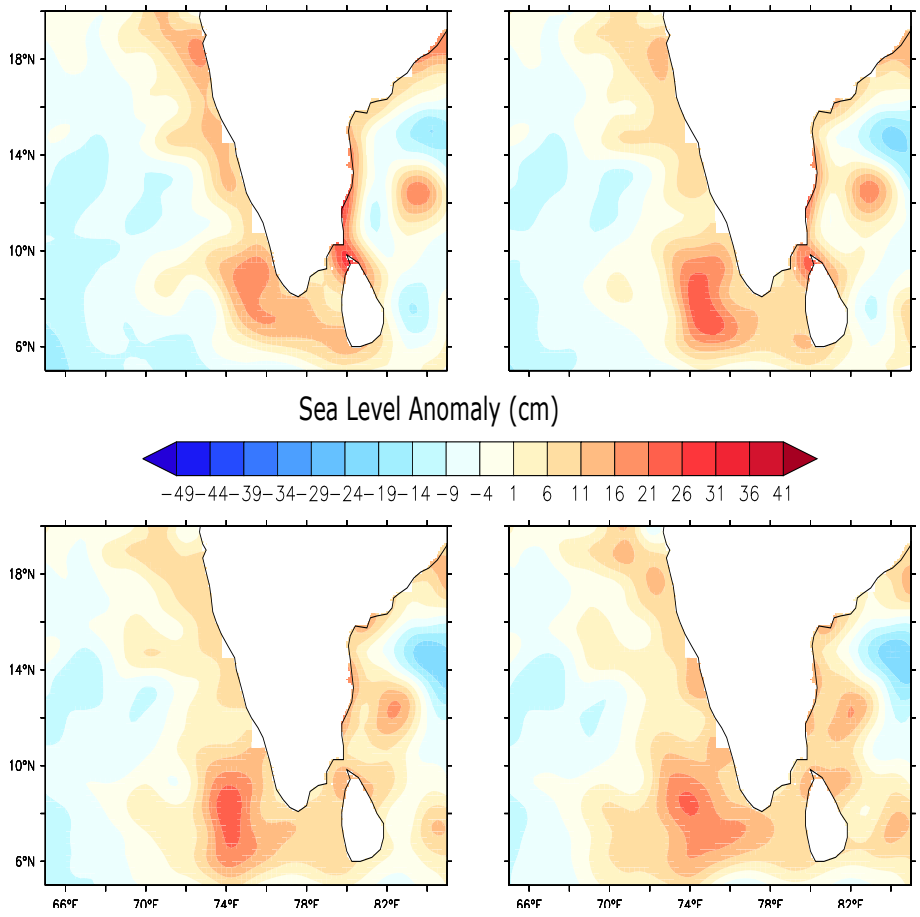

Figure 8.5: SLA in the Northern Indian Ocean during 49 to 52 weeks

Appendix-2

The following are the list of publications that form part of doctoral work

1 Chiranjivi Jayaram, TVS Udaya Bhaskar, Ajith Joseph K and Balchand A.N., (2011): " Variability of Wind stress and its influence on upwelling, Chlorophyll-a and Mixed layer in southeastern Arabian Sea as observed from satellite data".(Communicated).

2 Chiranjivi Jayaram, Neethu Chacko, Ajith Joseph K and Balchand A.N., (2010): Interannual Variability of Upwelling Indices in the Southeastern Arabian Sea: A Satellite Based Study. Ocean Science Journal, Vol. 45, No. 1, pp. 27 - 40.

3 Chiranjivi Jayaram, Nandini Menon N, Ajith Joseph K and Balchand A N (2010): Monitoring of Trichodesmium Spp. in the Arabian Sea from *in-situ* and Satellite data products. Oral Presentation at SAFARI - International Symposium on "Remote Sensing and Fisheries" held during February 2010 at Kochi, India.

4 Chiranjivi Jayaram, Ajith Joseph K and Balchand A.N., (2009): "Modulation of upwelling in the southeastern Arabian Sea during extreme climatic conditions: A remote sensing perspective". Awarded as the best poster during the Indo-Russian workshop on Regional Climate Change under the DST (Govt. Of India) - RFBR (Russian Federation) Call – 2009, held at Cochin during October 8 - 9, 2009.

5 Chiranjivi Jayaram, Ajith Joseph K and Balchand A.N., (2009): "Decreasing trend of chlorophyll-a concentration in southeastern

Arabian Sea - Observed from the satellite data". Presented at National Conference of Ocean Society of India held at Visakhapatnam during March 19 - 21, 2009.

6 Chiranjivi Jayaram (2009): "Differential response of the Arabian Sea productivity trends". Oral presentation at Indo- Norwegian conference on operational ocean modeling held at INCOIS, Hyderabad, India during March 2009.

7 Chiranjivi Jayaram, Ajith Joseph K and Balchand A.N., (2008): "Applications of SARAL - AltiKa altimeter in the coastal upwelling studies in synergy with Oceansat - II in the southeastern Arabian Sea". Oral presentation at SARAL - AltiKa meeting held at Space Applications Centre - ISRO, Ahmedabad in September 2008.

8 Chiranjivi Jayaram, Ajith Joseph K and Balchand A.N., (2008): "Indications of upwelling in the Lakshadweep Sea derived from ARGO and Satellite Observations". Oral presentation at First Indian ARGO users workshop held at INCOIS, Hyderabad in July2008.